

1

2

The Andes and Hotspots: Mutual Evidence

3

Rex H Pilger, Jr

4

10630 W 66th Avenue

5

Arvada, Colorado USA

6

rexpilger@yahoo.com

7

<https://orcid.org/my-orcid?orcid=0000-0003-3715-5084>

8

9

Key Points

10

Subduction beneath western South America of two hotspot traces on the Nazca Plate since 70 Ma is reflected in gaps and eastward displacement of the Andean volcanic arc as a result of trace-induced low-angle subduction.

11

12

13

The locations of the inferred effects of subducted traces in the Andean magmatic record are consistent with a single hotspot reference frame beneath the Pacific extending from Hawaii to the Juan Fernandez island-seamount chain offshore Chile and covering at least 140 Ma

14

15

16

The role of variations in convergence rate on Andean magmatism from 80 Ma to the Present is not obvious in the distribution of isotopic dates, perhaps correlations with geochemical trends would provide more insight in the future.

17

18

19

Abstract

20

Improved plate-to-plate reconstructions in the southwest Pacific, South Atlantic, and southwest Indian Ocean, and plate-to-hotspot models for the Pacific plate, combined with published igneous dates of the South American Andes produce apparent correspondence of predicted with observed magmatic patterns in the mountain range. The inferred Easter-Nazca (EN) and Juan Fernandez (JF) hotspot traces, long inferred to control low-angle subduction and contemporary volcanic gaps along the Andean crest, when reconstructed, match the traces' present bathymetric expression and seismic clusters within the South American plate. Global reconstructions of the Nazca to the South American plate predict the subducted portions of the traces through time. Gaps in magmatism over the past 10-15 Ma correspond with the reconstructed position of the traces beneath Peru (EN) and Chile and Argentina (JF). The predicted JF trace also matches trends in magmatism, especially mafic rocks, including eastward shifts and gaps as early as 60 Ma in Bolivia, southern Peru, Chile, and Argentina from the 80-90 Ma segments of the trace. The magmatic pattern provides a kind of "image" of the hotspot traces projected onto the Cenozoic of the Andes. The correspondences also increase confidence in the existence of a stable hotspot reference frame beneath the plates of the Pacific over the past ~90 m. y.

21

22

23

24

25

26

27

28

29

30

31

32

33

34

Key Words

35

3040 Plate tectonics

36

8157 Plate motions: past

37

8178 Tectonics and magmatism

38

3037 Oceanic hotspots and intraplate volcanism

39

40 Plain Text Summary

41 Application of advances in plate tectonic theory to the Andes of South America strengthens models of
42 anomalous oceanic plate from mantle hotspots which produce low-angle subduction and volcanic gaps and
43 shifts as oceanic and continental plates converge. Combined plate reconstructions and hotspot models of
44 the Pacific predict when and where anomalous parts of the oceanic plate encountered South America; the
45 calculated positions correspond with observed gaps and shifts in volcanism in the Andes over the past 60
46 million years.

47 1. Introduction

48 The South American Andes, which has developed above a continuously active subduction zone for the
49 plates beneath the Pacific throughout the Cenozoic and extending into the Late Cretaceous, provides the
50 ongoing opportunity for understanding the mutual relationships of mountain-building, magmatism, and
51 subduction to plate kinematics, oceanic plate age, subducting plate fracture zones, and hotspot traces.
52 Ongoing enhancements to the characterization of the ocean basins from magnetic and bathymetric surveys
53 and satellite geoid and gravity measurements, resulting in higher resolution plate reconstructions, provide
54 comparable evolving resolution of global reconstructions of the Nazca/Farallon and Antarctic plates relative
55 to South America. Similarly, studies of the contemporary configuration of the subduction zone from
56 seismicity, tomography, and potential field modeling, and the structure and magmatic evolution of the
57 mountain range, provide a basis of comparison with the plate reconstructions and kinematics. From such
58 analysis, insight into other mountain ranges formed above oceanic subduction zones may be provided, as
59 well as improved characterization of geohazards and effective development of existing and newly
60 discovered mineral resources.

61 The hotspot/plume hypothesis of Wilson (1963) and Morgan (1971, 1972) continues to influence research
62 on plate kinematics, as well as dynamics, both whether hotspots provide one or more distinct reference
63 frames, and the nature of their origin and relation to the driving mechanism. An auxiliary proposal, that
64 island-seamount chains, inferred traces of hotspots, decrease the angle of subduction, thereby
65 extinguishing or shifting loci of arc magmatism and resulting in Rocky Mountain-type deformation and back
66 arc subsidence (e.g. Cross and Pilger, 1978b, 1982; Pilger, 1981, 1984; Jarrard, 1986), has simmered,
67 lacking an abundance of data to establish a correspondence of observed island-seamount chains and their
68 inferred, reconstructed traces with magmatic patterns in the one mountain range in which it is possible, the
69 South American Andes. Since the original limited 1981 and 1984 tests for the Andes a number of workers
70 have applied the idea of gaps in magmatism as indicative of low-angle subduction (although periods of
71 reduced convergence rate, arc-parallel displacement between plates, and/or spreading ridge subduction
72 may also play a role), without application of particular kinematic models for the production of near-flat
73 subduction. Additional implications for magmatic, deformational, and dynamic elevation effects from
74 variations in subduction kinematics have also been a matter of speculation, even as global reconstructions
75 have increased in resolution.

76 Progressive advances in a wide variety of fields over the intervening forty-plus years provides the
77 opportunity for addressing the magmatic history, plate kinematics, hotspot-frame, and trace subduction
78 effects together for the past 80 Ma. The advances include the generation and publication of thousands of
79 isotopic dates of igneous rocks in the Andes by multiple laboratories in the Americas, Europe, Asia, and
80 Australia, and improved, higher resolution plate-pair reconstructions (especially recent results from the
81 South Atlantic and Southwest Indian Oceans to supplement earlier Southwest Pacific Ocean studies) and
82 plate-hotspot reconstructions (especially in the Pacific Ocean, based on more accurate argon-argon dating
83 and improved modeling techniques).

84 2. Rationale and Methodology

85 At present, the Andean subduction zone is readily subdivided into five zones, as recognized and defined
 86 from the seismicity by Barazangi and Isacks (1976, 1979), three with a maximum dip of 40-45 degrees of
 87 the descending plate between 100 to 300 km in depth, and two with nearly horizontal dips just below 100
 88 km in depth (Figure 1). Deeper seismicity appears to be separated from the shallow zone, within 500 and
 89 800 km. The shallow, low-angle segments, beneath central Chile and adjacent Argentina and beneath
 90 central and northern Peru, are also distinctive in the absence of active volcanism along the Andean crest, in
 91 contrast with the other three, more steeply dipping shallow segments.

92 Three inferred hotspot traces on the Nazca plate appear to be undergoing subduction beneath the Andes of
 93 South America, the Juan Fernandez chain, the Nazca Ridge, and the Carnegie Ridge. The first two are
 94 offshore of the contemporary low-angle subduction segments prompting the suggestion of a genetic
 95 relationship of the traces to the anomalous subduction (e.g., Pilger, 1981); the third may be responsible for
 96 incipient low-angle subduction beneath Colombia. The traces' inferred sources are, respectively, the
 97 proposed Juan Fernandez (JF), Easter-Nazca (EN), and Galapagos-Carnegie (GC) hotspots (Figure 1).

98 Numerous kinematic models for the production of the hotspot traces on the Pacific plate, assuming
 99 relatively fixed hotspots, have been produced since Morgan's (1971) original proposal. Pilger and
 100 Handschumacher (1981) showed how the models of Clague and Jarrard (1973) and Jarrard and Clague
 101 (1977) could be extended to the three inferred traces on the Nazca plate via relative reconstructions of the
 102 Pacific and Nazca/Farallon plates (the Nazca plate is the largest of several to have formed from the
 103 fragmentation of the larger Farallon plate at about 25 Ma as recognized by Handschumacher, 1976).

104 Reconstructions of the Nazca plate relative to the South American plate, first calculated by Pilger (1981,
 105 extended in 1983) were derived via the plate pair circuit South American > African > Indian > Antarctic >
 106 Pacific > Nazca (SA > AF > IN > AN > PC > NF). Subsequently, in Pilger (1984), the circuit was shortened
 107 when newly published AF > AN reconstructions could replace the longer and less precisely defined AF >
 108 IN > AN sub-circuit. A number of other workers have provided updates to the reconstructions within the
 109 circuit, including Cande (1985), Cande and Leslie (1986), Pardo-Casas and Molnar (1987), Somoza (1998),
 110 Martinod et al. (2010), Somoza and Ghidella (2012), Muller et al. (2016, 2019), Bello-González et al., 2020,
 111 and Quiero et al. (2022). (Reconstructions by Yáñez et al. and two of three models of Martinod et al. are
 112 based on the absolute motions of the Nazca and South American plates according to Gordon and Jurdy,
 113 1986, assuming that the hotspot frameworks of the Pacific and Atlantic are fixed relative to one another. All
 114 of the other reconstructions cited do not make this assumption, relying only on relative plate-pair
 115 reconstructions.) Recognition that East and West Antarctica have acted at times as separate plates (Cande
 116 and Stock, 2000) introduced their replacement of a single Antarctic plate within the circuit, included in the
 117 circuit calculations, of the last four works, plus one of Martinod et al.'s models). In each ocean basin,
 118 periodically updated plate-pair reconstructions have been published by a number of workers. Thus it is
 119 possible to derive documented NF > SA reconstructions as early as 84 Ma (for earlier times, the connection
 120 through Antarctica to the Pacific is speculative). A few alternate circuits have been proposed, as further
 121 considered below.

122 As noted, the correspondence of the two hotspot traces with segments of low-angle subduction could be
 123 genetic (other mechanisms have also been proposed in combination with hotspot traces or independent of
 124 them; see below). Thickened plate beneath aseismic ridges, formed at spreading centers could decrease
 125 the density contrast with the shallow asthenosphere at the subduction zone, resulting in shallower
 126 inclination of the oceanic plate. Intraplate hotspot traces might produce a decreased contrast due to heating
 127 of the plate along with marginal increase in thickness of the crust by the magmatic activity. Both proposed
 128 mechanisms have been modeled by several workers with divergent results. As shown by Pilger and
 129 Handschumacher (1981), the Nazca ridge was likely formed at the PC-NZ spreading center between 50 to

130 25 Ma, perhaps beginning even earlier (with older portions undergoing subduction beneath Peru). The Juan
 131 Fernandez chain is clearly younger than the surrounding Nazca plate and smaller in dimensions than the
 132 Nazca Ridge, so its effect on the subduction zone might be expected to be less significant than that of the
 133 Easter/Nazca trace, unless hotspot activity were of greater magnitude in the past.

134 The contemporary correspondence of hotspot traces and low-angle subduction can be further tested by
 135 reconstructions of the hotspot traces relative to the Nazca -Farallon (NF) plate (extending the Pacific >
 136 hotspot, PC > HS, models via PC > NF plate-pair reconstructions), and the latter relative to the South
 137 American (SA) plate, via the global circuit, for comparison with the magmatic history of the Andes. Pilger
 138 (1981, 1984) applied this approach with lower-resolution plate-pair reconstructions and a very small number
 139 of published isotopic dates of Andean igneous rocks. Then available dates showed the expected
 140 correspondence over the last 13 to 15 m. y., for the Easter-Nazca (EN) and Juan Fernandez (JF) traces;
 141 that is, within the two studied segments, dated magmatism along the Andean crest and younger than the
 142 calculated timing of trace subduction was observed to be absent. However, the paucity of dating over much
 143 of the Andes limited confidence in the anticipated correspondence, especially reconstructions for earlier
 144 times.

145 Higher resolution plate pair reconstructions are now available within some plate pairs within the circuit
 146 South American > African > East Antarctic > West Antarctic > Pacific > Nazca/Farallon (SA > AF > AN >
 147 WA > PC > NF), although a few limitations persist. One of the most significant shortcomings is the inability
 148 to propagate reconstruction uncertainties throughout since common magnetic isochrons for plate pair
 149 reconstructions within the circuit do not exist.

150 Over the past forty years thousands of isotopic dates of Andean igneous rocks have been produced by
 151 laboratories in South and North America, Europe, Asia, and Australia. A compilation of greater than 20,000
 152 dates on igneous rocks from the Andes and adjacent areas from published sources (including more than
 153 10,000 dates younger than 100 Ma) provides a basis for comparison with the reconstructions.

154 If the hotspot trace subduction effect exists, gaps or landward shifts in the magmatic foci should be
 155 observed for dates on the order of or younger than the reconstructed hotspot traces. (In addition, the
 156 reconstructions are also an implicit test of models of relatively fixed hotspots beneath the Pacific Ocean and
 157 the separate Atlantic-Indian Ocean hotspots.)

158 Other postulated controls on subduction zone configuration, such as convergence rate, motion of the upper
 159 plate relative to the deeper mantle (i.e., "absolute motion"), and age of the subducting oceanic plate may
 160 also be relevant (e.g., Cross and Pilger, 1982), but, with the exception of the first, are not so easily
 161 distinguished. Convergence rate variations are readily calculated from the reconstructions, so semi-
 162 quantitative comparisons are possible, recognizing the limitation of unknown uncertainties. Convergence
 163 rate inferences made in the first few decades of reconstructions (e.g., Pilger, 1983; Pardo-Casas and
 164 Molnar, 1987) suffered from inaccuracies and imprecision in the geomagnetic time scale, which appear to
 165 have decreased in recent years as more isotopic dating of sedimentary and volcanic sequences and
 166 correlation with solar cycle measurements have been incorporated (e.g. Gradstein et al., 2020).

167 Unfortunately, motion of the South American plate in a hotspot frame is poorly constrained and of relatively
 168 low resolution in most extended models (e.g., Pilger, 2007); some analysis may be tentatively undertaken,
 169 nevertheless.

170 3. Relative Plate Reconstructions

171 Table 1 lists the primary sources of the relative plate-pair reconstructions within the SA > AF > AN > WA >
 172 PC > NF and SA > AF > AN > WA > NF circuits and HS > PC, HS > AF; these pairs are addressed further
 173 below). Supplementary Table 1 lists the actual parameters and assigned ages. DeMets et al. (2015) and
 174 DeMets and Merkoviev (2019) have provided high resolution reconstructions for AF > EA (since ~20 Ma)

175 and SA > AF (since ~34 Ma), while Croon et al. (2008) have calculated high resolution reconstructions for
 176 WA > PC for virtually the full time interval of interest. Pérez-Díaz and Eagles' (2014) parameters complete
 177 SA > AF, while Royer and Chang (1991), Cande et al. (2010), Bernard et al. (2005), Nankivell (1997)
 178 complete AF > AN, at variable resolution. Wilder's (2003) PC > NF reconstructions are confined to the
 179 interval 12 to 28 Ma, supplemented by partial reconstructions of Wright et al. (2015) and Seton et al. (2012)
 180 from the North Pacific for older times and two PC > NF reconstructions younger than 12 Ma, calculated from
 181 Tebbens and Cande's (1987) WA > NF and Croon et al.'s WA > PC parameters (PA > NF is equivalent, of
 182 course, to PA > WA > NF, but with perhaps added uncertainty). A shorter circuit, involving SA > AN directly
 183 but of lower resolution, is also presented in Table 1 from Livermore et al. (2005), Eagles and Vaughn
 184 (2009), and Eagles and Jokat (2014). It is comparable to the primary circuit below.

185 The circuit reconstructions require interpolation since only a few isochrons are identified within all of the
 186 plate pairs. Conventional interpolation (e.g., Atwater and Molnar, 1973) utilizes constant stage poles and
 187 rates of rotation (introduced by Pitman and Talwani, 1972, and Weissel and Hayes, 1972) between
 188 reconstructed isochrons at discrete times. Piecewise polynomial interpolation (e.g., cubic splines) is an
 189 alternative approach (Pilger, 1981b, 2003, 2007), which allows for continuous change in kinematics;
 190 constant stage poles and rates force changes to correspond with the discrete isochron reconstructions (the
 191 most confidently identified isochrons are those formed during apparent periods of constant rotation pole, if
 192 not constant rate; forcing changes to correspond with just such times is very likely incorrect). Rather than
 193 select discrete isochrons, reconstruction parameters are calculated at unit m. y. intervals via the splines.
 194 Logically, meaningful reconstruction uncertainties cannot be determined by interpolation; by definition,
 195 interpolation provides synthetic parameters for times in which such parameters are unavailable.

196 Uncertainties for discrete reconstructions derived by conventional means (e.g., Kirkwood et al., 1997) are
 197 linearized approximations of nonlinear forms which do *not* have a temporal dependency since they are
 198 derived for individual isochrons whose assigned ages are identical and irrelevant to the uncertainties.
 199 (Livermore et al. 2014, did apply a method of simultaneous PC reconstructions of sequences of isochrons via
 200 flowlines, including uncertainties, after Shaw and Cande, 1990, but the approach has not been expanded
 201 upon, probably because the number of reconstruction and flowline parameters sought can become
 202 unwieldy.)

203 The geomagnetic timescale of Ogg (2020) is utilized for the reconstructions and cubic spline interpolation.
 204 The spline interpolation is applied to each plate pair, converting the spherical coordinates to Cartesian with
 205 magnitude equal to the average rotation rate. The algorithms of Press et al. (1992) produce the spline
 206 coefficients and interpolated pseudovector parameters, converted to quaternion parameters. The latter
 207 parameters are combined utilizing the derivation of Francheteau (1973; also in LePichon et al. 1973) and
 208 ultimately converted back to spherical coordinates. (Supplementary Table 2 provides the interpolated
 209 parameter sets for each pair at 1 m. y. intervals.)

210 Table 2 provides the calculated parameters for the reconstructions of the Nazca/Farallon plate to the South
 211 American plate at 1 m. y. Intervals. Resolution is best achieved between 12 and 20 Ma, and, to a lesser
 212 extent, between 20 and 33 Ma. Pacific to Nazca/Farallon reconstructions are probably the least certain in
 213 the primary circuit because of the sparsity of magnetic survey coverage of the east-central Pacific Ocean;
 214 this is particularly unfortunate since this boundary has the highest average spreading rates of the entire
 215 circuit (e.g. Pilger, 1983), thereby providing the greatest contribution to the net kinematics and potential
 216 variability.

217 4. Hotspot - Plate Reconstructions

218 Since Morgan's (1972) original parameterization of the Hawaiian-Emperor (H-E) hotspot trace (together with
 219 the Tuamotus and Line Islands) a number of workers have revised the parameters based on progressive

isotopic dating of volcanism along not only the H-E trace, but also others on the Pacific plate. Critical to modeled parameters was the introduction of argon-argon dating which demonstrated many measured island/seamount potassium-argon dates are apparently too young, most familiarly, the bend in the H-E chain, which is now accepted to be closer to 48 Ma based on argon-argon dating (Sharp and Clague, 2006; O'Connor et al. 2013) rather than the K/Ar date of 43 Ma and an even earlier, projected 27 Ma (Clague and Jarrard, 1973), while the Line Islands are much more complex than Morgan had interpreted. Interestingly, Harada and Hamano's (2000) model for the Pacific hotspot traces produced an implicit age of 48 Ma for the bend, even before Sharp and Clague's (2006) revised date was published and independent of relative plate motion evidence.

The most recent models of Pacific - hotspot motion which incorporate the 48 Ma age for the bend and other, newly recognized traces, are Wessel and Kroenke (2008) and Gaastra et al. (2022). Some workers argue that the dating and paleomagnetic measurements require significant relative motion of the Hawaiian and Louisville hotspots; Gaastra et al. (see sources cited in their paper) show that one issue is the presumption of where the point in the Louisville chain corresponding to the HE bend is located; their revised model, without such an assumption, fits the two primary traces plus parts of additional traces recognized on the Pacific plate resulting in minimal motion between hotspots.

It should be noted that most Pacific hotspot models do not take the apparent traces on the Nazca and Cocos plates into account; one exception is that of Pilger and Handschumacher (1981; also Pilger, 1983) who noted that the Easter-Nazca trace is better fit by an age for the HE bend close to isochron 21 or 22, now dated between 45.724 and 49.344 Ma (Ogg, 2020), than the then widely accepted 43 Ma; the older age also corresponds with a significant change in motion of the Farallon and Pacific plates, another point of contention with the 43 Ma date (e.g., Norton, 1995). Hu et al., (2022) document a variety of circum-Pacific changes at 50 Ma, which also support that age for the bend. That dates from seamounts may be as much as 3 m. y. younger than the onset of their formation has been suggested by O'Connor et al. (1995) and Ray et al. (2012) as applied to the Easter-Nazca chain (Maia et al. 2005, based on magnetic surveys and modeling of the near-ridge part of the Foundation seamount chain on the Pacific Plate, argue that some seamount formation occurs within a period as short as 1 m. y.).

Because both models, Wessel and Kroenke (2008) and Gaastra et al. (2022), for Pacific-hotspot motion are based entirely on isotopic ages, they do not need to be adjusted for changes in the geomagnetic time scale. However, in order to test the models against the traces on the Nazca plate, which involve magnetic reversal isochrons for the PC > NF plate reconstructions, it is necessary to document the timescale used, in this case, that of Ogg (2020). For this work, the parameters of Gaastra et al. (2022) are utilized, with ages from 25 to 48 Ma linearly reassigned from 25 to 50 Ma, and from 48 to 80 Ma from 50 to 80 Ma. Wessel and Kroenke's (2008) parameters from 78 Ma through 144 Ma are used for calculating stage parameters which are linearly interpolated and then combined with Gaastra et al.'s parameters at 80 Ma to produce total rotation parameters from 80 to 140 Ma. Supplementary Table 1 includes the two Pacific-hotspot model parameter sets; Supplementary Table 2 includes the cubic spline-interpolated parameters by the same procedure used for the relative plate reconstructions plus the calculated Nazca-hotspot parameters for the two hotspot models.

5. Nazca and Cocos Plate Hotspot Loci at Present

Note: It is suggested that the reader obtain the Keyhole Markup Language files in the Supplementary Data and display them in Google Earth (or another GIS software program which also displays regional geographic features, such as physiography, coastlines, trenches, islands and seamounts, and country boundaries). The descriptions in the next sections are more easily visualized in this manner.

265 Figure 2 illustrates back-tracked loci of individual dated volcanic samples from inferred hotspot traces on the
 266 Pacific, Nazca, and Cocos plates, using the model of Gaastra et al. (2022; “GGW22”) for Pacific-hotspot
 267 motion, extended to the two other plates; at the scale of the two figures, the model of Wessel and Kroenke
 268 (2008, “WK08”) would not produce obvious differences for the Pacific plate. Figure 3 shows loci for the two
 269 models of hotspot motion relative to the Nazca/Farallon plate (from revised dating of the Hawaiian-Emperor
 270 bend, as described above; see also Supplementary Keyhole Markup Language, “*.kml,” files), based on
 271 WK08, and GGW22, are calculated for the three inferred contemporary hotspots with respect to the Nazca-
 272 Farallon plate, propagated from the Pacific plate as described above. The hotspot locations are adjusted to
 273 best fit the bathymetric expression of each trace to the GGW22 loci. (There are a number of published
 274 dates for the JF, EN, and GC hotspot traces, included in a Supplementary Data *kml* file; they are not
 275 inconsistent with the calculated loci described in this paper.)

276 The extensions of the modeled loci into the South American plate (Figure 3 and subsequent illustrations
 277 below) are *not* adjusted for the configuration of the subducted slab, since the kinematic path along the slab
 278 is unknown, nor, for past reconstructions, is the slab configuration independently known; the individual loci
 279 would be relocated several tens of kilometers or more to the southwest or west of the modeled surface
 280 locations if the configuration were confidently known.

281 Figure 3 shows that both WK08 and GGW22 fit the 25 Ma bend in the EN trace fairly well, but with different
 282 inferred locations for the Easter hotspot (its contemporary location is poorly constrained). However, there is
 283 a significant deviation of the younger part of the JF and GC loci from the observed bathymetry for those
 284 based on the WK08 model compared with the GGW22 model; the WK08 model would fit better if the
 285 contemporary JF hotspot location were further southwest of the westernmost extent of the JF chain; even
 286 so, its orientations are still significantly different than those of the JF and GC traces.

287 For the purposes of this study, the recalibrated GGW22 Pacific-hotspot model is utilized because of its
 288 better fit to the observed portions of the JF and GC traces and the other data presented below. Before
 289 further consideration of the relationship of the GGW22 loci to other geological observations, it is convenient
 290 to summarize the shape of the loci through time. The JF locus, from present into the past extended east-
 291 west from 0 to ~25 Ma, to the northeast between ~25 and ~85 Ma, more easterly from ~85 to ~110 Ma, and
 292 northerly between ~110 to ~120 Ma; it then curves back to the west to north-north easterly from ~120 to
 293 ~140 Ma. (The part of the locus between 105 and 125 Ma, termed herein the “hammerhead,” appears in
 294 another guise below.) The abrupt “kink” in the locus about 50 Ma is inherited from the parameters of the
 295 GGW22 Pacific-hotspot model close to the HE bend and is independent of the PC > NF parameters. (The
 296 80 to 140 Ma part of GGW22 is based on the equivalent part of WK08A combined with the 80 Ma GGW22
 297 parameters.)

298 It is possible that the older parts of the locus, assumed attached to the Farallon plate, may never have
 299 formed in the first place as another plate may well have existed above the JF hotspot at that time, if the
 300 hotspot, also, then existed. Other evidence for the trace and plate is essential to provide support for the
 301 hotspot’s existence and expression at progressively earlier times.

302 Returning to the younger part of the loci, the GGW22 modeled JF trace corresponds well with the shallow-
 303 to-intermediate-depth seismicity pattern in central Chile extending into Argentina (Figure 4), and lesser
 304 shallow seismic clusters appear along the GGW22 extensions of the EN and GC loci (Figure 1; see also
 305 Alvarez et al., 2014). If the ridges indeed extend where the model suggests, instead of hotter, partially
 306 molten asthenosphere in the wedge between the subducting slab and the upper plate, drag against the
 307 upper plate by the shallowly dipping lower plate could induce resistance, propagating enhanced shallow
 308 deformation and seismicity into the upper (South American) plate above the subducting trace.

309 As recognized by Barazangi and Isacks (1976), contemporary volcanism along the crest of the Andes is
 310 present within the more steeply dipping segment of the subduction zone from southern Peru into northern

311 Chile, and absent within the low-angle subduction segments. The respective presence and absence of the
 312 asthenospheric wedge is invoked to explain the difference (see also Cross and Pilger, 1982).
 313 The reconstructed loci in their contemporary locations require only the Pacific-hotspot kinematic models and
 314 Pacific-Nazca/Farallon reconstructions (without attempting to address their deformation in the subduction
 315 zone). To compare the loci through time relative to the magmatic history of the Andes requires the global
 316 circuit plate reconstructions.

317 6. Nazca Plate Hotspot Loci Relative to South America since 80 Ma

318 The three Model GGW22 hotspot trace loci (Figure 3) are further reconstructed relative to South America for
 319 discrete times, via the global circuits to 80 Ma. (The hotspot traces themselves are reconstructed from the
 320 Pacific to the Nazca plate to 140 Ma.) Figure 5 shows the loci in relation to the continental plate at 1 m. y.
 321 intervals. From the figure one may infer that essentially east-west subduction at the latitude of the JF Ridge
 322 occurred over the last twenty million years, with most rapid convergence of the Nazca and South American
 323 plates between 25 and 15 Ma (higher resolution analysis of convergence rate and direction variations is
 324 addressed further, below). Additionally, the reconstructions imply that subduction of the JF trace was largely
 325 confined to the contemporary zone of low-angle subduction for the past ~13 m. y. (which is consistent with
 326 Pilger's 1984 reconstructions over the same period). Between 25 and 13 m. y., the locus intersection with
 327 the trench progressed southward from northernmost to central Chile. (Since the trench may have been in a
 328 more oceanward position, the intersection points would be farther to the southwest relative to the stable
 329 interior of the South American plate.) From ~45 to ~25 Ma, the reconstructed JF trace implies roughly east-
 330 west convergence within a narrow zone beneath southern Peru, northern Chile, Bolivia, and northern
 331 Argentina; the reconstructed trace first encountered the subduction zone about between 70 and 65 Ma.
 332 The reconstructed Easter-Nazca (EN) trace first encountered the Trench offshore present-day northern
 333 Colombia between 45 and 40 Ma (Figure 3), maintaining a southwesterly migrating intersection with the
 334 trench onshore Colombia and Ecuador until about 18 Ma, when the intersection migrated to the south-
 335 southeast more rapidly, to its contemporary position off southern Peru. As with the JF trace, the position of
 336 the trench may have been farther west relative to the interior of the continent at progressively earlier times,
 337 contributing some additional uncertainty to the intersection locales.

338 The reconstructed GC trace first intersected the Nazca-Pacific boundary between 35 and 30 Ma (Figure 3),
 339 near the contemporary Caribbean-South American-Nazca triple junction, extending beneath the complex
 340 Caribbean-South American boundary of northern Colombia and Venezuela (Figure 1). It is possible that the
 341 hotspot location could be farther east, resulting in onset of low-angle subduction at an earlier time.

342 As observed above, the older parts of the loci may never have developed on the older part of the Farallon
 343 plate if the corresponding portions of the latter did exist; the projected part of the Farallon plate is based on
 344 isochrons in the Northwest Pacific. Corresponding parts of the Pacific plate with those projected under
 345 South America are also unknown because they are presumably beneath the northeastern Australian plate,
 346 having been subducted, if they, also, ever did exist. The reconstructions of Clennett et al. (2020), focused
 347 on the northeast Pacific, do include an existent, subducting Farallon plate offshore South America as early
 348 as 80 Ma; prior to that time, they infer accreting terranes, island arc fragments, as far south as Colombia,
 349 with another intervening plate which completed subduction before the end of the Cretaceous. (Clennett et
 350 al.'s reconstruction circuit includes most of the components of the circuit utilized in this study, except their
 351 primary concern is North, not South, America relative to the plates of the Pacific and Mesozoic accreted
 352 terranes. Bello-González et al., 2020, utilizing essentially the same database as Clennett et al., produces
 353 positions of the hotspot traces in the global average reference frame.)

7. Volcanic history of the Andes and reconstructed hotspot loci

As anticipated, the patterns of magmatism in the Andes apparently reflected interaction with subducting hotspot loci in spatial/temporal gaps or landward displacement of igneous foci from then sparsely available potassium-argon isotopic dates (Pilger, 1981, 1984). The more recently acquired abundant dating, much of it argon-argon and uranium-lead, by multiple workers from the Andes and adjacent areas (compiled as part of the current study and provided in Supplementary Data; to be accessible via GEOROC, <http://georoc.mpch-mainz.gwdg.de/georoc/>) provides additional testing of the hypothesis. Display of four-dimensional data in comparison with reconstructed loci is a challenge, however, and would require a large number of two-dimensional maps and graphs and/or projection into three dimensions via digital goggles and sophisticated visualization software. In order to produce a small set of two-dimensional and pseudo-three-dimensional portrayals, the intersections of loci with the trench and sub-parallel landward segmented lines have been calculated for display in age versus distance from the trench graphs in addition to the maps provided in the Supplementary Data (the data sets are also available in spreadsheet and kml formats within Supplementary Data files).

(In the Supplementary Data, Google Earth views of the JF and EN hotspot trace loci and isotopic dates of igneous rocks in the Andes in 10 m. y. increments from 80 Ma to the Present are displayed together with the preferred model loci. It is apparent in such views that it is difficult to recognize the correlation of the JF trace with magmatic patterns except for the most recent period, 0-10 Ma. To a greater extent the apparent absence of significant magmatism for the same period from central to northern Peru, corresponds with the reconstructed EN loci.)

Plots of magmatic isotopic age versus distance along the Andes are more enlightening. Figure 6a illustrates the Peru-Ecuador-Colombia part of the Nazca-South American boundary in a set of charts with the trench, dates, and loci rotated 24.5° around a pole at 15.8° S latitude and -74.8° W longitude (the rotation parameters are chosen to approximately orient the Andean crest and the average trench north-south). Each chart incorporates rotated dates and loci points (calculated at 1 m. y.) in intervals of 1° east-west distance (~111 km) from the trench along parallels (rotated coordinates). The distribution of the isotopic dates from Peru and Ecuador younger than 15 Ma closely corresponds, as expected, with the projected locus points of the Easter-Nazca trace, producing a time-transgressive cessation from north to south, parallel with the locus intersections, lagging the loci (Figure 6a A-D), and strengthening the tentative correlation previously observed with the much sparser data set (Pilger, 1984). Resumption of magmatism is apparent along the northern part of the segment. Loci from the Juan Fernandez hotspot also reach into this segment and largely correspond with gaps in dates between 40 and 30 Ma. (There are obvious limitations with the rotated dates in the southern part of the segment in that the trend of the Andes undergoes a change from NNW to nearly NS.) Even with the increase in number of isotopic dates from the mid-1980s, there is still a paucity from northern Peru, although it is possible that a significant igneous history is hidden by late Cenozoic sedimentation in the upper Amazon basin, which appears to have formed in response to the onset of low-angle subduction (Cross and Pilger, 1978b).

Figure 6b shows a similar (unrotated) plot for the isotopic dates between 0 to 80 Ma, south of 15.8° S latitude, in 1° intervals, similarly bounded by the project loci points as in Figure 6a; a more subtle correlation appears to be present. The cessation of volcanism above the contemporary central Chilean-northern Argentinian low-angle subduction segment is inferred to have begun at approximately 13 Ma along the Andean crest, based on the isotopic dates; the locus of the projected Juan Fernandez trace stabilized in the segment at approximately the same time, as Pilger (1981, 1984) showed. Figure 7 illustrates projection of dates to the trench, utilizing the modeled convergence rates; in addition, the calculated intersections of the JF and EN traces with the trench are included.

399 What was not obvious in previous work, due to sparsity of data, was an apparent correspondence of date
400 distributions with the JF loci prior to 13 Ma. The significantly larger number of isotopic dates from Chile,
401 Argentina, Bolivia, and southernmost Peru allow for closer examination. For dates within 300 km of the
402 trench, the absence of such dates for the last 10 m. y. in the region where the JF locus intersects the trench
403 and the parallel line segments 150 and 300 km east of the trench is quite apparent, as noted above – the
404 contemporary zone of low-angle subduction (Barazangi and Isacks, 1979). Earlier, between 25 and 13 Ma
405 there is an onset of increasing density of dates paralleling the JF locus extending from north to south from
406 the contemporary low-angle segment in each chart. For dates greater than 300 km from the trench, there is
407 an even greater correspondence with the loci; that is, a greater density of dates far from the trench is
408 observed paralleling and the locus intersections from 3 to 7° (approximately 333 to 777 km). There are a
409 number of earlier dates apparent prior to the predicted location of the JF ridge. What is the significance of
410 the correlation? It is inferred that the JF trace produced a tentative increase in magmatism *after* it had
411 progressively moved from north to south; in other words, a short-lived period of low-angle subduction
412 interrupted normal subduction and was quickly followed by resumption of magmatism after passage of the
413 trace; the low-angle subduction expanded the zone of magmatism to the east which then persisted after
414 passage of the ridge beneath. Note that the oldest parts of the loci in each diagram (Figure 6b-A) records
415 the “hammerhead” in map view above (Figure 5); note also that the distribution of oldest igneous dates in
416 Figure 6b B-E, and F, also produce a similar shape, but older than the trace points.
417 That the loci intersections overlap with somewhat older dates in the same area with other factors may be
418 involved; the other possible mechanisms include: (1) the age progression along the Hawaiian trace may be
419 older than the combined GGW22 and W08 model, which would increase the age of the intersection of the
420 consequently longer and more easterly trending JF locus; (2) the JF hotspot may be located farther east; (3)
421 reconstructions between the Pacific and Nazca/Farallon plate since about 25 Ma are in error, due to
422 sparsity of isochron identifications (the high resolution identifications across the other plate-pair boundaries
423 are unlikely to be significantly erroneous); (4) the north-south zone of influence of the subducting trace may
424 have been significantly wider, affecting magmatism to the south of the southward-migrating intersection
425 (note the width of the magmatic zone from 0 to 5 Ma, Figure 8).
426 That Juan Fernandez ridge subduction has been responsible for rotation of the region south of 15°S, i.e.,
427 oroclinal bending (Isacks, 1988), has been proposed by a number of workers (e.g., Martinod, 2010,
428 Arriagada et al., 2013). The magnitude and timing of this deformation, ~20-25 Ma, is supported in part by
429 paleomagnetic evidence (e.g., Dupont-Nivet et al., 1996, Arriagada et al. 2013, Puigdomenech et al., 2021)
430 and corresponds with the calculated intersection of the JF trace with the trench (Pilger, 1981, 1984, this
431 paper).
432 O’Driscoll et al. (2015) suggest that a Farallon plate complement to the western Pacific Manihiki Plateau
433 (MP) may have been responsible for the orocline; however, their reconstructions are inconsistent with those
434 present here; herein the modeled JF trace first intersected the trench off Peru about ~65 Ma, continuing to
435 ~45 Ma before migrating south off Chile; the position O’Driscoll et al. illustrate for the MP relative to SA at
436 50 Ma would imply its subduction after JF subduction began. However, the present MP is west of the oldest
437 part of the synthetic JF trace extended to the Pacific plate, implying subduction of an MP complement on
438 the Farallon plate (to the east of JF) before JF trace subduction began beneath Peru.
439

440 8. Mafic Magmatic Evidence

441 With the exception of data 13 Ma and younger, the evidence for JF interaction in the magmatic evidence
442 shown above might be questioned by some: in a progressive north-to-south increased intensity in magmatic
443 activity represented by the increased density of isotopic dates, in parallel with the trace intersections? In an

444 effort to examine evidence for possible back-arc extension, independent of testing for the proposed JF
 445 “effect,” isotopically dated samples of identified mafic rocks were filtered from the larger Andean igneous
 446 data set. These included basalt, basaltic andesite, diabase, and gabbro as well as more generally defined
 447 mafic and basic rock types. Identifications appear to extend from field examination to thin section analysis in
 448 the original publications. (Modal analyses based on geochemistry of dated samples are not as common,
 449 and, therefore, are not incorporated.)

450 Figure 9 illustrates the mafic samples, binned into segments of 1° of arc from the trench (measured along
 451 parallels). Adjacent segments are shown in Figure 10A-E along with modeled JF and EN hotspot traces,
 452 using the reconstruction model (and rotation of northern samples) as described above.

453 Note that the modeled traces serve as incomplete envelopes bracketing magmatic episodes older and
 454 younger than the traces at each latitudinal point. On the older side, the JF trace bounds mafic samples
 455 which progress from west to east and north (~12° S) to south (35° S), terminating from ~80 Ma to the
 456 present. In some cases, the mafic magmatic episodes appear to expire several million years prior to the
 457 calculated intersection of the trace. On the younger side, the JF trace bounds the onset of mafic
 458 magmatism, particularly farther east from the trench, from 50 Ma at 15° S to the Present at 28° S. This
 459 pattern appears to be more obvious than within the total data set from 0-80 Ma (Figure 6), although the
 460 interpreted larger data distribution relative to the modeled traces is consistent with the more obvious pattern
 461 in the mafic dates. The mafic data from the northern Andes is consistent with the location of the EN trace
 462 intersections recognized in the larger data set, without obvious trends in inception and cessation of mafic
 463 magmatism.

464 The mafic dates are more clearly consistent with JF interaction as modeled by the reconstructions,
 465 strengthening the inference as applied to the larger data set. The full as well as the smaller mafic data sets
 466 are also consistent with interaction of the EN trace with the Andean subduction zone. Further, simple
 467 comparison of loci calculated in the other hotspot reference frames indicates a “best fit” of the extended,
 468 older GGW22 model.

469

470 9. Alternatives

471 A number of workers have proposed alternative mechanisms for the production of low-angle subduction,
 472 especially the two segments of the Andes in which flat slabs are observed, including Espurt et al. (2008),
 473 DeCelles et al. (2009), Skinner and Clayton (2013), Schepers et al. (2017), and Schellart (2020). In each
 474 case, some aspects of convergence rate, age of subducted plate, crustal thickening within the upper plate,
 475 duration of subduction episode, and/or surface erosion are invoked to explain the “anomalous” subduction
 476 with or without or minimizing the hotspot trace convergence effect. In some cases the workers have
 477 considered the contemporary structures and phenomena without considering the geohistorical evolution of
 478 the region; testing of plate reconstructions of the plates and hotspot traces over time is not incorporated into
 479 some of the models, nor evidence for the evolution of the volcanic gaps through time. Subduction of very
 480 young lithosphere may well occur at a low angle for the same reason as hotspot traces: young hot, thin
 481 plate, thinned lithosphere due to intraplate magmatism, is of lower net density than older and, therefore,
 482 colder plate.

483 Other factors may also be important in the back-arc region, depending on the motion of the upper plate
 484 relative to the subducting slab, and, perhaps, independent of whether normal or anomalous plate is being
 485 consumed (e.g., Cross and Pilger, 1982; Jarrard, 1986). Skinner and Clayton (2013) pointed to seeming
 486 exceptions – subducting aseismic ridges with no obvious effect on subduction configuration, including a
 487 small shallow aseismic ridge offshore of northern Chile, which Cande and Haxby (1991) originally proposed
 488 represented a propagating fracture zone by matching it with a corresponding feature on the Pacific plate. In

489 addition to apparent fracture offsets, the anomalous depth might indicate the ridge could have formed from
 490 a hotspot under the spreading center which localized the fractures; a candidate for the ridges' hotspot is the
 491 same melting center assumed to have produced the Foundation seamount chain on young Pacific plate
 492 (Contreras-Reyes, 2021). Utilizing Gaastra et al.'s (2022) parameters with the same age modifications as
 493 described above, the resulting loci come close to the two corresponding ridges (Figure 11); when one
 494 compares the age of the hypothetical hotspot trace with the age of adjacent lithosphere from magnetic
 495 isochron studies (i.e., the latest GSFMC compilation: Seton et al., 2014, included links) it is apparent that
 496 only a short section of the locus could have formed on the Farallon plate, that corresponds with the
 497 observed, offshore Chile ridge; the rest of the loci segments are older than the plate above which they are
 498 constructed and, therefore, could not have formed on the Farallon plate or at the spreading center; rather
 499 the hotspot would have been under the Pacific plate. If the locus is approximately correct, the short ridge
 500 segment on the Nazca plate has only limited extent and has not yet encountered the trench. Is it possible
 501 that older portions of the inferred Foundation trace were subducted? It seems unlikely, as the older part of
 502 the trace is still probably older than the corresponding subducted plate, at least within a few hundred
 503 kilometers inland of the trench.

504
 505 The inferred inadequacy of a buoyancy effect in some calculated models may point to the need to consider
 506 auxiliary phenomena if the modeling cannot reproduce low-angle subduction. The observation of low-
 507 velocity mantle deeper beneath the subducting slab under southern Peru (Bishop et al., 2017) – the
 508 recognized continuation of the Nazca ridge – is particularly striking. That is, the buoyancy effect of the
 509 thickened crust may be augmented by low-density mantle beneath the subducting plate. Paleomagnetic
 510 evidence from southern Peru indicates late Cenozoic deformation of the Andes (Rousse et al., 2017). This
 511 corresponds with the progressive southern migration of the Nazca ridge along the Andes, and, by inference,
 512 the subducting ridge and its underlying anomaly. Other aspects of apparent Nazca ridge migration, on the
 513 trench side, and the foreland side of the Peruvian arc are also worthy of further investigation. Might such
 514 anomalies exist under intraplate hotspot traces? If so, and especially beneath younger traces, this might
 515 explain the negligible effect of subduction of old traces in the western Pacific have (Cross and Pilger, 1982;
 516 Jarrard, 1986; Skinner and Clayton, 2013); such anomalies, if of thermal origin, could have decayed over
 517 time.

518
 519 3
 520 One remaining issue is the persistence of low-angle subduction beneath northern Peru after inferred
 521 passage of the Easter-Nazca trace beneath, as the contemporary position of the trace is predicted to
 522 continue well to the east. Note that all trace reconstructions do not incorporate conformance of the traces
 523 onto the inferred subduction zone. Were such calculations added, the position of the trace would be farther
 524 to the west, but it is not clear if the apparent anomaly would be fully resolved by such a "correction." One
 525 more possible factor may be relevant: younger plate is undergoing subduction beneath northern Peru than
 526 plate beneath central and southern Peru. As noted above and is apparent beneath southern Chile, younger
 527 plate subducts at lower angles than older plate (Figure 12; see also Cande and Leslie, 1986, for discussion
 528 of the offshore southern Chile example).

529 10. Convergence Rates and Directions

530 The reconstructions derived in this study also provide estimates of variations in convergence rate and
 531 direction across the Nazca/Farallon - South American plate boundary. Significant revisions to the
 532 geomagnetic timescale result in differing convergence rate calculations from those in the 1980s (e.g., Pilger,
 533 1981, 1983; Cande, 1985; Pardo-Casas and Molnar, 1987) on top of the higher resolution of newer plate-

534 pair reconstructions. Cande and Kent's (1995) timescale has been the standard for most subsequent plate
535 kinematic analyses, e.g. Muller et al. (2019) and previous University of Sydney syntheses; the latest
536 timescale of Ogg (2020), utilized in this study, produces results not that much different from Cande and
537 Kent, even as it is aligned with the orbital-tuning refinements incorporated into the latest geological time
538 scale (Harland et al. 2020).

539
540 Figure 13A illustrates the calculated instantaneous convergence rate variations over the last 80 m. y., as
541 derived from the global plate reconstructions via spline interpolation of pseudo-vectors and their gradients
542 (Pilger, 1983, 2003) at several locations along the South American-Nazca plate boundary. At a resolution of
543 1 m. y. variations in apparent rates are significant, but perhaps misleading. The variations could represent
544 uncertainties in isochron picks, the spline interpolation, and/or the geomagnetic timescale which are
545 magnified by calculation of the gradient.

546
547 By undertaking a moving average (Figure 13B) four distinct relative peaks in convergence rates are
548 recognizable. The first, just before the end of the Cretaceous, between 78 and 68 Ma, is followed by a deep
549 minimum between 65 and 55 Ma. Three more peaks, each greater than the previous, follow, between 54
550 and 49, 45 and 40, and 22 and 15 Ma. The drop-off since 18 Ma includes some apparent stationarity
551 between 14 and 9 Ma, with a smaller "shoulder" around 7 to 5 Ma. It is important to keep in mind that the
552 highest rates of motion in the circuit are between the Nazca/Farallon and South American plates, which has
553 the lowest resolution, especially in the past 15 m. y., and prior to 30 Ma.

554
555 A simple histogram of all of the compiled dates 80 Ma or younger, at 5 m. y. bins (Figure 14A), when
556 compared with the convergence rates, does not demonstrate any obvious visual correspondence. Perhaps
557 a finer comparison, focused on date frequency relative to distance from the trench and age would reveal a
558 better correlation (Figures 14B-G); however, there still is no obvious correspondence.

559
560 If there is a correlation between convergence rate and magmatism, it might be manifested in a certain
561 amount of lag time between the time of subduction and its manifestation in a change in magmatic volume
562 (for which the dates are a proxy). Simple correlation of the number of dates in one-million-year bins versus
563 convergence rate normal to the margin produces a value of 0.26. For simple convergence rate, the value is
564 0.07. Cross-correlation over 0-80 m. y., at a 1 m. y. is displayed in Figure 15. The absence of a sharp peak
565 implies the absence of a simple lag from subduction to magmatism. The broad peak, cresting between 13
566 and 22 m. y. could be interpreted as an integrated effect of waves of magmatism complexly correlated with
567 convergence rate over a broad lag in time. Of course, it is important to recognize that sampling of the
568 igneous activity in the Andes has not been focused on measuring changes in volumes of magmatism over
569 time; that is the histograms maybe only vaguely indicative of magmatic intensity.

570 11. Southern Andes and Spreading Center - Trench Interaction

571 The southern Andes differ from the central and northern parts of the range insofar as the latter have
572 apparently interacted with the Nazca/Farallon plate most of the Cenozoic, while the former has been
573 inferred to be affected by proximity to the Nazca-West Antarctic spreading center for at least the Late
574 Cenozoic (Cande and Leslie, 1986) and, consequently, slow subduction of the young, hot WA plate. The
575 updated global reconstructions as part of this study have been applied to identified WA-NF isochrons and
576 restored to both their apparent positions relative to SA at the time they formed but also projected forward in
577 time at 1 m. y. increments to provide apparent positions of younger, now subducted isochrons
578 reconstructed to the SA plate as well (Figure 16). The synthetic assumption for the younger reconstructed

579 isochrons is that spreading continued after subduction at the same rate and geometry as the rest of the still
 580 active part of the NF-WA spreading center. So the reconstructed isochrons approximate the hypothetical
 581 spreading center beneath SA at the age of the rotated isochron. This is not to imply that spreading actually
 582 did persist for millions of years after the first encounter of the ridge with the trench. However, the pattern of
 583 the reconstructed isochrons relative to the pattern of isotopic ages from the same nearest the trench are
 584 intriguing: Reconstructed isochrons along the trench and along segmented lines approximately parallel to
 585 the trench at 150 km spacings are plotted along with isotopic ages in age versus latitude charts (Figure 17).
 586 Note the similarity in patterns of reconstructed isochrons along the trench, 150 km east of the trench and
 587 isotopic ages between the two segmented lines (Figure 17). The near-trench patterns have two obvious
 588 implications: hotter subducting plate resulted in closer proximity of volcanism, very similar to the pattern
 589 observed in the North Pacific as parts of the Farallon-Pacific spreading center approached the California
 590 subduction zone beginning about 25 Ma (Pilger and Henyey, 1979). The corresponding patterns in the
 591 southern Andes, with this interpretation, provide additional support for the resilience of the global plate
 592 reconstructions for the past 45 m. y., while the hotspot trace patterns described above support the
 593 reconstructions since at least 60 Ma.

594 12. Other Hotspot Reference Frames

595 It is not enough to demonstrate an apparent correspondence of hotspots in one reference frame, in the
 596 Pacific, with subduction-related magmatic patterns. Other hotspot reference frames outside of the Pacific
 597 have also been proposed. Müller et al.'s classic (1993; "M93") hotspot-plate model for the plates of the
 598 Indian and Atlantic Oceans is one example and a globally averaged hotspot reference frame is another
 599 (Müller et al., 2019, "M19").

600 There are two rationales for using Müller et al. (1993) in addition to their own documentation. As first
 601 recognized by Oxburgh and Turcotte (1974), mid-to-late Cenozoic isotopic dates from East Africa imply a
 602 southward progression of volcanic inception; Pilger (2003), based on a larger data set, inferred two
 603 southward progressions of inception, from 60 Ma (southern progression – the one Oxburgh and Turcotte
 604 recognized) and from 40 Ma (northern progression). What is intriguing is that the progressions are both
 605 consistent with M93. That is, the asthenospheric magmatic sources responsible for the two groups of East
 606 African volcanism appear to be fixed relative to the other hotspots that comprise the foundation of M93.
 607 The second rationale is provided by Müller et al. (1999) who showed that reconstructions of the paleo-
 608 positions of the Caribbean island arc are also consistent with the M93 reference frame. Using Pindell and
 609 Kennen's (1991) reconstructions of the Caribbean plate relative to North America, restoration via the circuit
 610 Caribbean > North American > African > Hotspot, the restored arc positions overlie one another. That is, the
 611 Caribbean subduction zone apparently maintained a stable position in the same reference frame as the
 612 hotspots beneath the Indian and Atlantic Oceans, as defined by M93. In contrast, the moving hotspot
 613 reference frame, M19, and its earlier progenitors (e.g., O'Neill et al., 2005, and Torsvik et al., 2010,
 614 Doubrovine, 2012) do not both fit the East African volcanic date pattern and restore the Caribbean arc as
 615 well as M93.

616 Assuming the three hotspots of the Nazca plate are fixed to each of those reference frames, connected
 617 through the global relative reconstruction circuit used above, reconstructed JF loci along with the GGW22
 618 locus are shown in Figure 18. One recognizes overall similarities in the calculated loci to those constructed
 619 from GGW22, with the 25 Ma bend present in all three, along with the "hammerhead." The extension of M93
 620 to the Nazca plate shows the 25 Ma bend farther east and extended M19 farther west from the extended
 621 GGW22 model. The similarity in bends is not surprising, as the Pacific-Nazca spreading center, with its
 622 prominent 25 Ma motion change, at the time of fragmentation of the southern Farallon plate into the Cocos
 623 and Nazca plates, dominates contributions to the global reconstruction circuit (Pilger, 1983). The alternative

624 models are also displaced from the observed JF and GC traces; depending on the location of the Easter
 625 hotspot, each of the three loci could fit the Easter trace, with the extended M19 and M93 models having
 626 comparable orientations to the Nazca Ridge. Comparison of the alternative models with the Andean isotopic
 627 dates shows a significant offset of the predicted loci intersections from the igneous patterns, however, again
 628 realizing that the placement of the Easter hotspot is critical to the position of the loci intersections relative to
 629 the Peruvian trench. In sum, the extended GW22 model, with older ages for pre-25 Ma parameters,
 630 appears to fit all of the data sets (physiography, shallow seismicity clusters, igneous isotopic dates) better
 631 than those of WK08, M93, and M19, in the context of the same global reconstruction circuit (for the latter
 632 two models).

633 13. Conceptual Implications: Gap and Delamination?

634 If one tentatively accepts the possible correlation of the intersection of the Juan Fernandez hotspot trace
 635 with the Andean subduction zone and onset of increased magmatism shortly after, the question naturally
 636 arises: what is the mechanism for apparent increased melting of source material in relation to the trace?
 637 This scenario is envisioned: (1) Normal subduction of the Farallon plate is accompanied by modest
 638 magmatism along the Andean crest, as a result of the encounter of the top of the oceanic plate with the
 639 asthenosphere beneath the South American plate. (Primary melt sources are the subducting crust,
 640 sedimentary overburden – if any, asthenospheric wedge, and/or lower part of upper plate enhanced by
 641 dewatering of the crust and sediments.) (2) At a particular latitude along the trench the hotspot trace begins
 642 to be subducted; when the top of the thickened oceanic plate reaches ~100 km in depth, the lesser net
 643 density of the subducting plate begins moving horizontally, cutting off melting and therefore the supply of
 644 magma, resulting in gradual cessation of volcanism. (3) Eventually the oceanic crust of the hotspot trace
 645 experiences the phase change from basalt/gabbro to denser eclogite and begins to sink at a steeper angle,
 646 coming into contact with the asthenosphere at a larger distance from the trench, with minor magmatism
 647 resulting. (4) While subduction is nearly east-west, the orientation of the subducting trace results in
 648 migration of the intersection with the trench from north to south. Each intersection zone experiences a short
 649 period of low-angle subduction of the trace, followed by resumption of subduction of normal oceanic plate.
 650 (4) As the last part of the trace reaches a depth of ~100 km and moves horizontally, the normal oceanic
 651 plate detaches from the thicker part and begins to sink at a steeper angle. (5) The remaining part of the
 652 trace continues to move to the east, resulting in a gap emerging between the trace and the detached, now
 653 normally subducting plate. As a consequence, asthenospheric mantle begins to fill in the gap and a rapidly
 654 widening flare of magmatism begins behind the horizontally moving hotspot trace. The contemplated gap
 655 may be associated with inferred delamination of the South American plate (e.g., Kay et al., 1994, Risse et
 656 al., 2013) beginning beneath the Central Andes of Bolivia and northern Chile and Argentina (Kay et al.,
 657 2019) and extending to just north of the contemporary low-angle subduction segment beneath Chile and
 658 Argentina (Mulcahy et al., 2014).

659 The proposed gap between the subducting hotspot trace fragment and reinstated normally subducting
 660 oceanic plate is geometrically comparable to, if significantly smaller than, the conjectured window in the
 661 Southern Andes between the subducted of the Nazca- (West) Antarctic spreading center and the remnant
 662 of the subducting Nazca plate (Cande and Leslie, 1986; and, e.g., Navarette et al., 2020). Only minor
 663 subduction of the West Antarctic plate, if any, follows the cessation of spreading.

664 Thus, the subducting JF trace, while producing only a short hiatus in magmatism as it obliquely subducts, is
 665 followed by a flare of magmatism. The hiatus is almost unobservable in the total data set, but more
 666 apparent in the smaller mafic data set, because of the remnant of magmatic activity from the prior episode
 667 of normal subduction and the following flare. The apparent intensification of magmatism following the
 668 oblique trace subduction may represent decompression melting of quickly rising, hotter and/or more fertile

669 asthenosphere previously beneath the thickened subducting plate and under the accompanying
 670 delaminating upper plate,
 671 The zone of concentrated mafic dates at 27-28°S from ~13 Ma to the Present is approximately located
 672 above the inferred gap between moderate and low-angle subduction. Perhaps the gap is responsible for the
 673 enhanced mafic magmatism in this locale as well as the inferred delamination at an earlier time, farther
 674 north.

675 14. Hotspots and Reference Frames

676 While the primary focus of this investigation has been on the magmatic evolution of the Andes in relation to
 677 subduction of inferred hotspot traces, the implications of the recognition of additional evidence for the
 678 subduction effect for the nature of hotspots themselves is worthy of further consideration. The evidence for
 679 the trace effect on subduction in the context of the Pacific hotspot reference frame and distinct from an
 680 Atlantic-Indian Ocean reference frame prompts questions about the reference frames themselves. That the
 681 motions of the plates relative to hotspots of the two domains apparently incompatible with one another was
 682 recognized already in the 1980s by the work of Molnar and colleagues (e.g., Molnar and Atwater, 1973;
 683 Molnar and Francheteau, 1975). Resolution of the inconsistency between the Pacific and Atlantic/Indian
 684 Ocean domains would require detection of a yet unrecognized plate boundary between the central South
 685 Pacific and the Indian Ocean, most likely within the Antarctic plate. Cenozoic movement between East and
 686 West Antarctic within the Cenozoic has indeed been documented, but the detected displacement (Cande
 687 and Stock, 2000; Granot et al., 2013; Granot and Dyment, 2018).is inadequate relative to the discrepancy
 688 between the two hotspot frames. The idea of a “moving hotspot” reference frame (O’Neill et al., 2005)
 689 presents other difficulties, however. Each hotspot within the Atlantic and Indian Ocean domain is assumed
 690 to move semi-independently from one another, in effect displaced by a kind of mantle wind. Modeling of
 691 whole earth convection with embedded hotspots is the mechanism assigned to such movement; however,
 692 the scheme suffers from several defects. Most importantly, it is profoundly underdetermined; perturbations
 693 of convection are performed so as to fit each of a small number of hotspot traces, constrained by gross
 694 mantle structure (seismic velocity with inferred density and viscosity), plate boundaries and kinematics.
 695 Parameters describing hotspot motion, conventional pole latitude and longitude and rotation angle relative
 696 to either the global frame or one of the continental plates (usually Africa) are difficult to rationalize; they may
 697 describe an individual hotspot’s motion relative to a particular frame, but how are such parameters
 698 interpolated? That is, the approach does not provide a means of estimating the motion of other hotspots
 699 which are not part of the framework; the application of M19, above, to the JF trace, illustrates the problem.
 700 Does a global convection model fit the hotspots of the Pacific? Oddly, as Gaastra et al. (2022) show, a
 701 single hotspot reference frame appears to provide a satisfactory reference frame for the hotspots of the
 702 Pacific plate; extrapolated to the Nazca plate, it also appears to fit the Andean “images” of subducted
 703 hotspot traces, with slight adjustments to the age progression. Koivisto et al. (2015) further argue that a
 704 single reference frame fits the Pacific and Atlantic/Indian frames since Hawaiian-Emperor bend time;
 705 however the discrepancy between the modified Gaastra et al. (2022) and M19 (Figure 18) seem too great to
 706 accept that inference.
 707 What are the implications of the observation that (1) a single reference frame beneath the Pacific Ocean
 708 appears to have existed for at least 80 m. y. and (2) an inferred hotspot reference frame beneath the Indian
 709 and Atlantic Oceans fits volcanic patterns in northeast Africa for 60 m. y. and “anchors” a Caribbean island
 710 arc for 70 Ma? Further, (3) the motion of the Pacific plate in the Hawaiian hotspot frame also fits the
 711 orientation of lineations in the observed gravity field (Haxby and Weissel, 1986), structures that have a
 712 shallow origin? Collectively, the evidence implies that the hotspot reference frames are shallow – not

713 manifestations of the locations of deep mantle plumes, even if the plumes do originate at depth (see also
714 Pilger, 2003, 2007).

715 15. Conclusion

716 This short contribution is built upon an enormous amount of data produced by many workers: field
717 observation, petrographic, geochemical and isotopic laboratory analysis, shipboard magnetic and
718 bathymetric profiling, aeromagnetic surveying, satellite navigation and geoid observation with gravity
719 extraction and bathymetric estimation, magnetic isochron modeling and identification, fracture zone
720 characterization, marine dredging and drilling, plate pair reconstruction, data compilation... Much finer
721 analysis of the isotopic date distribution and the plate reconstructions could be undertaken, especially
722 incorporating more detailed petrology and geochemistry. The relationship to the deformation and uplift
723 history of the Andes since 80 Ma is not explored in this study, other than the observation that late Cenozoic
724 faulting in the Pampean Ranges of northern Argentina occurs within the low-angle subduction segment in
725 which the reconstructions imply subduction of the Juan Fernandez trace for over 10 m. y., thus a genetic
726 relationship (originally recognized by Pilger, 1981). Further, the reconstructions that indicate apparent
727 subduction of the older parts of the JF trace between 60 and 45 Ma beneath northernmost Chile and
728 Argentina, southernmost Peru, and Bolivia may indicate contribution of the trace to the intense deformation
729 that produced the so-called Andean orocline (Isacks, 1987) and its associated structures.

730
731 It is apparent that the two reconstructed hotspot traces compared with seismicity, bathymetry, and igneous
732 isotopic ages, imply controlling influences on the angle of dip of the Andean subduction zone and
733 consequent location of volcanic loci by the traces. The Easter-Nazca trace-igneous date correspondence is
734 clearer than the Juan Fernandez trace, perhaps indicative of the significantly larger dimensions of the
735 Nazca Ridge than the Juan Fernandez trace, with a larger, more persistent low-angle subduction effect.
736 Pilger (1981) had suggested that the “mirror-image” of the Nazca Ridge on the Pacific plate might have
737 contributed further to the extent of the low-angle subduction segment, a suggestion other workers have
738 subsequently made (it is difficult to point to any other independent evidence in support of this auxiliary
739 proposal).

740
741 The reconstructions and corresponding patterns of magmatism in the Andes provide indirect support of the
742 hypothesis that the hotspots of the Pacific Ocean form a stable self-consistent reference frame extending
743 beyond the limits of the Pacific plate. That is, the combined and modified model of Gaastra et al. (2022) and
744 Wessel and Kroenke (2008) extended to the Nazca and South American plates not only fits the observed
745 parts of the Easter-Nazca and Juan Fernandez island-seamount-ridges, but also the distribution of
746 magmatic activity in the central and northern Andes for the past 65-70 m. y.

747
748 It is difficult to recognize obvious relations of convergence rate and magmatism in the Andes from the
749 reconstructions and age distribution of igneous isotopic dates. Similarly, the relation of motion of South
750 America to the hotspots beneath the Atlantic and Indian Oceans and any possible control on Andean
751 magmatism has been proposed by numerous authors. The most recent models for these hotspots imply
752 motion relative to one another as well as those of the Pacific set (e.g., Müller et al., 2019, and references
753 therein). Consequently, it is uncertain how to extend the model to the South American plate for testing
754 beyond the simple examples presented above.

755
756 Subduction of very young plate and the actual spreading center appears to be manifest in the igneous
757 history of the southern Andes as Cande and Leslie (1986) first recognized. Patterns of igneous activity

758 appear to correspond closely with reconstructed isochrons. This correspondence provides additional
 759 confidence in the robustness of the global plate reconstructions for at least the last 40-50 Ma, on top of the
 760 correspondences of the hotspot trace “images” mentioned above.

761

762 That the Juan Fernandez and Hawaiian hotspot traces, along with the other traces of the Pacific and Nazca
 763 plates can be characterized by an internally consistent reference frame is an additional striking result of this
 764 study. While the propagation of uncertainties in the reconstructions is not possible using contemporary
 765 formulations and existing isochron identifications and their derivative reconstruction parameters, the visual
 766 correspondences with Andean igneous dates should motivate higher resolution magnetic and bathymetric
 767 surveys of the older parts of the SA-AF and AF-EA systems and especially the PA-NF and WA-NF systems
 768 for the full time period since Chron 34. The PA-NF pair, with the highest average spreading rates in the full
 769 circuit, is an especially desirable target for near-future surveys; one might expect to find evidence of multiple
 770 small plates, like the present-day Easter plate (e.g., Handschumacher et al., 1981; Naar and Hey, 1991)
 771 which only high-resolution surveys could resolve. Could semi-autonomous, solar-powered drones, with
 772 satellite GPS, three-component magnetometers and laser ranging, and intermittent satellite connection for
 773 data uploads provide a relatively economical fleet for aeromagnetic surveys of the remote regions of the
 774 South Pacific and southwest Indian Oceans most lacking in data? The correspondences demonstrated in
 775 this work may motivate the additional proposed study, especially in relation to continued mineral exploration
 776 and development, geothermal prospecting for electrical energy generation, geological hazards related to
 777 contemporary volcanism, uplift, and hydrothermal activity, and enhanced geoclimatic history in and of
 778 Andes. Such improved understanding may provide useful analogs for studies of other subduction-related
 779 mountain belts.

780 Supplementary Data

781 Spreadsheets and keyhole markup language (*.kml, *.kmz) files include the dates, charts, reconstruction
 782 parameters, and map data sets are included in the Supplementary Data. The full compilation of isotopic
 783 dates from igneous rocks beyond what is used in this study is to be archived by GEOROC.

784

785 Acknowledgements

786 The research made use of the following software: Microsoft Office, Visual Studio C++, Google Earth,
 787 Google Sheets, Google Docs, and Numerical Recipes algorithms. The principal algorithms, in C, are
 788 available in Pilger (2003). Other calculations utilizing MS Excel are included in the supplementary data
 789 spreadsheets. The author thanks the reviewers for their suggestions and calling attention to related
 790 contributions whose alternate interpretations could be addressed.

791

792 References

793

794 Alvarez, O., Gimenez, M. E., Martinez, M. P., Lincklinger, F., and Braitenberg, C., 2014, *Geological Society of*
 795 *London Special Publications*, New insights into the Andean crustal structure between 32° and 34°S from GOCE
 796 satellite gravity data and EGM2008 model, Sepulveda, S. A., Giambiagi, L. B., Moreiras, S. M., Pinto, L., Tunik, M.,
 797 Hoke, G. D. and Farias, M., editors, *Geodynamic Processes in the Andes of Central Chile and Argentina*. 399,
 798 <http://dx.doi.org/10.1144/SP399.3>

- 799 Arriagada, César, Ferrando, Rodolfo, Córdova, Loreto, Morata, Diego, Roperch, Pierrick, 2013, *Andean Geology*, The
800 Maipo Orocline: A first scale structural feature in the Miocene to Recent geodynamic evolution in the central Chilean
801 Andes. *Andean Geology*, 40, 419-437, <http://dx.doi.org/10.5027/andgeoV40n3-a02>
802 Atwater, T, and Molnar, P., 1973, Relative motion of the Pacific and North American plates deduced from sea-floor
803 spreading in the Atlantic, Indian, and South Pacific Oceans. Proceedings Conference on Tectonic Problems of the
804 San Andreas Fault System, XIII, School of Earth Sciences, Stanford Univ. Publications, Stanford, CA, USA, 136-148.,
805 Barazangi, Muawia, and Isacks, Bryan L., 1976, *Geology*, Spatial distribution of earthquakes and subduction of the
806 Nazca plate beneath South America. *Geology*, 4, 686–692., [https://doi.org/10.1130/0091-](https://doi.org/10.1130/0091-7613(1976)4%3C686:SDOEAS%3E2.0.CO;2)
807 [7613\(1976\)4%3C686:SDOEAS%3E2.0.CO;2](https://doi.org/10.1130/0091-7613(1976)4%3C686:SDOEAS%3E2.0.CO;2)
808 Barazangi, Muawia, and Isacks, Bryan L., 1979, *Geophysical Journal International*, Subduction of the Nazca plate
809 beneath Peru: evidence from spatial distribution of earthquakes. *Geophysical Journal International*, 57, 537–555,
810 <https://doi.org/10.1111/j.1365-246X.1979.tb06778.x>.
811 Bello-González, Juan Pablo, Contreras-Reyes, Eduardo, Arriagada, César, 2018, *Gondwana Research*, Predicted
812 path for hotspot tracks off South America since Paleocene times: Tectonic implications of ridge-trench collision along
813 the Andean margin. *Gondwana Research*, 64, 216-234, DOI: 10.1016/j.gr.2018.07.008
814 Bernard, A., Munsch, M., Rotstein, Y, and Sauter, D., -2005, *Geophysical Journal International*, Refined spreading
815 history at the Southwest Indian Ridge for the last 96 Ma, with the aid of satellite gravity data. . *Geophysical Journal*
816 *International*, 162, 765-778, <https://doi.org/10.1111/j.1365-246X.2005.02672.x>
817 Bishop, Brandon T., Beck, Susan L., Zandt, George, Wagner, Lara, Long, Maureen D., Knezevic, Antonijevic, Sanja,
818 Kumar, Abhash, and Tavera, Hernando, 2017, *Geosphere*, Causes and consequences of flat-slab subduction in
819 southern Peru. *Geosphere*, 13, 1392-1407, <https://doi.org/10.1130/GES01440.1>.
820 Cande, Steven C., 1985, Nazca-South America plate interactions since 50 M. Y.B.P.. Ocean Margin Drilling Program,
821 Regional Atlas Series, Atlas 9, Hussong, D. M., Dang, S. P., Kulm, L. D., Couch, R. W., and Hilde, T. W. C., Editors.,
822 Peru-Chile Trench Off Peru
823 Cande, Steven C., and Leslie, Rob B., 1986, *Journal of Geophysical Research: Solid Earth*, Late Cenozoic tectonics
824 of the Southern Chile Trench. *Journal of Geophysical Research: Solid Earth*, 91, 471-496,
825 <https://doi.org/10.1029/JB091iB01p00471> .
826 Cande, S. C., and Kent, D. V., 1995, *Journal of Geophysical Research: Solid Earth*, Revised calibration of the
827 geomagnetic polarity timescale for the Late Cretaceous and Cenozoic. *Journal of Geophysical Research: Solid Earth*,
828 100, 6093-6095, <https://doi.org/10.1029/94JB03098>
829 Cande, S. C., Raymond, C. A., Stock, J., and Haxby, W. F., 1995, *Science*, Geophysics of the Pitman fracture zone
830 and Pacific-Antarctic plate motions during the Cenozoic. *Science*, 270, 947-953,
831 <https://doi.org/10.1126/science.270.5238.947>
832 Cande, S. C., Stock, J. M., Müller, R. D., and Ishihara, T., 2000, *Nature*, Cenozoic motion between East and West
833 Antarctica. *Nature*, 404, 145-150., <https://doi.org/10.1038/35004501>
834 Cande, Steven C., and Stock, Joann M., 2004, *Geophysical Journal International*, Pacific–Antarctic–Australia motion
835 and the formation of the Macquarie Plate. *Geophysical Journal International*, 157, 399–414,
836 <https://doi.org/10.1111/j.1365-246X.2004.02224.x>
837 Cande, S. C., Patriat, P., and Dymant, J., 2010, *Geophysical Journal International*, Motion between the Indian,
838 Antarctic and African plates in the early Cenozoic. *Geophysical Journal International*, 183, 127-149.,
839 <https://doi.org/10.1111/j.1365-246X.2010.04737.x>
840 Cande, Steven C., and Patriat, Philippe, 2015, *Geophysical Journal International*, The anticorrelated velocities of
841 Africa and India in the Late Cretaceous and early Cenozoic. *Geophysical Journal International*, 200, 227–243.,
842 <https://doi.org/10.1093/gji/ggu392>
843 Clague, David A., and Jarrard, Richard D., 1973, *Geological Society of America Bulletin*, Tertiary Pacific Plate Motion
844 Deduced from the Hawaiian-Emperor Chain. *Geological Society of America Bulletin*, 84, 1135–1154,
845 [https://doi.org/10.1130/0016-7606\(1973\)84<1135:TPPMDF>2.0.CO;2](https://doi.org/10.1130/0016-7606(1973)84<1135:TPPMDF>2.0.CO;2)
846 Clennett, E. J., Sigloch, K., Mihalynuk, M. G., Seton, M., Henderson, M. A., Hosseini, K., et al., 2020, *Geochemistry*
847 *Geophysics Geosystems*, A quantitative tomotectonic plate reconstruction of western North America and the eastern
848 Pacific basin. *Geochemistry. Geochemistry Geophysics Geosystems*, 20, e2020GC009117,
849 <https://doi.org/10.1029/2020GC009117>
850 Coira, B., Kay, S.M., and Viramonte, J., 1993, *International Geology Review*, Upper Cenozoic magmatic evolution of
851 the Argentine Puna—A model for changing subduction geometry. *International Geology Review*, 35, 677–720.,
852 <https://doi.org/10.1080/00206819309465552>
853 Contreras-Reyes, Eduardo, Obando-Orrego, Sebastián, Geersen, Jacob, Bello-González, Juan Pablo,
854 2021, Density structure, flexure, and tectonics of the Iquique Ridge, northern Chile, *Journal of South*
855 *American Earth Sciences*, 111, 103423, <https://doi.org/10.1016/j.jsames.2021.103423>, .

- 856 Croon, M. B., Cande, S. C., and Stock, J. M., 2008, *Geochemistry Geophysics Geosystems*, Revised Pacific-Antarctic
857 plate motions and geophysics of the Menard Fracture Zone. *Geochemistry Geophysics Geosystems*, 9, 7,
858 <https://doi.org/10.1029/2008GC002019>
- 859 Cross, T. A., and Pilger, R. H., Jr., 1978a, *American Journal of Science*, Constraints on absolute motion and plate
860 interactions inferred from Cenozoic igneous activity in the western United States. *American Journal of Science*, 278,
861 865-902., <https://doi.org/10.2475/ajs.278.7.865>
- 862 Cross, T. A., and Pilger, R. H., Jr., 1978b, *Nature*, Tectonic controls of Late Cretaceous sedimentation, western
863 interior, U.S.A.. *Nature*, 274, 653-657., <https://doi.org/10.1038/274653a0>
- 864 Cross, Timothy, and Pilger, Rex, 1982, *Geological Society of America Bulletin*, Controls of subduction geometry,
865 location of magmatic arcs, and tectonics of arc and back-arc regions. *Geological Society of America Bulletin*, 93, 545-
866 562, [https://doi.org/10.1130/0016-7606\(1982\)93%3C545:COSGLO%3E2.0.CO;2](https://doi.org/10.1130/0016-7606(1982)93%3C545:COSGLO%3E2.0.CO;2)
- 867 Dalrymple, G.B., and Clague, D.A., 1976, *Earth and Planetary Science Letters*, Age of the Hawaiian Emperor bend.
868 *Earth and Planetary Science Letters*, v. 31, 313-329, [https://doi.org/10.1016/0012-821X\(76\)90113-8](https://doi.org/10.1016/0012-821X(76)90113-8)
- 869 DeMets, C., Gordon, R.G., Argus, D.F., and Stein, S., 1990, *Geophysical Journal International*, Current plate
870 motions. *Geophysical Journal International*, 101, 425-78., <https://doi.org/10.1111/j.1365-246X.1990.tb06579.x>
- 871 DeMets, C., Gordon, R.G., Argus, D.F., and Stein, S., 1994, *Geophysical Research Letters*, Effect of recent revisions
872 to the geomagnetic reversal time scale on estimates of current plate motions. *Geophysical Research Letters*, v. 21,
873 2191-2194, <https://doi.org/10.1029/94GL02118>
- 874 DeMets, C., Gordon, R.G., and Argus, D.F., 2010, *Geophysical Journal International*, Geologically current plate
875 motions. *Geophysical Journal International*, 181, 1-80, <https://doi.org/10.1111/j.1365-246X.2009.04491.x>
- 876 DeMets, C., Merkuriev, S., and Sauter, D., 2015, *Geophysical Journal International*, High-resolution estimates of
877 Southwest Indian Ridge plate motions, 20 Ma to present. *Geophysical Journal International*, 203, 1495-1527,
878 <https://doi.org/10.1093/gji/ggv366>
- 879 DeMets, C., and Merkuriev, S., 2019, *Geophysical Journal International*, High-resolution reconstructions of
880 Nubia, North America, and Antarctic plate motions relative to South America: 34 Ma to present. *Geophysical Journal*
881 *International*. *Geophysical Journal International*, 217(3), 1821-1853. <https://doi.org/10.1093/gji/ggz087>
- 882 Doubrovine, P. V., Steinberger, B., and Torsvik, T. H., 2012, *Journal of Geophysical Research*, Absolute plate motions
883 in a reference frame defined by moving hot spots in the Pacific, Atlantic, and Indian oceans. *Journal of Geophysical*
884 *Research*, 117, B09101, <https://doi.org/10.1029/2011JB009072>
- 885 Dupont-Nivet, G., Roperch, P., Gautier, P., Chauvin, A., Gerard, M., and Carlier, G., 1996, Clockwise rotations in
886 northern Chile: oroclinal bending and in situ tectonic rotations. Third ISA, St. Malo, 355-358., France
- 887 Eagles, Graeme, Gohl, Karsten, and Larter, Robert D., 2008, *Tectonophysics*, Animated tectonic reconstruction of the
888 Southern Pacific and alkaline volcanism at its convergent margins since Eocene times. *Tectonophysics*, 464, 21-29,
889 <https://doi.org/10.1016/j.tecto.2007.10.005>
- 890 Eagles, Graeme, and Jokat, Wilfried, 2014, *Tectonophysics*, Tectonic reconstructions for paleobathymetry in Drake
891 Passage. *Tectonophysics*, 611, 28-50, <https://doi.org/10.1016/j.tecto.2013.11.021>
- 892 Eagles, Graeme, and Vaughan, Alan P. M., 2009, *Geophysical Research Letters*, Gondwana breakup and plate
893 kinematics: Business as usual. *Geophysical Research Letters*, 36, L10302, <https://doi.org/10.1029/2009GL037552>
- 894 Engebretson, D.C., Cox, A., and Gordon, R.G., 1985, *Geological Society of America Special Papers*, Relative motions
895 between oceanic and continental plates in the Pacific basin. *Geological Society of America Special Papers*, 206, 1-
896 60, [http://dx.doi.org/10.1130/SPE206-p1.Espurt\[RP1\]](http://dx.doi.org/10.1130/SPE206-p1.Espurt[RP1])
- 897 Francheteau, Jean, 1970, *Paleomagnetism and Plate Tectonics*. PhD dissertation, University of California, San
898 Diego.,
- 899 Funiello, F., Faccenna, C., and Giardini, D., 2004, *Geophysical Journal International*, D. Role of lateral mantle flow in
900 the evolution of subduction systems: insights from laboratory experiments. *Geophysical Journal International*, 157,
901 1393-1406, <https://doi.org/10.1111/j.1365-246X.2004.02313.x>
- 902 Francesca Funiello, Claudio Faccenna, Domenico Giardini, Klaus Regenauer-Lieb, 2003, *Journal of Geophysical*
903 *Research*, Dynamics of retreating slabs: 2. Insights from three-dimensional laboratory experiments. *Journal of*
904 *Geophysical Research*, 108, 2207-2216, <https://doi.org/10.1029/2001JB000896>
- 905 Gaastra, Kevin Mitchell, Gordon, Richard G., and Woodworth, Daniel, 2022, *Tectonics*, Quantification of Pacific Plate
906 Hotspot Tracks Since 80 Ma and the Relative Timing of Eocene Plate Tectonic Events. *Tectonics*, (submitted),
907 <https://doi.org/10.1002/essoar.10506394.2>
- 908 Gaina, C., Müller, D. R., Royer, J.-Y., Stock, J., Hardebeck, J., and Symonds, P., 1998, *Journal of Geophysical*
909 *Research*, The tectonic history of the Tasman Sea: A puzzle with 13 pieces. *Journal of Geophysical Research*,
910 103(B6, 12413- 12433, <https://doi.org/10.1029/98JB00386>
- 911 Gradstein, F. M., and Ogg, J. G., 2020, *Geologic Time Scale*, The chronostratigraphic scale. *Geologic Time Scale*,
912 Gradstein, F. M., Ogg, J. G., Schmitz, M. D., Ogg, G. M., editors, Elsevier, Amsterdam, 1, 21-32.,
- 913 Granot, R., Cande, S. C., Stock, J. M., and Damaske, D., 2013, *Geophysical Research Letters*, Revised Eocene-
914 Oligocene kinematics for the West Antarctic rift system. *Geophysical Research Letters*, 40, 279-284,
915 <https://doi.org/10.1029/2012GL054181>

- 916 Hamilton, W., 1969, *Oregon Department of Mineral Industries Bulletin*, The volcanic Central Andes: A modern model
 917 for the Cretaceous batholiths and tectonics of western North America. Oregon Department of Mineral Industries
 918 Bulletin, 655, 175-1984.,
 919 Handschumacher, D.W., 1976, Post-Eocene plate tectonics of the Eastern Pacific. in *The Geophysics of the Pacific*
 920 *Ocean Basin and its Margins*, AGU Monograph 19, ed.G.H.Sutton, et al., American Geophysical Union, Washington,
 921 pp. 177-202.,
 922 Harada, Y., and Hamano, Y., 2000, Recent progress on plate motions relative to hot spots. in *The History and*
 923 *Dynamics of Global Plate Motions*, Geophysical Monograph Series, 121, edited by Richards, M. A., Gordon, R. G.,
 924 and van der Hilst, R. D., 327–338, AGU, Washington, D. C.,
 925 Haxby, W.F., and Weissel, J.K., 1986, *Journal of Geophysical Research*, Evidence for small-scale mantle convection
 926 from Seasat altimeter data. *Journal of Geophysical Research*, 91, <https://doi.org/10.1029/JB091iB03p03507>
 927 Hayes, G. P., Moore, G. L., Portner, D. E., Hearne, M., and Flamme, H., Furtney, M., and Smocsyk, G. M., 2018,
 928 *Science*, Slab2, a comprehensive subduction zone geometry model. *Science*, 362, 48-61.,
 929 <https://doi.org/10.1126/science.aat4723>
 930 Herron, E. M., 1972, *Geological Society of America Bulletin*, Sea-floor spreading and the Cenozoic history of the east-
 931 central Pacific. *Geological Society of America Bulletin*, 83, 1671-1692., [https://doi.org/10.1130/0016-](https://doi.org/10.1130/0016-7606(1972)83[1671:SSATCH]2.0.CO;2)
 932 [7606\(1972\)83\[1671:SSATCH\]2.0.CO;2](https://doi.org/10.1130/0016-7606(1972)83[1671:SSATCH]2.0.CO;2)
 933 Hu, Jiashun, Gurnis, Michael, Rudi, Johann, Stadler, Georg, and Muller, R. Dietmar, 2022, *Nature Geoscience*,
 934 Dynamics of the abrupt change in Pacific Plate motion around 50 million years ago. *Nature Geoscience*, 15, 74-78,
 935 <https://www.nature.com/articles/s41561-021-00862-6>
 936 Isacks, Bryan L., 1988, *Journal of Geophysical Research: Solid Earth*, Uplift of the Central Andean Plateau and
 937 Bending of the Bolivian Orocline. *Journal of Geophysical Research: Solid Earth*, 93, 3211-3231,
 938 <https://doi.org/10.1029/JB093iB04p03211>
 939 Jarrard, R. D., 1986, *Tectonophysics*, Causes of compression and extension behind trenches. *Tectonophysics*, 132,
 940 89 – 102, [https://doi.org/10.1016/0040-1951\(86\)90027-2](https://doi.org/10.1016/0040-1951(86)90027-2)
 941 Jarrard, R.D., and Clague, D.A., 1977, *Reviews of Geophysics and Space Physics*, Implications of Pacific Island and
 942 seamount ages for the origin of volcanic chains. *Reviews of Geophysics and Space Physics*, 15, 57-76.,
 943 <https://doi.org/10.1029/RG015i001p00057>
 944 Kay, S. M., Coira, B., and Viramonte, J., 1994, *Journal of Geophysical Research*, Young mafic back arc volcanic rocks
 945 as indicators of continental lithospheric delamination beneath the Argentine Puna Plateau, central Andes. *Journal of*
 946 *Geophysical Research*, 99(B12), 24323– 24339, <https://doi.org/10.1029/94JB00896>
 947 Kay, S. M., and Abbruzzi, J. M., 1996, *Tectonophysics*, Magmatic evidence for Neogene lithospheric evolution of the
 948 Central Andean flat-slab between 30 and 32°S. *Tectonophysics*, 259, 15-28, [https://doi.org/10.1016/0040-](https://doi.org/10.1016/0040-1951(96)00032-7)
 949 [1951\(96\)00032-7](https://doi.org/10.1016/0040-1951(96)00032-7)
 950 Kay, Suzanne M., Kato, Joseph J., Coira, Beatriz L., and Jimenez, N., 2018, Isotopic and Geochemical Signals of the
 951 Neogene Los Frailes Volcanic Complex as Recorders of Delamination and Lower Crustal Flow under the Southern
 952 Altiplano of the Central Andes. South American symposium on isotope geology, 11th SSAGI, Cochabamba, Bolivia,
 953 22-25 July.,
 954 Kirkwood, B. H., Royer, J. Y., Chang, T. C., and Gordon, R. G., -1999, *Geophysical Journal International*, Statistical
 955 tools for estimating and combining finite rotations and their uncertainties. *Geophysical Journal International*, 137(2),
 956 408– 428., <https://doi.org/10.1046/j.1365-246X.1999.00787.x>
 957 Koivista, E. A., Andrews, D. L., and Gordon, R.G., 2015, *Journal of Geophysical Research*, Tests of fixity of the Indo-
 958 Atlantic hot spots relative to Pacific hot spots. *J. Geophys. Res. . Journal of Geophysical Research*, 119, 661–675,
 959 <https://doi.org/10.1002/2013JB010413>
 960 König, Matthias, and Jokat, Wilfried, 2010, *Geophysical Journal International*, Advanced insights into magmatism and
 961 volcanism of the Mozambique Ridge and Mozambique Basin in the view of new potential field data. *Geophysical*
 962 *Journal International*, 180, 158 - 180, <https://doi.org/10.1111/j.1365-246X.2009.04433.x>
 963 Larter, Robert D., Cunningham, A. P., Barker, P. F., Gohl, K., and Nitsche, F. O., 2002, *Journal of Geophysical*
 964 *Research-Solid Earth*, Tectonic evolution of the Pacific margin of Antarctica 1. Late Cretaceous tectonic
 965 reconstructions. *Journal of Geophysical Research-Solid Earth*, 107, EPM 6-1-EPM 6-20,
 966 <https://doi.org/10.1029/2002JB001897>
 967 Le Pichon, X., Francheteau, J., and Bonnin, J., 1973, *Elsevier*, Plate Tectonics. Elsevier, Amsterdam, 300 p.,
 968 Livermore, Roy, Nankivell, Adrian, Eagles, Graeme, and Morris, Peter, 2005, *Earth and Planetary Science Letters*,
 969 Paleogene opening of Drake Passage. *Earth and Planetary Science Letters*, 236, 459 – 470,
 970 <https://doi.org/10.1016/j.epsl.2005.03.027>
 971 Lonsdale, P., 2005, *Tectonophysics*, Creation of the Cocos and Nazca plates by fission of the Farallon plate.
 972 *Tectonophysics*, 404, 237-264, <https://doi.org/10.1016/j.tecto.2005.05.011>
 973 Maia, Marcia, Dymant, Jérôme, and Jouannetaud, David, 2005, *Earth and Planetary Science Letters*, Constraints on
 974 age and construction process of the Foundation chain submarine volcanoes from magnetic modeling. *Earth and*
 975 *Planetary Science Letters*, 235, 183-199, <https://doi.org/10.1016/j.epsl.2005.02.044>.

- 976 Marks, K., and Stock, J., 2001, *Marine Geophysical Researches*, Evolution of the Malvinas Plate South of Africa.
 977 *Marine Geophysical Researches*, 22, 289–302, <https://doi.org/10.1023/A:1014638325616>
- 978 Matthews, K. J., Williams, S. E., Whittaker, J. M., Müller, R. D., Seton, M., and Clarke, G. L., 2015, *Earth-Science*
 979 *Reviews*, Geologic and kinematic constraints on Late Cretaceous to mid Eocene plate boundaries in the southwest
 980 Pacific. *Earth-Science Reviews*, 140, 72–107, <https://doi.org/10.1016/j.earscirev.2014.10.008>
- 981 Molnar, P., and Francheteau, J., 1975, *Geophysical Journal of the Royal Astronomical Society*, The relative motion of
 982 hotspots in the Atlantic and Indian Oceans during the Cenozoic. *Geophysical Journal of the Royal Astronomical*
 983 *Society*, 43, 763–774, <https://doi.org/10.1111/j.1365-246X.1975.tb06194.x>
- 984 Martinod, J., and Husson, N., 2010, *Earth and Planetary Science Letters*, Horizontal subduction zones, convergence
 985 velocity and the building of the Andes. *Earth and Planetary Science Letters*, 299, 299–309,
 986 <https://doi.org/10.1016/j.epsl.2010.09.010>
- 987 Martinod, Joseph, Gérard, Mélanie, Husson, Laurent, Regard, Vincent, 2020, *Earth Science Reviews*, Widening of
 988 the Andes: an interplay between subduction dynamics and crustal wedge tectonics. *Earth Science Reviews*, 204,
 989 103170, <https://doi.org/10.1016/j.earscirev.2020.103170>
- 990 Morgan, W.J., 1971, *Nature*, Convection plumes in the lower mantle. *Nature*, 230, 42-43.,
 991 <https://doi.org/10.1038/230042a0>
- 992 Morgan, W.J., 1972, *Geological Society of America Memoir*, Plate motions and deep mantle convection. *Geological*
 993 *Society of America Memoir*, 132, 7-22, Colorado Colorado, 44764, <https://doi.org/10.1130/MEM132-p7>
- 994 Mulcahy, P., C.Chen, S.M.Kay, L. D. Brown, B. L. Isacks, E. Sandvol, B.Heit, X.Yuan, and B.L.Coira, 2014, *Tectonics*,
 995 Central Andean mantle and crustal seismicity beneath the Southern Punaplateau and the northern margin of the
 996 Chilean-Pampean flat slab. *Tectonics*, 33, 1636–1658, <https://doi.org/10.1002/2013TC003393>
- 997 Müller, R.D., Royer, J.-Y., and Lawver, L. A., 1993, *Geology*, Revised plate motions relative to the hotspots from
 998 combined Atlantic and Indian Ocean hotspot tracks. *Geology*, 21, 275–278., [https://doi.org/10.1130/0091-](https://doi.org/10.1130/0091-7613(1993)021%3C0275:RPMRTT%3E2.3.CO;2)
 999 [7613\(1993\)021%3C0275:RPMRTT%3E2.3.CO;2](https://doi.org/10.1130/0091-7613(1993)021%3C0275:RPMRTT%3E2.3.CO;2)
- 1000 Müller, R.D., Cande, S.C., Royer, J.-Y., Roest, W.R., and Maschenkov, S., 1999, New constraints on the Late
 1001 Cretaceous/Tertiary plate tectonic evolution of the Caribbean. in *Caribbean Basins*, edited by P. Mann, 39-55,
 1002 Elsevier, Amsterdam,
- 1003 Müller, R. Dietmar, Roest, Walter R., Royer, Jean-Yves, Gahagan, Lisa M., and Sclater, John G., 1997, *Journal of*
 1004 *Geophysical Research*, Digital isochrons of the world's ocean floor. *Journal of Geophysical Research*, 102, 3211-
 1005 3214, <https://doi.org/10.1029/96JB01781>
- 1006 Müller, R. D., Sdrolias, M., Gaina, C., and Roest, W. R., 2008, *Geochemistry Geophysics Geosystems*, Age,
 1007 spreading rates, and spreading asymmetry of the world's ocean crust. *Geochemistry Geophysics Geosystems*, 9,
 1008 Q04006, <https://doi.org/10.1029/2007GC001743>
- 1009 Müller, D.R., Seton, M., Zahirovic, S., Williams, S.E., Matthews, K.J., Wright, N.M., Shephard, G.E., Maloney, K.T.,
 1010 Barnett-Moore, N., Hosseinpour, M., Bower, D.J., and Cannon, J., 2016, *Annual Review of Earth and Planetary*
 1011 *Sciences*, Ocean basin evolution and global-scale plate reorganization events since Pangea breakup. *Annual Review*
 1012 *of Earth and Planetary Sciences*, 44, 107–138. <https://doi.org/10.1146/annurev-earth-060115-012211>.
- 1013 Müller, R. D., Zahirovic, S., Williams, S. E., Cannon, J., Seton, M., Bower, D. J., Tetley, Michael G., Heine, Christian,
 1014 Le Breton, Eline, Liu, Shaofeng, Russell, Samuel H. J., Yang, Ting, Leonard, Jonathon, and Gurnis, Michael, 2019,
 1015 *Tectonics*, A global plate model including lithospheric deformation along major rifts and orogens since the Triassic.
 1016 *Tectonics*, 38, 1884–1907, <https://doi.org/10.1029/2018TC005462>
- 1017 Naar, D. F., and Hey, R. N., 1991, *Journal of Geophysical Research*, Tectonic evolution of the Easter Microplate.
 1018 *Journal of Geophysical Research*, 96, 7961 – 7993., <https://doi.org/10.1029/90JB02398>
- 1019 Nankivell A.P., 1997, Tectonic evolution of the southern ocean between Antarctica, South America and Africa over the
 1020 last 84 Ma. PhD thesis, University of Oxford,
- 1021 Navarrete, César, Gianni, Guido, Massafiero, Gabriela, and Butler, Kristina, 2020, *Earth-Science Reviews*, The fate of
 1022 the Farallon slab beneath Patagonia and its links to Cenozoic intraplate magmatism, marine transgressions and
 1023 topographic uplift. *Earth-Science Reviews*, 210, 103379, <https://doi.org/10.1016/j.earscirev.2020.103379>
- 1024 Norton, I.O., 1995, *Tectonics*, Plate motions in the North Pacific: the 43 Ma non-event. *Tectonics*, 14, 1080-1094.,
 1025 <https://doi.org/10.1029/95TC01256>
- 1026 Norton, I. O., 2000, Global hotspot reference frames and plate motion. in Richards, M.A., Gordon, R. G., and van der
 1027 Hilst, R. D., editors, *The History and Dynamics of Global Plate Motions*, American Geophysical Geophysical
 1028 *Monograph*, 121, 339–357.,
- 1029 Nürnberg, D., and Müller, R. D., 1991, *Tectonophysics*, The tectonic evolution of the South Atlantic from Late Jurassic
 1030 to present. *Tectonophysics*, 191, 27-53, [https://doi.org/10.1016/0040-1951\(91\)90231-G](https://doi.org/10.1016/0040-1951(91)90231-G)
- 1031 O'Connor, J. M., Stoffers, P., and McWilliams, M. O., 1995, *Earth and Planetary Science Letters*, Time-space
 1032 mapping of Easter Chain volcanism. *Earth and Planetary Science Letters*, 136, 197-212,
 1033 [https://doi.org/10.1016/0012-821X\(95\)00176-D](https://doi.org/10.1016/0012-821X(95)00176-D)
- 1034 O'Connor, John M., Steinberger, Bernhard, Koppers, Anthony A. P., Wijbrans, Jan R., Haase, Karsten M., Stoffers,
 1035 Peter, Jokat, Wilfried, and Garbe-Schönberg, Dieter, 2013, *Geochemistry Geophysics Geosystems*, Constraints on

- past plate and mantle motion from new ages for the Hawaiian-Emperor Seamount Chain. *Geochemistry Geophysics Geosystems*, 14, <https://doi.org/10.1002/ggge.20267>,
- O'Driscoll, Leland J., Richards, Mark A., and Humphreys, Eugene D., 2012, *Tectonics*, Nazca–South America interactions and the late Eocene–late Oligocene flat-slab episode in the central Andes. *Tectonics*, 31, TC2013, doi:10.1029/2011TC003036.[RP3]
- Ogg, J. G., 2020, Geomagnetic Polarity Time Scale. in *Geologic Time Scale 2020*, Gradstein, F. M., Ogg, J. G., Schmitz, M. D., Ogg, G. M., editors, Elsevier, Amsterdam, 1, 159-192.,
- O'Neill, Craig, Müller, R. Dietmar, and Steinberger, Bernhard, 2005, *Geochemistry-Geophysics-Geosystems*, On the uncertainties in hot spot reconstructions and the significance of moving hot spot reference frames. *Geochemistry-Geophysics-Geosystems*, 6, Q04003, <https://doi.org/10.1029/2004GC000784>
- Pardo Casas, Frederico, and Molnar, Peter, 1987, *Tectonics*, Relative motion of the Nazca (Farallon) and South American Plates since Late Cretaceous time. *Tectonics*, 6, 233-248., <https://doi.org/10.1029/TC006i003p00233>
- Pérez-Díaz, L., and G. Eagles, 2014, *Tectonics*, Constraining South Atlantic growth with seafloor spreading data. *Tectonics*, 33, 1848–1873, <https://doi.org/10.1002/2014TC003644>
- Pilger, Rex H., Jr., 1978, *Geophysical Research Letters*, A method for finite plate reconstructions, with applications to Pacific-Nazca Plate evolution. *Geophysical Research Letters*, 5, 469-472, <https://doi.org/10.1029/GL005i006p00469>.
- Pilger, Rex H., Jr., and Henyey, T., 1979, *Tectonophysics*, Pacific-North American plate interaction and Neogene volcanism in coastal California. *Tectonophysics*, 57, 189-209, [https://doi.org/10.1016/0040-1951\(79\)90148-3](https://doi.org/10.1016/0040-1951(79)90148-3)
- Pilger, Rex H., Jr., 1981a, *Geological Society of America Bulletin*, Plate reconstructions, aseismic ridges, and low-angle subduction beneath the Andes. *Geological Society of America Bulletin*, 92, 448–456, [https://doi.org/10.1130/0016-7606\(1981\)92<448:PRARAL>2.0.CO;2](https://doi.org/10.1130/0016-7606(1981)92<448:PRARAL>2.0.CO;2)
- Pilger, Rex H., Jr., and Handschumacher, David, 1981, *Geological Society of America Bulletin*, The fixed-hotspot hypothesis and origin of the Easter—Sala y Gomez—Nazca trace. *Geological Society of America Bulletin*, 92, 437–446, [https://doi.org/10.1130/0016-7606\(1981\)92<437:TFHAOO>2.0.CO;2](https://doi.org/10.1130/0016-7606(1981)92<437:TFHAOO>2.0.CO;2)
- Pilger, Rex H., Jr., 1981b, Interpolation of plate reconstructions using cubic splines: a means of estimating instantaneous kinematics. AGU Annual Meeting, San Francisco, CA, USA, EOS Transactions, American Geophysical Union, 62, 45, 44875, TE-1-A-1.,
- Pilger, Rex H., Jr., 1983, Kinematics of the South American subduction zone from global plate reconstructions. In *Geodynamics of the Eastern Pacific Region, Caribbean and Scotia Arcs* Geodynamics of the Eastern Pacific Region, Caribbean and Scotia Arcs, 9, Editor: Cabré, Ramón, S.J., <https://doi.org/10.1029/GD009p0113>,
- Pilger, Rex H., Jr., 1984, *Journal of the Geological Society*, Cenozoic plate kinematics. subduction and magmatism: South American Andes. *Journal of the Geological Society*, 141, 793-802, <https://doi.org/10.1144/gsjgs.141.5.0793>
- Pilger, Rex H., Jr., 2003, *Springer*, Geokinematics - Prelude to Geodynamics. Springer, New York, DOI:10.1007/978-3-662-07439-8
- Pilger, Rex H., Jr., 2007, *Geological Society of America Bulletin*, The Bend: Origin and significance. *Geological Society of America Bulletin*, 119, <https://doi.org/10.1130/B25713.1>
- Pilger, Rex H., Jr., 2012, *Marine Geophysical Research*, Fractal plate reconstructions with spreading asymmetry. *Marine Geophysical Research*, 33, <https://doi.org/10.1007/s11001-012-9152-6>
- Pindell, J., and Kennan, L., 2001, *Transactions Gulf Coast Association of Geological Societies.*, Kinematic evolution of the Gulf of Mexico and Caribbean. *Transactions Gulf Coast Association of Geological Societies.*, <https://doi.org/10.5724/gcs.01.21.0193>
- Pitman, Walter C., and Talwani, Manik, 1972, *Geological Society of America Bulletin*, Sea-Floor Spreading in the North Atlantic. *Geological Society of America Bulletin*, 83, 619–646, [https://doi.org/10.1130/0016-7606\(1972\)83\[619:SSITNA\]2.0.CO;2](https://doi.org/10.1130/0016-7606(1972)83[619:SSITNA]2.0.CO;2)
- Press, William H., Teukolsky, Saul A., Vetterling, William T., and Flannery, Brian P., 1992, *Numerical Recipes in C - The Art of Scientific Computing*. Second Edition, Cambridge University Press, Cambridge, UK, 994 p.,
- Puigdomenech, C., Alarcón, S., Ruiz González, V., Rossel, P., Orts, D., and Zaffarana, C., 2021, *Journal of South American Earth Sciences*, Tectonic rotations in central Chile: New insights on the southern limit of the Maipo Orocline. *Journal of South American Earth Sciences*, 106, <https://doi.org/10.1016/j.jsames.2020.103012>
- Quiero, Felipe, Tassara Andrés, Iaffaldano, Giampiero, and Rabbia, Osvaldo, 2022, *Nature Communications*, Growth of Neogene Andes linked to changes in plate convergence using high-resolution kinematic models. *Nature Communications*, 35-19, <https://doi.org/10.1038/s41467-022-29055-4>
- Ramos, Victor A., 1999, *Episodes*, Plate tectonic setting of the Andean Cordillera. *Episodes*, 22, 183-190.,
- Ramos, V. A., Cristallini, E. O., and Pérez, D.J., 2002, *Journal of South American Earth Sciences*, The Pampean flat-slab of the Central Andes. *Journal of South American Earth Sciences*, 15, 59–78., [https://doi.org/10.1016/S0895-9811\(02\)00006-8](https://doi.org/10.1016/S0895-9811(02)00006-8)
- Ray, Jyotiranjana S., Mahoney, John J., Duncan, Robert A., Ray, Jyotisankar, Wessel, Paul, and Naar, David F., 2012, *Journal of Petrology*, Chronology and Geochemistry of Lavas from the Nazca Ridge and Easter Seamount Chain: an ~30 Myr Hotspot Record. *Journal of Petrology*, 53, 1417–1448, <https://doi.org/10.1093/petrology/egs021>

- Raymond, C.A., Stock, J.M., and Cande, S.C., 2000, Fast Paleogene motion of the Pacific hotspots from revised global plate circuit constraints. in Richards, M.A., Gordon, R.G., and van der Hilst, R.D., editors, *History and Dynamics of Plate Motions*, AGU Geophysical Monograph, 121, 359-375.,
- Risse, A., Trumbull, R. B., Kay, S. M., Coira, B., and Romer, R. L., 2013, *Journal of Petrology*, Multi-stage Evolution of Late Neogene Mantle-derived Magmas from the Central Andes Back-arc in the Southern Puna Plateau of Argentina. *Journal of Petrology*, 54, 1963–1995, <https://doi.org/10.1093/petrology/egt038>
- Royer, J., and Chang, T., 1991, *Journal of Geophysical Research*, Evidence for relative motions between the Indian and Australian Plates during the last 20 m. y. From plate tectonic reconstructions: Implication for the deformation of the Indo-Australian plate. *Journal of Geophysical Research*, 96, <https://doi.org/10.1029/91JB00897>. issn: 0148-0227.
- Royer, J.-Y., Patriat, P., Bergh, H., and Scotese, C. R., 1988, *Tectonophysics*, Evolution of the Southwest Indian Ridge from the Late Cretaceous anomaly 34 to the middle Eocene anomaly 20. *Tectonophysics*, 155, 235-260., [https://doi.org/10.1016/0040-1951\(88\)90268-5](https://doi.org/10.1016/0040-1951(88)90268-5)
- Schellart, W. P., 2020, *Frontiers in Earth Science*, Control of subduction zone age and size on flat slab subduction. *Frontiers in Earth Science*, 0.3513888888888889, <https://doi.org/10.3389/feart.2020.00026>
- Schepers, G., van Hinsbergen, D., and Spakman, W. et al., 2017, *Nature Communications*, South-American plate advance and forced Andean trench retreat as drivers for transient flat subduction episodes. . *Nature Communications*, 8, 15249, <https://doi.org/10.1038/ncomms15249>[RP7]
- Seton, M., Müller, R.D., Zahirovic, S., Gaina, C., Torsvik, T., Shephard, G., Talsma, A., Gurnis, M., Turner, Maus, S., and Chandler, M., 2012, *Earth-Science Reviews*, Global continental and ocean basin reconstructions since 200Ma. *Earth-Science Reviews*, 113, 212 - 270, <https://doi.org/10.1016/j.earscirev.2012.03.002>
- Seton, M., Whittaker, J., Wessel, P., Müller, R. D., DeMets, C., Merkouriev, S., Cande, S., Gaina, C., Eagles, G., Granot, R., Stock, J., Wright, N., and Williams, S., 2014, *Geochemistry Geophysics Geosystems*, Community infrastructure and repository for marine magnetic identifications. *Geochemistry Geophysics Geosystems*, 5, 1629-1641, <https://doi.org/10.1002/2013GC005176>
- Sharp, W.D., and Clague, D.A., 2006, *Science*, 50-Ma Initiation of Hawaiian-Emperor Bend Records Major Change in Pacific Plate Motion. *Science*, 313: 1281-1284,
- Shaw, P., and Cande, S., 1990, *Journal of Geophysical Research*, High-Resolution Inversion for South Atlantic Plate Kinematics Using Joint Altimeter and Magnetic Anomaly Data. *Journal of Geophysical Research*, 80, 4815–4822., <https://doi.org/10.1029/JB095iB03p02625>
- Skinner, Steven, and Clayton, Robert W., 2013, *Earth and Planetary Science Letters*, The lack of correlation between flat slabs and bathymetric impactors in South America. *Earth and Planetary Science Letters*, 371-372, 44566, https://ui.adsabs.harvard.edu/link_gateway/2013E&PSL.371....1S/doi:10.1016/j.epsl.2013.04.013
- Somoza, Rubén, 2005, Cenozoic convergence in western South America: Subduction of the Nazca, Farallon, and Aluk plates. 6th International Symposium on Andean Geodynamics, ISAG 2005, Barcelona, Extended Abstracts: 681-684.,
- Somoza, Rubén, and Ghidella, M.E., 2005, *Revista de la Asociacion Geologica Argentina*, Convergence in the western margin of South America during the Cenozoic: Subduction of Nazca, Farallon and Aluk plates. *Revista de la Asociacion Geologica Argentina*, 60, 797-809, http://hdl.handle.net/20.500.12110/paper_00044822_v60_n4_p797_Somoza
- Somoza, Rubén, and Ghidella, M.E., 2012, *Earth and Planetary Science Letters*, Late Cretaceous to recent plate motions in western South America revisited. *Earth and Planetary Science Letters*, 331-332, 152-163., <https://doi.org/10.1016/j.epsl.2012.03.003>
- Tebbens, S. F., and Cande, S. C., 1997, *Journal of Geophysical Research: Solid Earth*, Southeast Pacific tectonic evolution from Early Oligocene to Present. *Journal of Geophysical Research: Solid Earth*, 102, 12061-12084., <https://doi.org/10.1029/96JB02582>
- Tetley, Michael G., Williams, S. E., Gurnis, Michael, Flament, Nicolas, and Müller, R. D., 2019, *Journal of Geophysical Research: Solid Earth*, Constraining Absolute Plate Motions Since the Triassic. *Journal of Geophysical Research: Solid Earth*, 124, <https://doi.org/10.1029/2019JB017442>
- Torsvik, Trond H., Steinberger, Bernhard, Gurnis, Michael, and Gaina, Carmen, 2010, *Earth and Planetary Science Letters*, Plate tectonics and net lithosphere rotation over the past 150My. *Earth and Planetary Science Letters*, 291, 106-112, <https://doi.org/10.1016/j.epsl.2009.12.055>
- Weissel, J. K., and Hayes, D. E., 1972, *Antarctic Research Series*, Magnetic anomalies in the Southeast Indian Ocean. *Antarctic Research Series*, 19, *Antarctic Oceanology II: The Australian-New Zealand Sector*, edited by D.E. Hayes, Washington, D.C., 165-196.,
- Wessel, P., and L. W. Kroenke, 2008, *Journal of Geophysical Research*, Pacific absolute plate motions since 145 Ma. *Journal of Geophysical Research*, 113, B06101, doi:10.1029/2007JB005499.
- Whittaker, J. M., Müller, R. D., Leitchenkov, G, Stagg, H, Sdrolias, M, Gaina, C, and Goncharov, A, 2007, *Science*, Major Australian-Antarctic plate reorganization at Hawaiian-Emperor bend time. *Science*, 318, 83–86, doi:10.1126/science.1143769.

- 1154 Wilder, D. T., 2003, Relative motion history of the Pacific-Nazca (Farallon) plates since 30 million years ago. M.S.
 1155 Thesis, University of South Florida.,
 1156 Williams, S. E., Whittaker, J. M., and Müller, R. D., 2011, *Tectonics*, Full-fit palinspastic reconstruction of the
 1157 conjugate Australian-Antarctic margins. . *Tectonics*, TC6012., <https://doi.org/10.1029/2011TC002912>
 1158 Wilson, J.T., 1963, *Canadian Journal of Physics*, A possible origin of the Hawaiian islands. *Canadian Journal of*
 1159 *Physics*, 41, 863-870., <https://doi.org/10.1139/p63-094>
 1160 Wright, Nicky, Müller, Dietmar, Seton, Maria, and Williams, Simon, 2015, *Geology*, Revision of Paleogene plate
 1161 motions in the Pacific and implications for the Hawaiian-Emperor bend. *Geology*, 43, 455-458,
 1162 <https://doi.org/10.1130/G36303.1>
 1163 Yáñez, G. A., Ranero, C. R., von Huene, R., and Díaz, J., 2001, *Journal of Geophysical Research*, Magnetic anomaly
 1164 interpretation across the southern central Andes (32°–34°S): The role of the Juan Fernández Ridge in the late Tertiary
 1165 evolution of the margin. *Journal of Geophysical Research*, 106, 6325–6345, <https://doi.org/10.1029/2000JB900337>
 1166

1167 Supplementary Table References, .

- 1168
 1169 Andrews, D. L., Gordon, R.G., and Horner-Johnson, B. C., 2006, *Geophysical Journal International*, Uncertainties in
 1170 plate reconstructions relative to the hot spots: Pacific-hot spot rotations and uncertainties for the past 68 million years.
 1171 *Geophysical Journal International*, 166, 939–951, <https://doi.org/10.1111/j.1365-246X.2006.03029.x>
 1172 Cande, S. C., and Kent, D. V., 1995, *Journal of Geophysical Research*, Revised calibration of the geomagnetic time
 1173 scale for the Late Cretaceous and Cenozoic. *Journal of Geophysical Research*, 100, 6093-6095.,
 1174 <https://doi.org/10.1029/94JB03098>
 1175 Eagles, Graeme, and Jokat, Wilfried, 2014, *Tectonophysics*, Tectonic reconstructions for paleobathymetry in Drake
 1176 Passage. *Tectonophysics*, 611, 28–50, <https://doi.org/10.1016/j.tecto.2013.11.021>
 1177 Eagles, Graeme, and Vaughan, Alan P. M., 2009, *Geophysical Research Letters*, Gondwana breakup and plate
 1178 kinematics: Business as usual. *Geophysical Research Letters*, 36, L10302, <https://doi.org/10.1029/2009GL037552>
 1179 Eagles, Graeme, Gohl, Karsten, and Larter, Robert D., 2008, *Tectonophysics*, Animated tectonic reconstruction of the
 1180 Southern Pacific and alkaline volcanism at its convergent margins since Eocene times . *Tectonophysics*, 464, 21-29,
 1181 <https://doi.org/10.1016/j.tecto.2007.10.005>
 1182 Granot, R., and Dymant, J., 2018, *Nature Communications*, Late Cenozoic unification of East and West Antarctica. .
 1183 *Nature Communications*, 9, 3189, <https://doi.org/10.1038/s41467-018-05270-w>
 1184 Royer, J.Y., and Chang, T., 1991, *Journal of Geophysical Research*, Evidence for relative plate motions between the
 1185 Indian and Australian plates during the last 20 m. y. from plate tectonic reconstructions: implications for the
 1186 deformation of the Indo-Australian plate. *Journal of Geophysical Research*, 96, 11779–11802.,
 1187 <https://doi.org/10.1029/91JB00897>
 1188 Seton, M., Whittaker, J., Wessel, P., Müller, R. D., DeMets, C., Merkouriev, S., Cande, S., Gaina, C., Eagles, G.,
 1189 Granot, R., Stock, J., Wright, N., and Williams, S., 2014, *Geochemistry Geophysics Geosystems*, Community
 1190 infrastructure and repository for marine magnetic identifications. *Geochemistry Geophysics Geosystems*, 5, 1629-
 1191 1641, <https://doi.org/10.1002/2013GC005176>
 1192 Steinberger, B., and Torsvik, T. H., 2008, *Nature*, Absolute plate motions and true polar wander in the absence of
 1193 hotspot tracks. *Nature*, 452, 620–623, <https://doi.org/10.1038/nature06824>
 1194 Torsvik, T. H., Müller, R. D., Van der Voo, R., Steinberger, B., and Gaina, C., 2008, *Review of Geophysics*, Global
 1195 plate motion frames: Toward a unified model. . *Review of Geophysics*, 46, RG3004,
 1196 <https://doi.org/10.1029/2007RG000227>
 1197 Torsvik, T. H., Van der Voo, R., Preeden, U., Mac Niocaill, C., Steinberger, B., Doubrovine, P. V., van Hinsbergen,
 1198 Douwe J.J., Domeier, Mathew, Gaina, Carmen, Tohver, Eric, Meert, Joseph G., McCausland, Phil J.A., and Cocks, L.
 1199 Robin M., 2012, *Earth Science Reviews*, Phanerozoic polar wander, paleogeography and dynamics. *Earth Science*
 1200 *Reviews*, 114, 325–368., <https://doi.org/10.1016/j.earscirev.2012.06.007>
 1201 Torsvik, T. H., Steinberger, B., Shephard, G. E., Doubrovine, P. V., Gaina, C., Domeier, M., et al., 2019,
 1202 *Geochemistry Geophysics Geosystems*, Pacific-Panthalassic reconstructions: Overview, errata and the way forward.
 1203 *Geochemistry Geophysics Geosystems*, 20, 3659–3689, <https://doi.org/10.1029/2019GC008402>
 1204 Wessel, P., Y. Harada, and L. W. Kroenke, 2006, *Geochemistry Geophysics Geosystems*, Toward a self-consistent,
 1205 high-resolution absolute plate motion model for the Pacific. *Geochemistry Geophysics Geosystems*, 7, Q03L12,
 1206 doi:10.1029/2005GC001000.
 1207
 1208
 1209

The Andes and Hotspots: Mutual Evidence – Tables & Figures

Rex H Pilger, Jr
10630 W 66th Avenue
Arvada, Colorado USA
rexpilger@yahoo.com
<https://orcid.org/my-orcid?orcid=0000-0003-3715-5084>

Circuit	Plate Pairs								
	SA - AF	SA - AN	AF - AN	AN - WA	WA - PC	PC - NF	AN - NF	HS - PC	HS - AF
SA - AF - AN - WA - PC - NF	DeMets & Merkouriev, 2019; Pérez-Díaz & Eagles, 2014		Cande et al., 2010; Cande and Patriat, 2015; DeMets & Merkouriev, 2015	Granot et al., 2013	Croon et al., 2008	Wilder, 2003; Wright et al., 2015; Seton et al., 2012			
SA - AF - AN - WA - NF	DeMets & Merkouriev, 2019; Pérez-Díaz & Eagles, 2014		Cande et al., 2010; Cande and Patriat, 2015; DeMets & Merkouriev, 2015	Granot et al., 2013			Tebbens and Cande, 1997		
SA - AN - WA - PC - NF		Eagles & Jokat, 2014; Livermore et al., 2005		Granot et al., 2013	Croon et al., 2008	Wilder, 2003; Wright et al., 2015; Seton et al., 2012			
SA - AN - WA - NF		Eagles & Jokat, 2014; Livermore et al., 2005		Granot et al., 2013			Tebbens and Cande, 1997		
HS - AF - AN - WA - PC - NF			Cande et al., 2010; Cande and Patriat, 2015; DeMets & Merkouriev, 2015	Granot et al., 2013	Croon et al., 2008	Wilder, 2003; Wright et al., 2015; Seton et al., 2012			Müller et al., 1993; Müller et al., 2019
HS - PC - NF						Wilder, 2003; Wright et al., 2015; Seton et al., 2012		Wessel and Kroenke, 2008; Gastra, 2022	

Table 1. Reconstruction sources for circuits. AF: African, AN: East Antarctic, HS: Hotspot, NF: Nazca/Farallon, PC: Pacific, SA: South American, WA: West Antarctic

Plate 1	Plate 2	Age (Ma)	Longitude (°E)	Latitude (° N)	Angle (CCW)
Nazca	South American	1	80.276	-51.577	0.658
Nazca	South American	2	80.848	-54.545	1.486
Nazca	South American	3	79.543	-55.485	2.319
Nazca	South American	4	78.382	-59.122	3.141

Nazca	South American	5	78.327	-61.340	3.959
Nazca	South American	6	78.131	-55.296	4.974
Nazca	South American	7	77.997	-49.677	6.011
Nazca	South American	8	78.566	-51.104	6.890
Nazca	South American	9	78.626	-55.923	8.155
Nazca	South American	10	78.719	-56.910	9.291
Nazca	South American	11	79.453	-57.193	10.494
Nazca	South American	12	80.470	-57.556	11.448
Nazca	South American	13	79.777	-58.836	12.322
Nazca	South American	14	76.250	-60.742	13.497
Nazca	South American	15	74.007	-61.666	15.006
Nazca	South American	16	75.654	-60.343	16.346
Nazca	South American	17	77.849	-59.123	17.976
Nazca	South American	18	80.570	-58.119	19.978
Nazca	South American	19	83.484	-57.231	22.520
Nazca	South American	20	84.899	-56.402	24.208
Nazca	South American	21	86.092	-56.118	25.345
Nazca	South American	22	87.687	-55.654	27.236
Nazca	South American	23	88.721	-55.515	28.381
Nazca	South American	24	88.715	-56.388	29.051
Nazca	South American	25	87.820	-58.145	29.519
Nazca	South American	26	86.283	-60.393	29.961
Nazca	South American	27	84.035	-62.722	30.260
Nazca	South American	28	81.299	-64.528	30.638
Nazca	South American	29	79.026	-65.663	31.244
Nazca	South American	30	76.797	-66.245	31.917
Nazca	South American	31	75.190	-66.552	32.720
Nazca	South American	32	74.060	-66.919	33.666
Nazca	South American	33	72.416	-67.330	34.519
Nazca	South American	34	70.359	-68.330	35.391
Nazca	South American	35	67.862	-69.932	36.370
Nazca	South American	36	64.267	-71.585	36.970
Nazca	South American	37	59.674	-73.548	37.878
Nazca	South American	38	53.884	-75.449	39.149
Nazca	South American	39	46.867	-76.876	40.576
Nazca	South American	40	39.726	-77.639	42.120
Nazca	South American	41	33.940	-77.690	43.610
Nazca	South American	42	29.884	-77.445	45.231
Nazca	South American	43	26.149	-77.089	46.545
Nazca	South American	44	22.081	-76.728	47.519
Nazca	South American	45	17.726	-76.409	48.337

Nazca	South American	46	13.329	-76.085	49.068
Nazca	South American	47	9.172	-75.727	49.766
Nazca	South American	48	5.562	-75.329	50.482
Nazca	South American	49	2.624	-74.909	51.231
Nazca	South American	50	0.115	-74.507	51.960
Nazca	South American	51	357.775	-74.143	52.639
Nazca	South American	52	355.408	-73.820	53.291
Nazca	South American	53	352.847	-73.530	53.946
Nazca	South American	54	350.080	-73.263	54.627
Nazca	South American	55	347.264	-73.002	55.337
Nazca	South American	56	344.589	-72.720	56.032
Nazca	South American	57	342.247	-72.395	56.654
Nazca	South American	58	340.399	-72.013	57.145
Nazca	South American	59	339.015	-71.576	57.528
Nazca	South American	60	337.931	-71.103	57.879
Nazca	South American	61	336.904	-70.604	58.257
Nazca	South American	62	335.688	-70.085	58.722
Nazca	South American	63	334.073	-69.546	59.340
Nazca	South American	64	332.397	-69.020	60.158
Nazca	South American	65	331.097	-68.541	61.155
Nazca	South American	66	330.131	-68.086	62.266
Nazca	South American	67	329.429	-67.624	63.431
Nazca	South American	68	328.917	-67.129	64.606
Nazca	South American	69	328.520	-66.574	65.751
Nazca	South American	70	328.175	-65.962	66.859
Nazca	South American	71	327.837	-65.317	67.935
Nazca	South American	72	327.470	-64.661	68.983
Nazca	South American	73	327.050	-64.012	69.995
Nazca	South American	74	326.567	-63.383	70.953
Nazca	South American	75	326.013	-62.783	71.842
Nazca	South American	76	325.396	-62.204	72.662
Nazca	South American	77	324.722	-61.631	73.421
Nazca	South American	78	323.999	-61.050	74.132
Nazca	South American	79	323.234	-60.444	74.805
Nazca	South American	80	322.437	-59.800	75.453

Table 2. South America-Nazca Reconstruction Parameters, 0-80 Ma.

Reference Frame	Plate	Age (Ma)	Longitude (°E)	Latitude (° N)	Angle (CCW)
Hawaiian Hotspot	Nazca	1	-81.507	-2.836	0.432

Hawaiian Hotspot	Nazca	2	-83.993	2.059	0.894
Hawaiian Hotspot	Nazca	3	-81.490	7.972	1.282
Hawaiian Hotspot	Nazca	4	-73.179	17.386	1.521
Hawaiian Hotspot	Nazca	5	-76.226	25.777	1.897
Hawaiian Hotspot	Nazca	6	-83.495	21.016	2.701
Hawaiian Hotspot	Nazca	7	-87.719	17.662	3.679
Hawaiian Hotspot	Nazca	8	-87.600	23.364	4.202
Hawaiian Hotspot	Nazca	9	-86.270	32.629	4.649
Hawaiian Hotspot	Nazca	10	-86.535	38.297	5.427
Hawaiian Hotspot	Nazca	11	-84.670	38.652	6.115
Hawaiian Hotspot	Nazca	12	-83.844	40.688	6.706
Hawaiian Hotspot	Nazca	13	-85.013	44.866	7.242
Hawaiian Hotspot	Nazca	14	-89.487	50.290	7.973
Hawaiian Hotspot	Nazca	15	-93.911	53.549	9.062
Hawaiian Hotspot	Nazca	16	-92.759	52.514	10.258
Hawaiian Hotspot	Nazca	17	-91.453	51.545	11.651
Hawaiian Hotspot	Nazca	18	-90.310	50.846	13.331
Hawaiian Hotspot	Nazca	19	-89.108	50.431	15.656
Hawaiian Hotspot	Nazca	20	-88.503	50.000	17.258
Hawaiian Hotspot	Nazca	21	-88.278	49.491	18.144
Hawaiian Hotspot	Nazca	22	-87.779	49.228	19.879
Hawaiian Hotspot	Nazca	23	-87.761	49.104	20.890
Hawaiian Hotspot	Nazca	24	-88.874	50.119	21.477
Hawaiian Hotspot	Nazca	25	-91.092	52.029	21.785
Hawaiian Hotspot	Nazca	26	-94.379	54.397	21.968
Hawaiian Hotspot	Nazca	27	-98.499	56.720	22.198
Hawaiian Hotspot	Nazca	28	-102.789	58.432	22.586
Hawaiian Hotspot	Nazca	29	-106.522	59.099	23.058
Hawaiian Hotspot	Nazca	30	-109.283	59.123	23.687
Hawaiian Hotspot	Nazca	31	-111.281	58.890	24.406
Hawaiian Hotspot	Nazca	32	-112.925	58.717	25.127
Hawaiian Hotspot	Nazca	33	-114.715	58.938	25.791
Hawaiian Hotspot	Nazca	34	-117.233	59.805	26.340
Hawaiian Hotspot	Nazca	35	-120.808	61.272	26.803

Hawaiian Hotspot	Nazca	36	-125.540	63.055	27.264
Hawaiian Hotspot	Nazca	37	-131.428	64.860	27.797
Hawaiian Hotspot	Nazca	38	-138.152	66.387	28.474
Hawaiian Hotspot	Nazca	39	-144.984	67.415	29.327
Hawaiian Hotspot	Nazca	40	-150.869	67.849	30.358
Hawaiian Hotspot	Nazca	41	-154.900	67.762	31.536
Hawaiian Hotspot	Nazca	42	-157.452	67.426	32.762
Hawaiian Hotspot	Nazca	43	-159.489	67.018	33.908
Hawaiian Hotspot	Nazca	44	-161.844	66.679	34.883
Hawaiian Hotspot	Nazca	45	-164.784	66.390	35.670
Hawaiian Hotspot	Nazca	46	-167.967	66.098	36.339
Hawaiian Hotspot	Nazca	47	-170.974	65.746	36.950
Hawaiian Hotspot	Nazca	48	-173.542	65.273	37.552
Hawaiian Hotspot	Nazca	49	-175.060	64.821	38.181
Hawaiian Hotspot	Nazca	50	-180.986	63.111	38.969
Hawaiian Hotspot	Nazca	51	-182.474	62.905	39.785
Hawaiian Hotspot	Nazca	52	-183.797	62.727	40.534
Hawaiian Hotspot	Nazca	53	-185.359	62.453	41.242
Hawaiian Hotspot	Nazca	54	-186.894	62.203	41.924
Hawaiian Hotspot	Nazca	55	-188.616	61.868	42.592
Hawaiian Hotspot	Nazca	56	-190.090	61.601	43.239
Hawaiian Hotspot	Nazca	57	-192.399	60.857	43.912
Hawaiian Hotspot	Nazca	58	-194.743	59.910	44.608
Hawaiian Hotspot	Nazca	59	-195.623	59.630	45.238
Hawaiian Hotspot	Nazca	60	-196.568	59.253	45.912
Hawaiian Hotspot	Nazca	61	-197.439	58.896	46.608
Hawaiian Hotspot	Nazca	62	-198.399	58.520	47.329
Hawaiian Hotspot	Nazca	63	-199.553	58.096	48.076
Hawaiian Hotspot	Nazca	64	-200.619	57.688	48.858
Hawaiian Hotspot	Nazca	65	-201.328	57.341	49.689
Hawaiian Hotspot	Nazca	66	-201.756	57.051	50.547
Hawaiian Hotspot	Nazca	67	-202.016	56.804	51.420
Hawaiian Hotspot	Nazca	68	-202.226	56.566	52.291
Hawaiian Hotspot	Nazca	69	-202.485	56.320	53.147

Hawaiian Hotspot	Nazca	70	-202.827	56.057	53.987
Hawaiian Hotspot	Nazca	71	-203.232	55.776	54.806
Hawaiian Hotspot	Nazca	72	-203.697	55.485	55.614
Hawaiian Hotspot	Nazca	73	-204.223	55.183	56.415
Hawaiian Hotspot	Nazca	74	-204.777	54.875	57.203
Hawaiian Hotspot	Nazca	75	-205.378	54.549	57.992
Hawaiian Hotspot	Nazca	76	-206.008	54.208	58.775
Hawaiian Hotspot	Nazca	77	-206.647	53.871	59.562
Hawaiian Hotspot	Nazca	78	-207.302	53.530	60.350
Hawaiian Hotspot	Nazca	79	-207.957	53.185	61.145
Hawaiian Hotspot	Nazca	80	-208.607	52.837	61.954
Hawaiian Hotspot	Nazca	81	-209.244	52.489	62.777
Hawaiian Hotspot	Nazca	82	-209.829	52.166	63.629
Hawaiian Hotspot	Nazca	83	-210.338	51.873	64.533
Hawaiian Hotspot	Nazca	84	-210.727	51.612	65.490
Hawaiian Hotspot	Nazca	85	-211.005	51.396	66.531
Hawaiian Hotspot	Nazca	86	-211.460	51.026	67.955
Hawaiian Hotspot	Nazca	87	-212.017	50.537	69.708
Hawaiian Hotspot	Nazca	88	-212.514	50.033	71.620
Hawaiian Hotspot	Nazca	89	-212.828	49.616	73.510
Hawaiian Hotspot	Nazca	90	-212.921	49.329	75.284
Hawaiian Hotspot	Nazca	91	-212.831	49.158	76.937
Hawaiian Hotspot	Nazca	92	-212.588	49.086	78.475
Hawaiian Hotspot	Nazca	93	-212.221	49.099	79.904
Hawaiian Hotspot	Nazca	94	-211.752	49.180	81.228
Hawaiian Hotspot	Nazca	95	-211.204	49.315	82.456
Hawaiian Hotspot	Nazca	96	-210.599	49.490	83.595
Hawaiian Hotspot	Nazca	97	-209.956	49.690	84.652
Hawaiian Hotspot	Nazca	98	-209.295	49.901	85.635
Hawaiian Hotspot	Nazca	99	-208.636	50.107	86.551
Hawaiian Hotspot	Nazca	100	-208.001	50.294	87.408
Hawaiian Hotspot	Nazca	101	-207.408	50.446	88.211
Hawaiian Hotspot	Nazca	102	-206.878	50.549	88.967
Hawaiian Hotspot	Nazca	103	-206.422	50.598	89.680

Hawaiian Hotspot	Nazca	104	-206.048	50.599	90.352
Hawaiian Hotspot	Nazca	105	-205.764	50.557	90.986
Hawaiian Hotspot	Nazca	106	-205.575	50.475	91.585
Hawaiian Hotspot	Nazca	107	-205.491	50.358	92.153
Hawaiian Hotspot	Nazca	108	-205.518	50.209	92.694
Hawaiian Hotspot	Nazca	109	-205.665	50.033	93.213
Hawaiian Hotspot	Nazca	110	-205.939	49.833	93.717
Hawaiian Hotspot	Nazca	111	-206.340	49.617	94.223
Hawaiian Hotspot	Nazca	112	-206.852	49.393	94.753
Hawaiian Hotspot	Nazca	113	-207.434	49.156	95.314
Hawaiian Hotspot	Nazca	114	-208.026	48.895	95.905
Hawaiian Hotspot	Nazca	115	-208.571	48.601	96.526
Hawaiian Hotspot	Nazca	116	-209.009	48.267	97.175
Hawaiian Hotspot	Nazca	117	-209.282	47.888	97.850
Hawaiian Hotspot	Nazca	118	-209.339	47.460	98.553
Hawaiian Hotspot	Nazca	119	-209.214	46.993	99.299
Hawaiian Hotspot	Nazca	120	-208.984	46.504	100.107
Hawaiian Hotspot	Nazca	121	-208.729	46.010	100.999
Hawaiian Hotspot	Nazca	122	-208.527	45.528	101.982
Hawaiian Hotspot	Nazca	123	-208.466	45.068	103.036
Hawaiian Hotspot	Nazca	124	-208.629	44.639	104.131
Hawaiian Hotspot	Nazca	125	-209.048	44.227	105.214
Hawaiian Hotspot	Nazca	126	-209.715	43.805	106.215
Hawaiian Hotspot	Nazca	127	-210.621	43.343	107.066
Hawaiian Hotspot	Nazca	128	-211.745	42.805	107.721
Hawaiian Hotspot	Nazca	129	-213.053	42.156	108.157
Hawaiian Hotspot	Nazca	130	-214.504	41.357	108.352
Hawaiian Hotspot	Nazca	131	-216.047	40.380	108.303
Hawaiian Hotspot	Nazca	132	-217.602	39.240	108.079
Hawaiian Hotspot	Nazca	133	-219.089	37.971	107.761
Hawaiian Hotspot	Nazca	134	-220.457	36.617	107.424
Hawaiian Hotspot	Nazca	135	-221.672	35.231	107.142
Hawaiian Hotspot	Nazca	136	-222.706	33.871	106.984
Hawaiian Hotspot	Nazca	137	-223.539	32.603	107.021

Hawaiian Hotspot	Nazca	138	-224.165	31.481	107.300
Hawaiian Hotspot	Nazca	139	-224.614	30.507	107.809
Hawaiian Hotspot	Nazca	140	-224.922	29.670	108.525

Table 3. Nazca-Hotspot Parameters - 0 - 140 Ma, as described in text.

Figure Captions

Figure 1. South American subduction zone: Surface from Hayes et al. (2012). Earthquakes from USGS (2022); depth: orange 0-33 km, yellow 33-70 km, green 70-150 km, blue 150-300 km. Red: 500-800 km. Note inferred hotspot traces in bathymetry. All map images are in Google Earth. Proposed hotspot traces: Juan Fernandez, Easter-Nazca, Galapagos-Carnegie in green.

Figure 2. Two views of Pacific Ocean island-seamount volcanic rock locations rotated back by isotopic age, +/- 2.5 m. y., producing loci, according to the model of Gaastra et al. (2022) and Wessel and Kroenke (for dates older than 80 Ma, as described in text); extended to the Nazca and Cocos plates by plate-pair reconstructions as also described in text. Names apply to loci clusters and inferred hotspots or hotspot groups. A. Central Pacific. B. Eastern Pacific. Google Earth format (*.kml) file is accessible in Supplementary Data files.

Figure 3. Hotspot loci for (south to north) Juan Fernandez, Easter, and Galapagos hotspots relative to Nazca plate (and Cocos plate for latter). Blue: Wessel and Kroenke (2008) Pacific hotspot model, 140-0 Ma. Green: Gaastra et al. (2022) Pacific-hotspot model for 80-0 Ma, Wessel and Kroenke (2008) for 140-80 Ma; (Loci are not “deformed” onto the subducting surface.) Note that the inferred location of the Easter hotspot differs between the two models so as to visually fit the Easter-Nazca trace; clearly there is a lot of freedom in regard to picking hotspot locations. Google Earth format (*.kml) files are accessible in Supplementary Data files.

Figure 4. Calculated locus for Juan Fernandez hotspot relative to Nazca plate based on Gaastra et al. (2022) Pacific-hotspot model propagated to Nazca plate; Earthquakes from USGS (2022); circles: orange 0-33 km, yellow 33-70 km, green 70-150 km, blue 150-300 km. (Loci are not “deformed” onto the subducting surface.) Image in Google Earth. Google Earth format (*.kml) files are accessible in Supplementary Data files.

Figure 5. Calculated loci based on combined Gaastra et al. (2022) (0-80 Ma) and Wessel and Kroenke (2008) (80-140 Ma) Pacific-hotspot model with 50 Ma Hawaiian-Emperor Bend calculated at 1 m. y. interval, extended to the Nazca plate, and reconstructed relative to (fixed) South America, at 1 m. y. interval (5 m. y. interval isochrons are in gold): (A) Galapagos-Carnegie, (B) Easter-Nazca and (C) Juan Fernandez (lower) hotspot traces on Nazca/Farallon plate, reconstructed relative to (fixed) South American plate. See Figure 3 for Easter hotspot location. The present positions of the loci are the most easterly portions. Apparent first contact, relative to the *current* continental boundary occurred for: Juan Fernandez trace, ~65 Ma; Easter trace, ~43 Ma; Galapagos-Carnegie, ~31 Ma. *Recall that the loci positions over the ocean, as well as land, is relative to South America, without projection onto the hypothesized subduction zones corresponding with the loci.* The western end of each locus is the apparent location of the hotspot relative to South America. Comparison of features in each locus with adjacent positions provides insight into the relative motion of the Nazca plate to South America over that interval. Thus, from 25-0 Ma, the Nazca plate was moving east-northeast across the trench relative to South America, 50-25 Ma, eastward, and northeastward from 80-50 Ma. Also, note rapid convergence between 20-15 Ma and 50-40 Ma, and very slow convergence 70-55 and 80-75 Ma. The proximity of the Juan Fernandez locus to the Andean bend (e.g., Isacks, 1988) at Latitude ~18° S is suggestive of possible influence on the formation of the bend between 35 to 20 Ma; enhanced convergence at that latitude could have induced shortening of the shallow crust between 25 to 18° S during

that period of time as Martinod et al. (2010) proposed. See Figure 13 for higher resolution portrayal of convergence rates. Google Earth format (*.kml) files are accessible in Supplementary Data files.

Figure 6a. Andes isotopic dates and calculated intersections of reconstructed Easter-Nazca (EN) and Juan Fernandez (JF) hotspot traces (see figure 5 for map views) with Peru-Chile trench-parallel lines, top to bottom: A. 0-1° of arc (0 to ~111 km) from trench. B. 1-2°; C. 2-3°, D. 3-4°; E. 4-5°; F. 5-6°. G. 6-7°. H. 7-8°. Note especially B and C in which cessation of magmatism parallels the Easter hotspot loci intersections, and most graphs in which onset or increase in magmatism is paralleled by Juan Fernandez hotspot loci intersections. Spreadsheets are accessible in Supplementary Data files.

Figure 6b. Close-up graphs as in Figure 6a, showing magmatic patterns and hotspot loci intersections. A & B: Easter-Nazca (EN) hotspot. Note apparent cessation of magmatism and predicted trace. C-E: Juan Fernandez (JF) hotspot trace: Note apparent parallelism of onset of magmatism and predicted trace.

Figure 7. Central Andes isotopic dates, projected to the trench at estimated time of encounter. Spreadsheet is accessible in Supplementary Data files.

Figure 8. Isotopic dates of silicic to intermediate igneous rocks younger than 5.0 Ma, central and southern Andes. Magmatism from the coast inland into northwestern Argentina extends over 500 km while the central zone of concentrated magmatism along the Andean crest typically exceeds 125 km in width. The western margins of the central zone correspond with the inferred first contact of the subducting Nazca plate with the asthenosphere (compare with Figure 3). Google Earth format (*.kml) file is accessible in Supplementary Data files.

Figure 9. Isotopic dates of mafic igneous 0-80 Ma.

Figure 10. Charts: Projected isotopic dates of mafic rocks in adjacent increments of 1 to 2° arc-distance from the trench along with projected intersections of modeled hotspot traces on segment boundaries, A: 0-2°, B: 2-3°, C: 3-4°, D: 4-5°, E: 5-6°. Traces are from modified GGW22 model (older Hawaiian-Emperor bend, 50 Ma) combined with WK08 incremental stages for traces older than 80 Ma, of Pacific-Hotspot reconstructions propagated to the Nazca plate and further reconstructed relative to South American plate. The traces can be thought of as partial envelopes around time-transgressive magmatic episodes. That is, in the middle of the graph, as it propagates north-south, the Juan Fernandez (JF) trace bounds older from younger mafic data points. The Easter-Nazca trace (EN) provides similar bounds on the northern part of the graph, although data points are sparser.

Figure 11. Hypothetical Foundation Seamounts hotspot loci (green curve, yellow squares) and identified magnetic isochrons (red circles): A. Southwestern Pacific (north is upper left). B. East-central Pacific, offshore Chile (north is top); yellow contours – outline of principal bathymetric anomaly rotated from Pacific plate after Skinner and Clayton (2013) in which ages of locus points and isochrons are very close to one another. Note proximity of loci age points to isochrons. If loci age is less than plate age, then the trace is possible. Correspondence of submarine ridges implies melting anomaly was close to the spreading center for a brief period of time, but mostly beneath Pacific plate 55 Ma to the Present; no ridge is apparent on Nazca/Farallon plate older than 43 Ma, and, therefore, none to be subducted, along the hotspot locus.

Figure 12. USGS earthquakes, SLAB configuration (Hayes et al., 2018), dated isochrons and mapped fracture zones (Seton et al., 2014, with links), and (pink) calculated locus of the Easter-Nazca ridge (this

paper), Peru and adjacent areas. Note the end of the fracture zone in the trench at 10.3°S latitude. Isochrons on the northwest side are ~7 m. y. younger; and, similarly, the next fracture zone north, 9°S, separates plate ~3 m. y. younger on the north from that on the south. Younger plate subducts at lower angles than does older plate (see, e. g, southern Chile subduction zone).

Figure 13. (Top to bottom:) A. Calculated total convergence rate, Nazca to South American plate, 80-0 Ma, calculated at 1 m. y. interval, deg of arc per m. y., at indicated points along the contemporary trench. B. Total convergence rate, as a, at 5 m. y., moving average. Spreadsheet is accessible in Supplementary Data files.

Figure 13. Histograms of igneous dates from Andes, 80-0 Ma. A. All dates 1 m. y. bins. B. As A, 5 m. y. bins. C. Within 0-150 km from trench. D. 150-300 km from trench. E. 300-450 km from trench. F. 450-600 km from trench. G. 600-750 km from trench.

Figure 15. Normalized cross-correlation of convergence rate versus bin date size.

Figure 16. Projected section of igneous isotopic dates, 0 to 2° arc east of Andean trench with reconstructed isochrons within 1° arc of trench (reconstructed isochrons in map view are in the Supplemental Data, Figure S7). Note near-trench igneous dates between 46 and 47° S latitude are closest to youngest reconstructed isochrons. Otherwise there is no obvious relationship of age of older subducting plate and position of magmatism.

Figure 17. Juan Fernandez hotspot traces in Hawaiian (green: combined Gaastra et al., 2022, and Wessel and Kroenke, 2008), Tristan (blue: Muller et al., 1993), and global average (orange: Muller et al., 2019) reference frames via plate-to-plate circuits. Hawaiian: HS > PC > NF; Tristan and global average: HS > AF > AN > WA > PC > NF.

Figure 1.

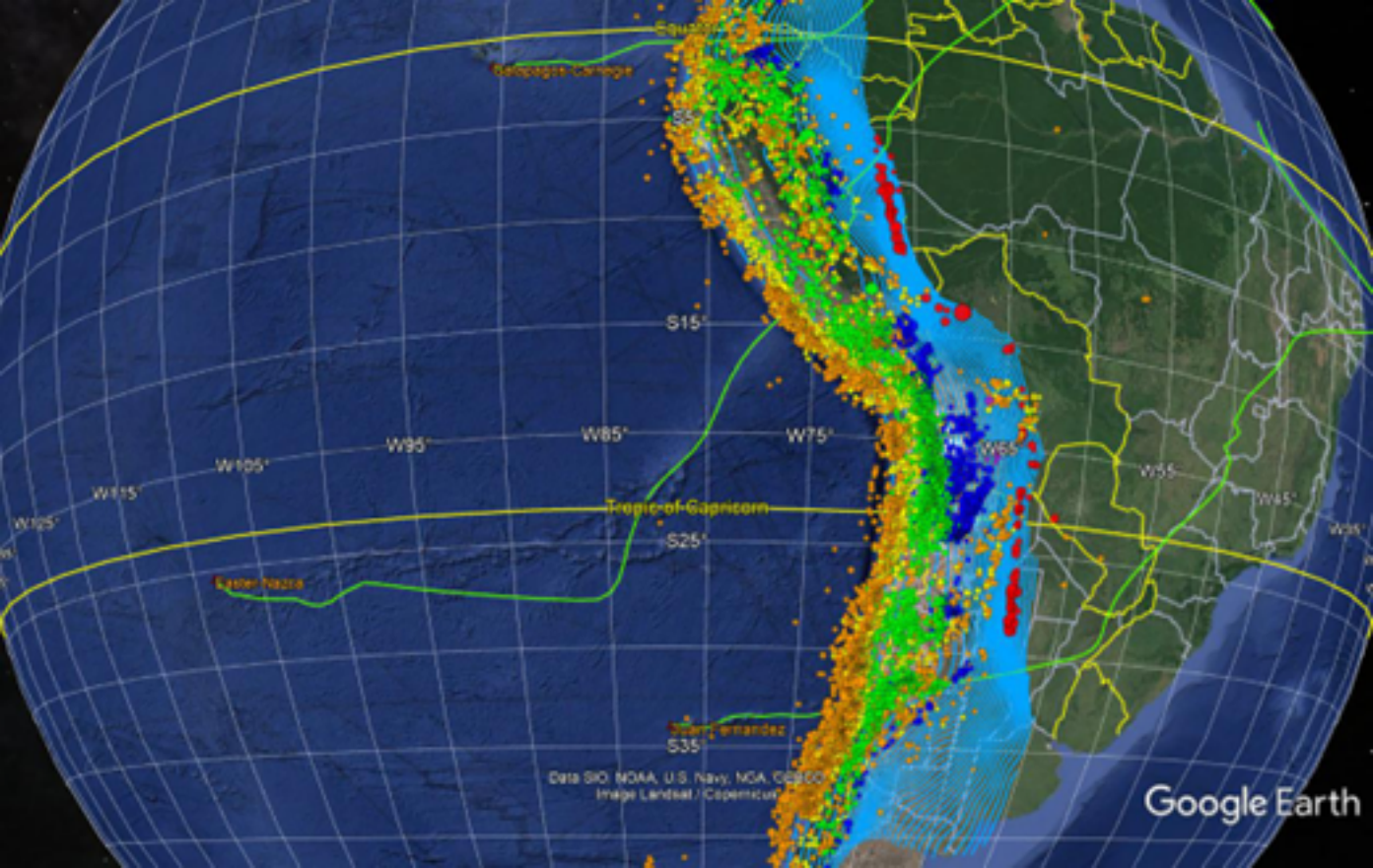
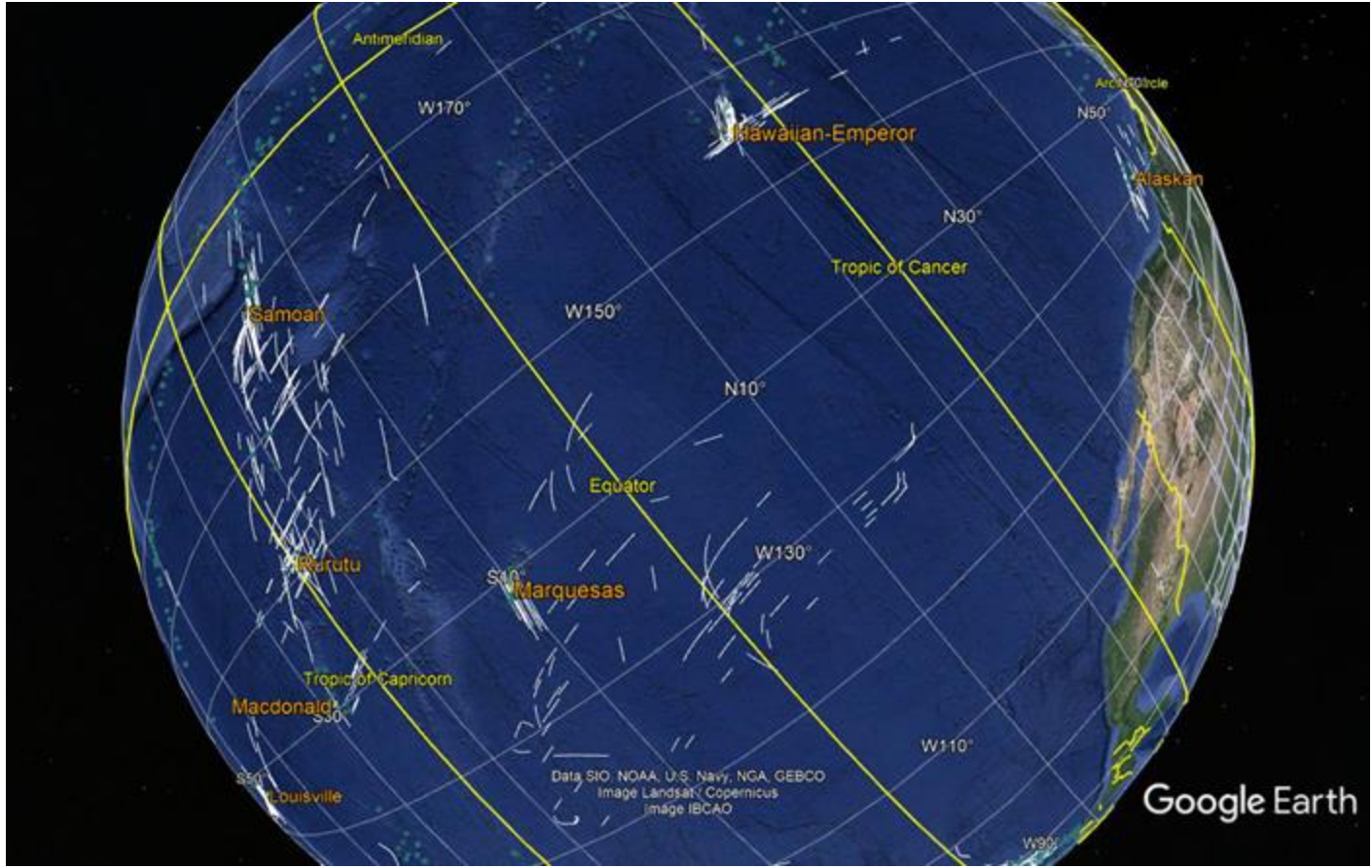


Figure 2.



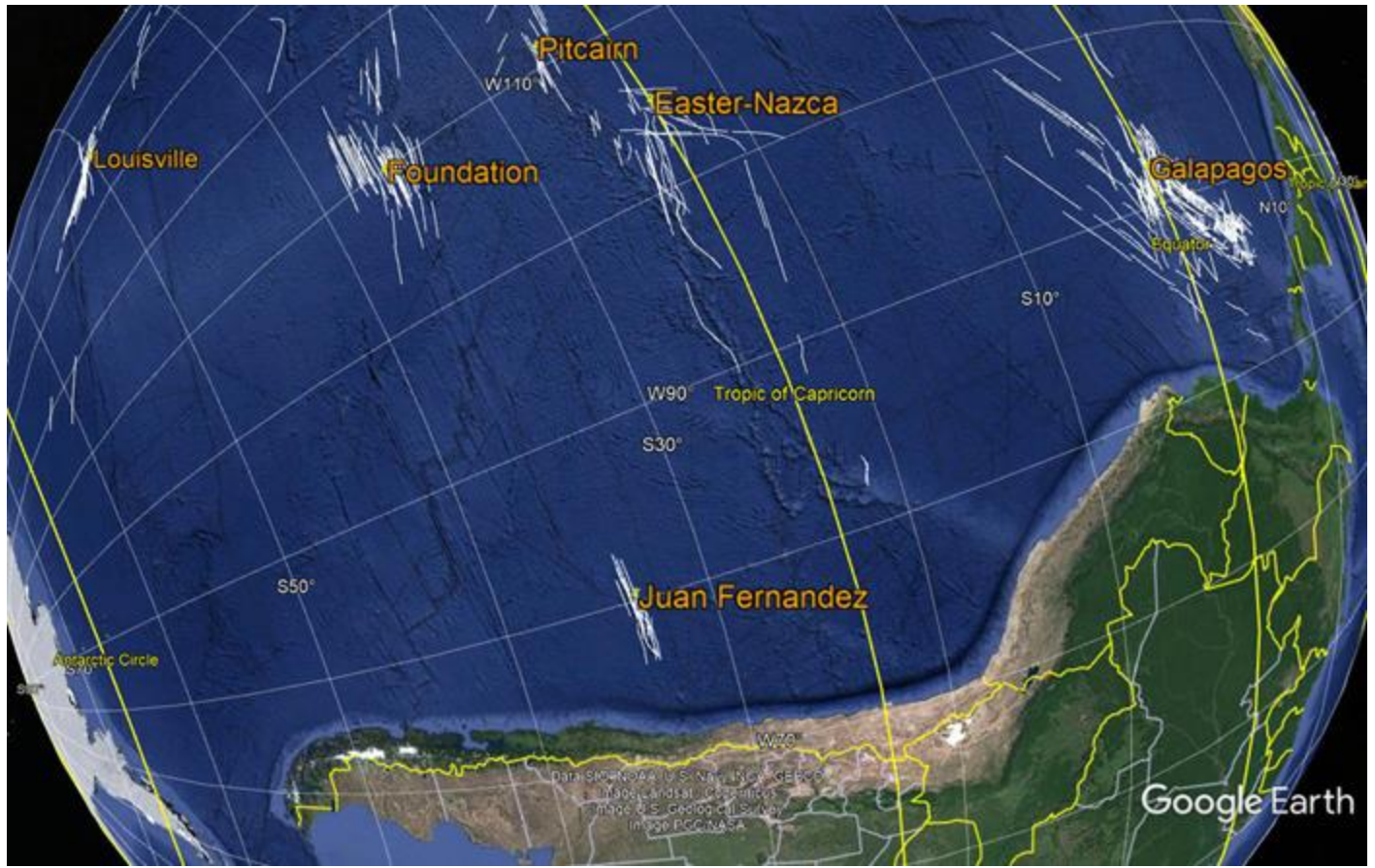


Figure 3.

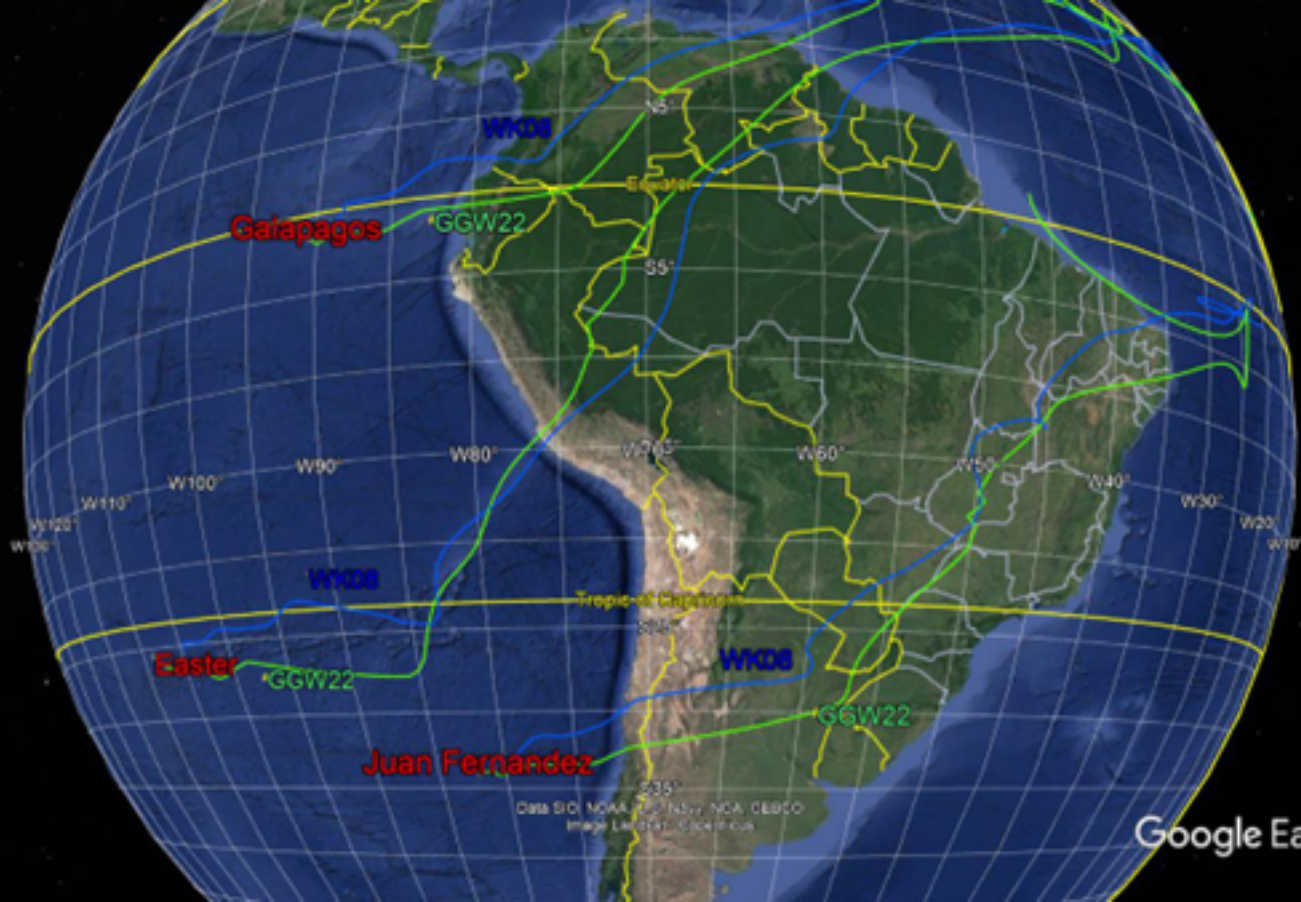
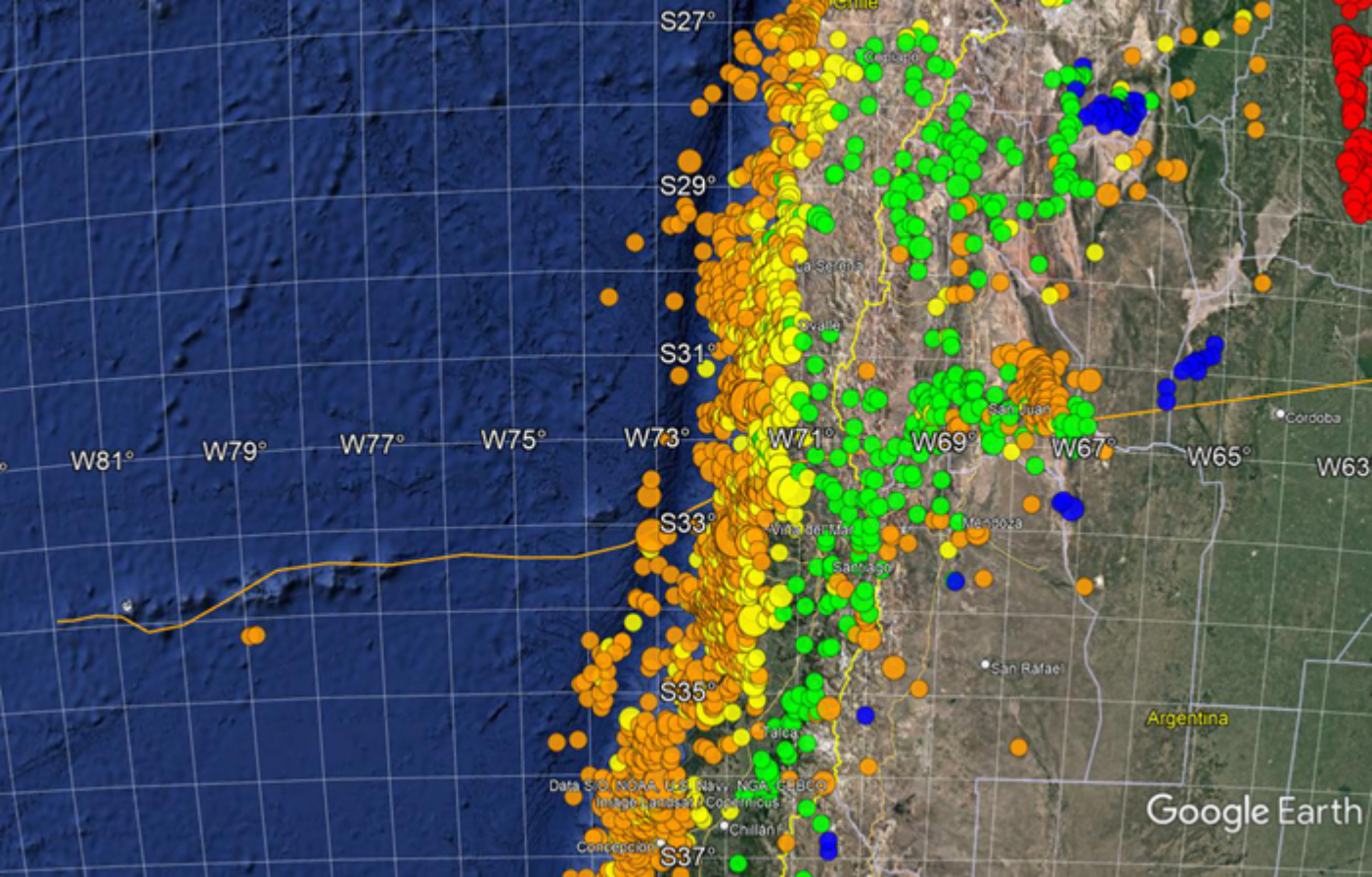


Figure 4.



S27°

S29°

S31°

S33°

S35°

S37°

W81°

W79°

W77°

W75°

W73°

W71°

W69°

W67°

W65°

W63°

Copiapó

La Serena

Ovalle

San Juan

Cordoba

Viña del Mar

Mendoza

Santiago

San Rafael

Talca

Chillan

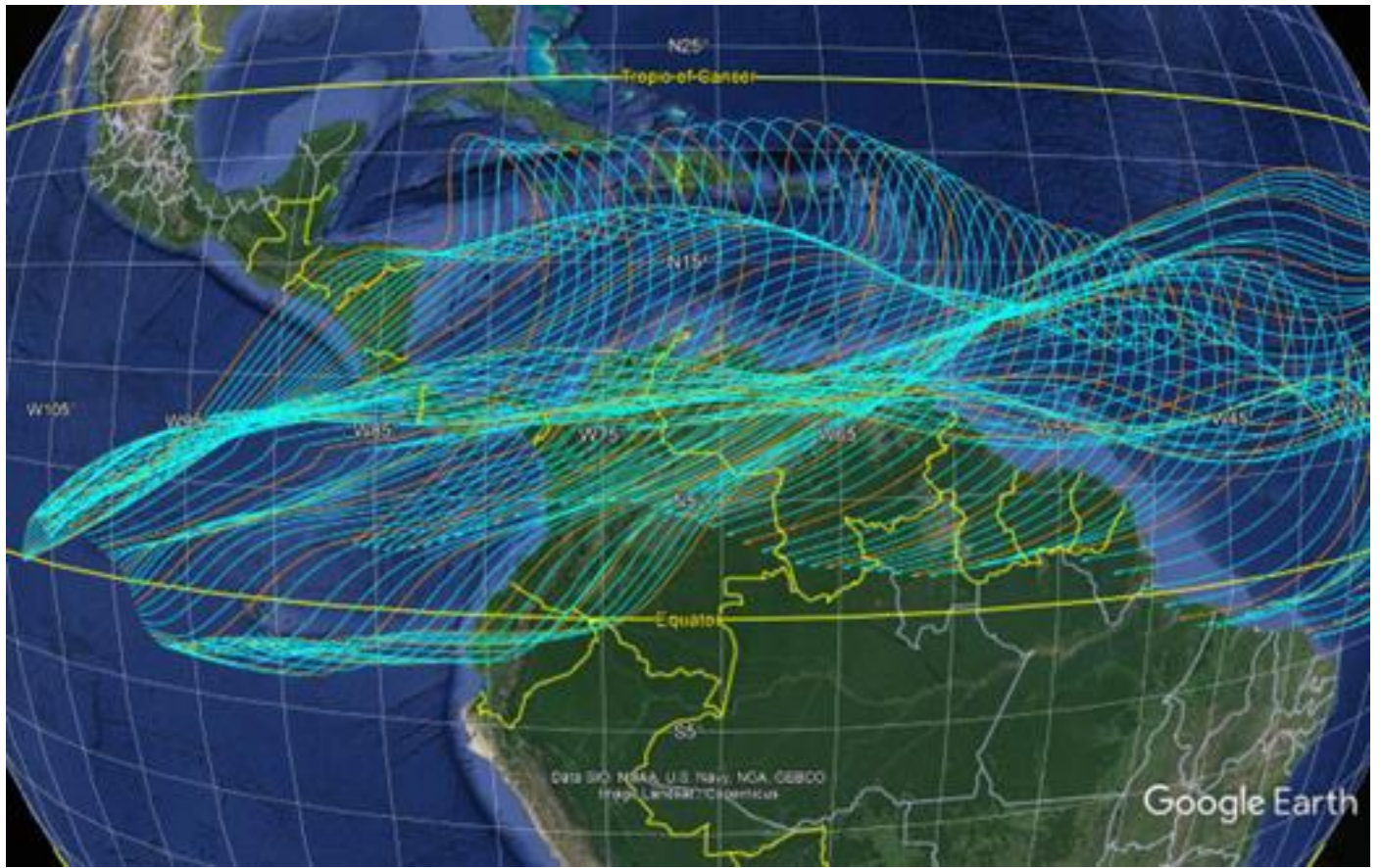
Concepcion

Argentina

Data S.O. NOAA, US Navy, NGA, GEBCO
Image Landsat/Copernicus

Google Earth

Figure 5.





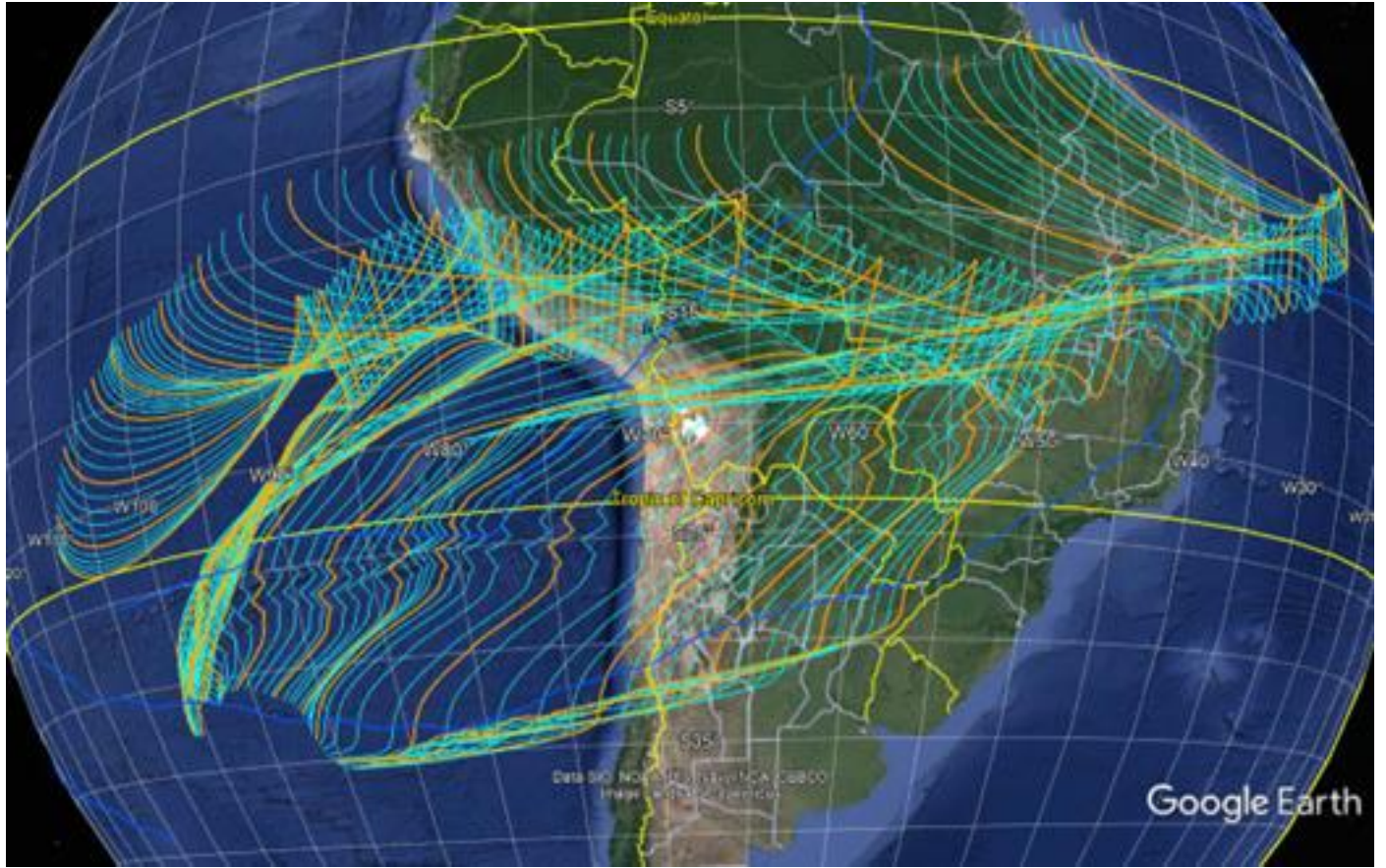
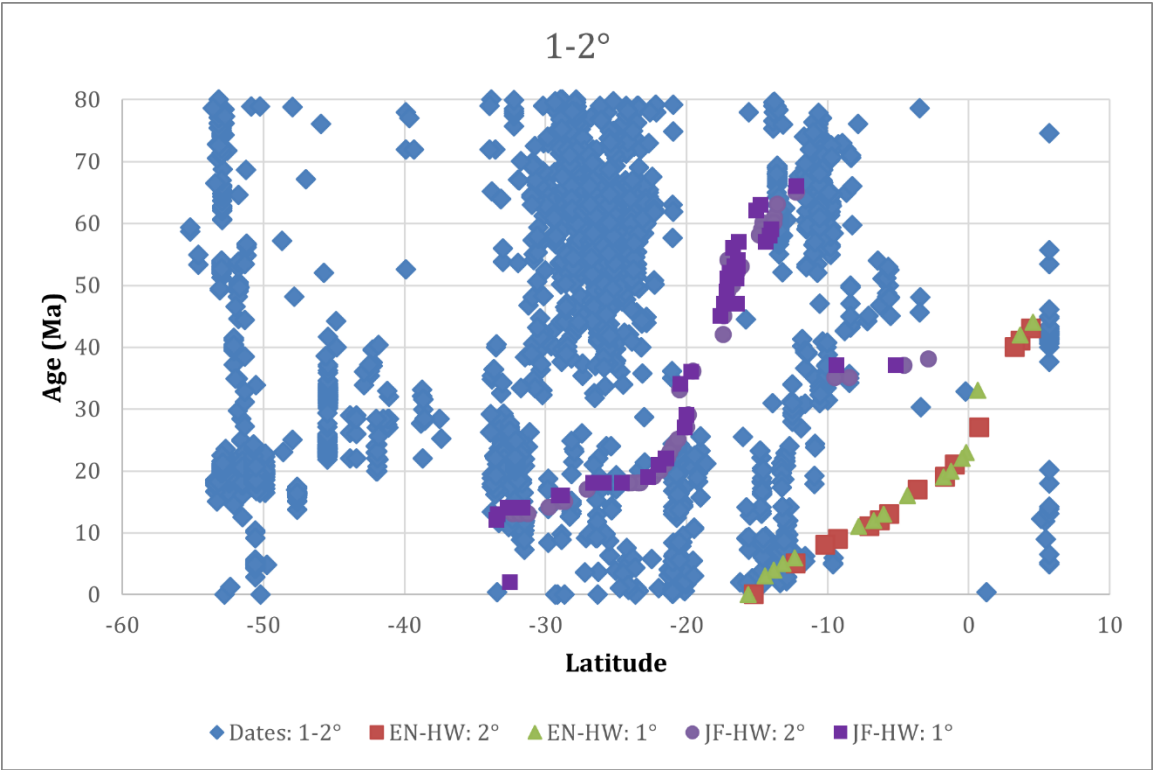
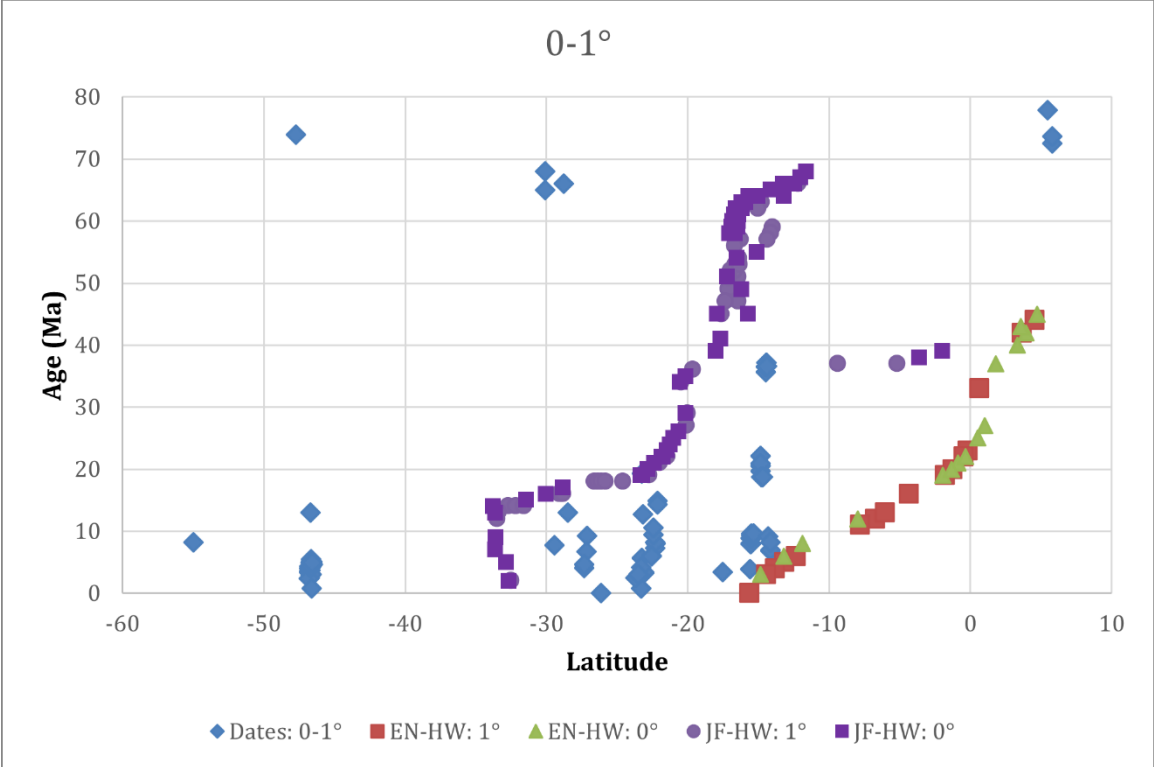
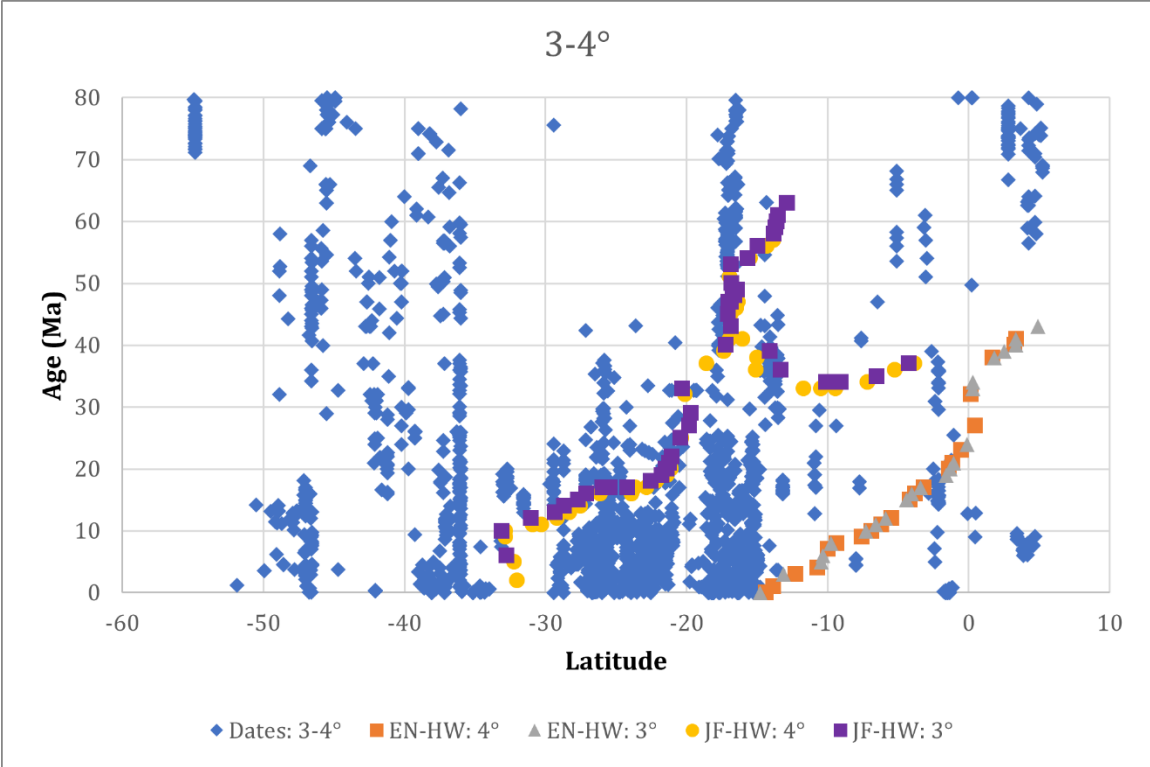
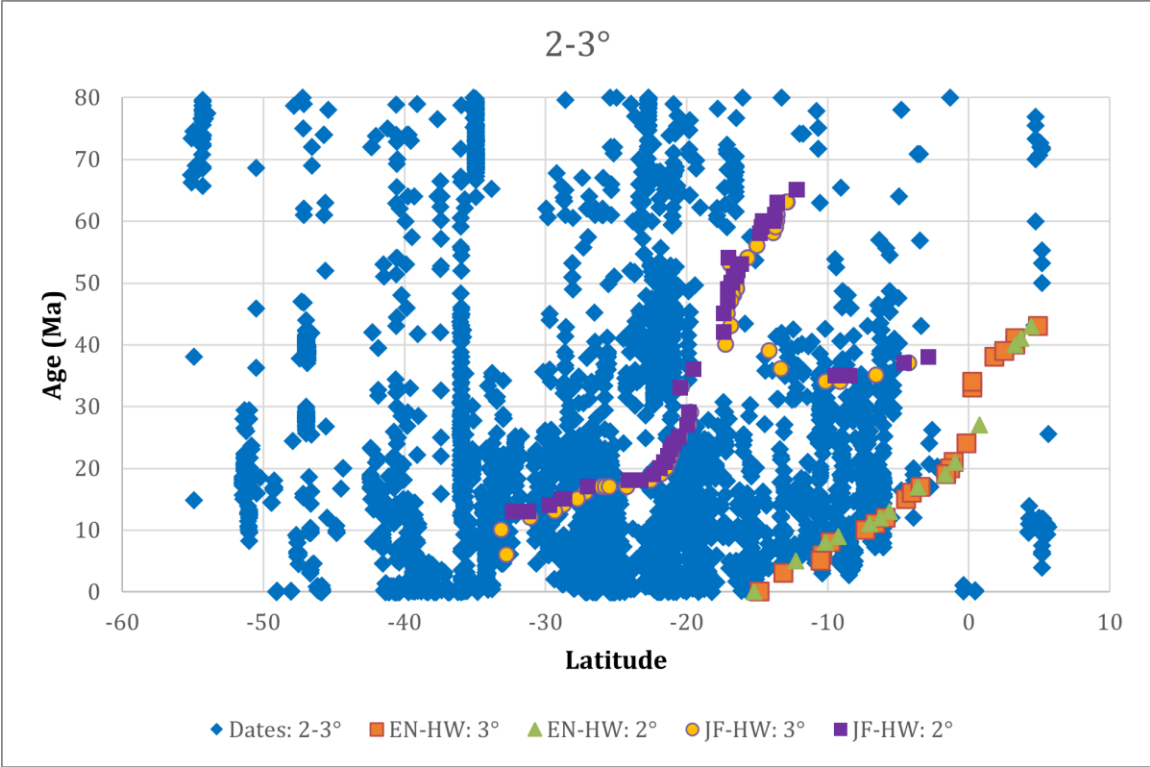
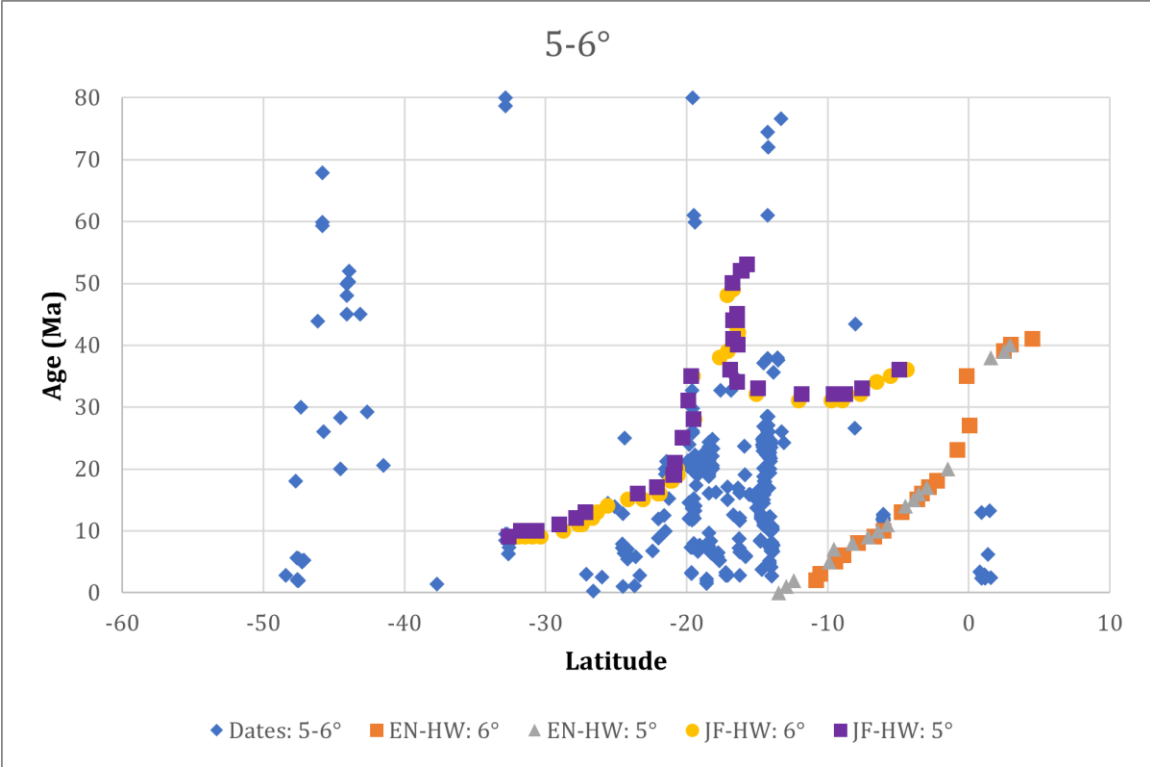
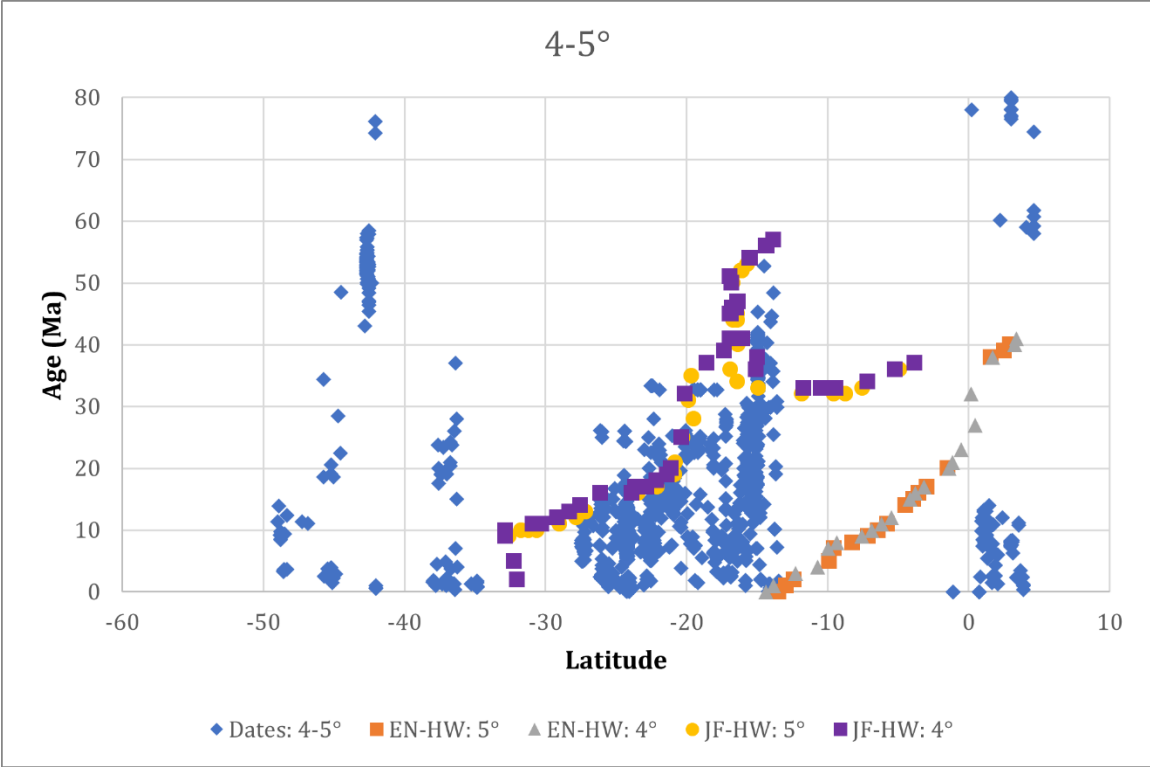
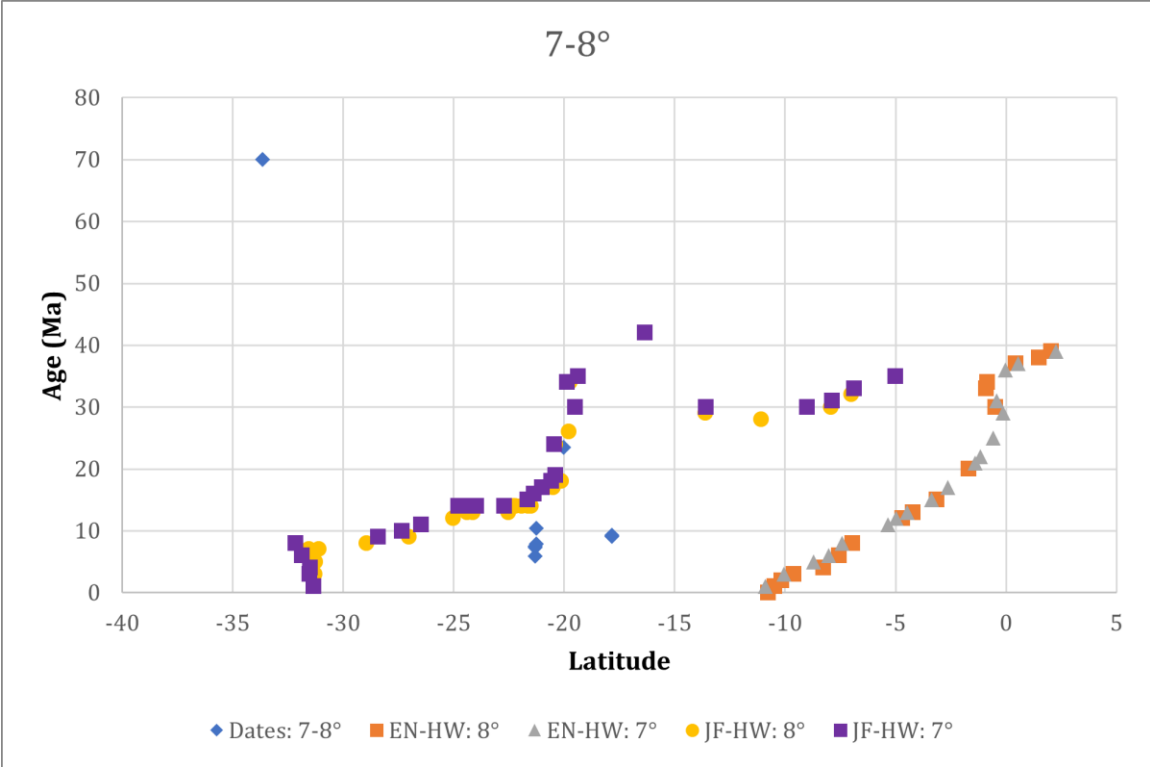
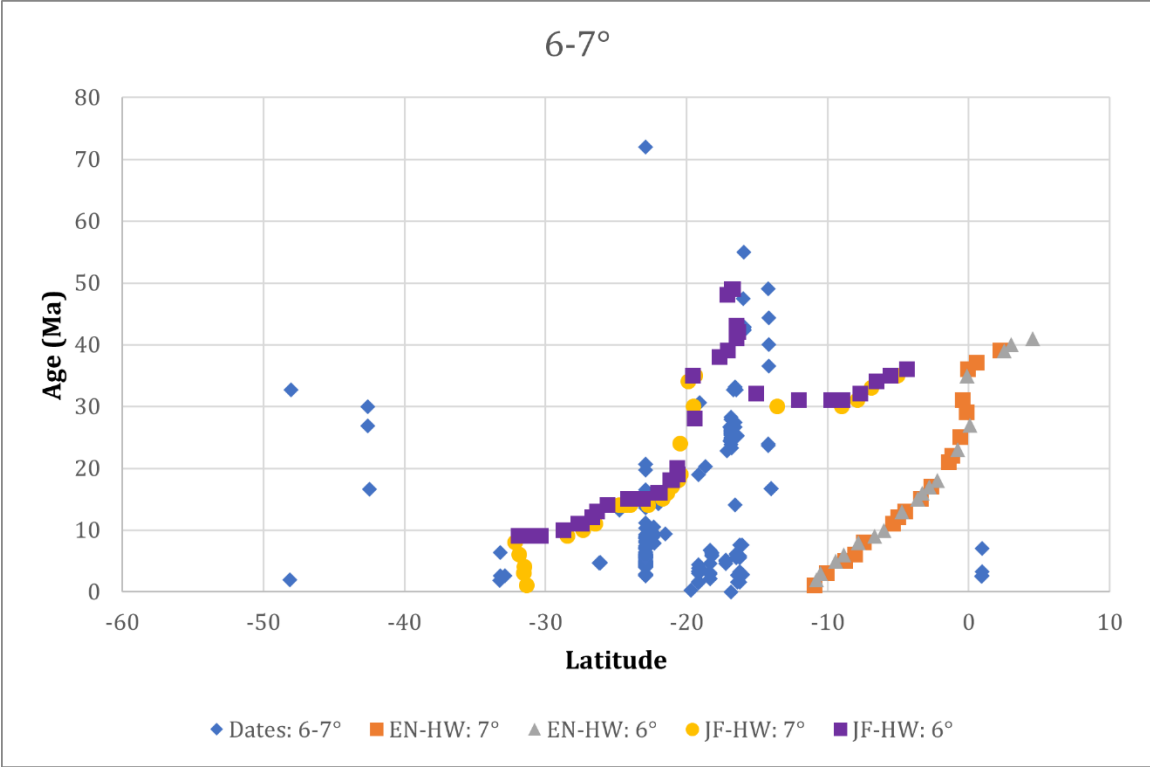


Figure 6.









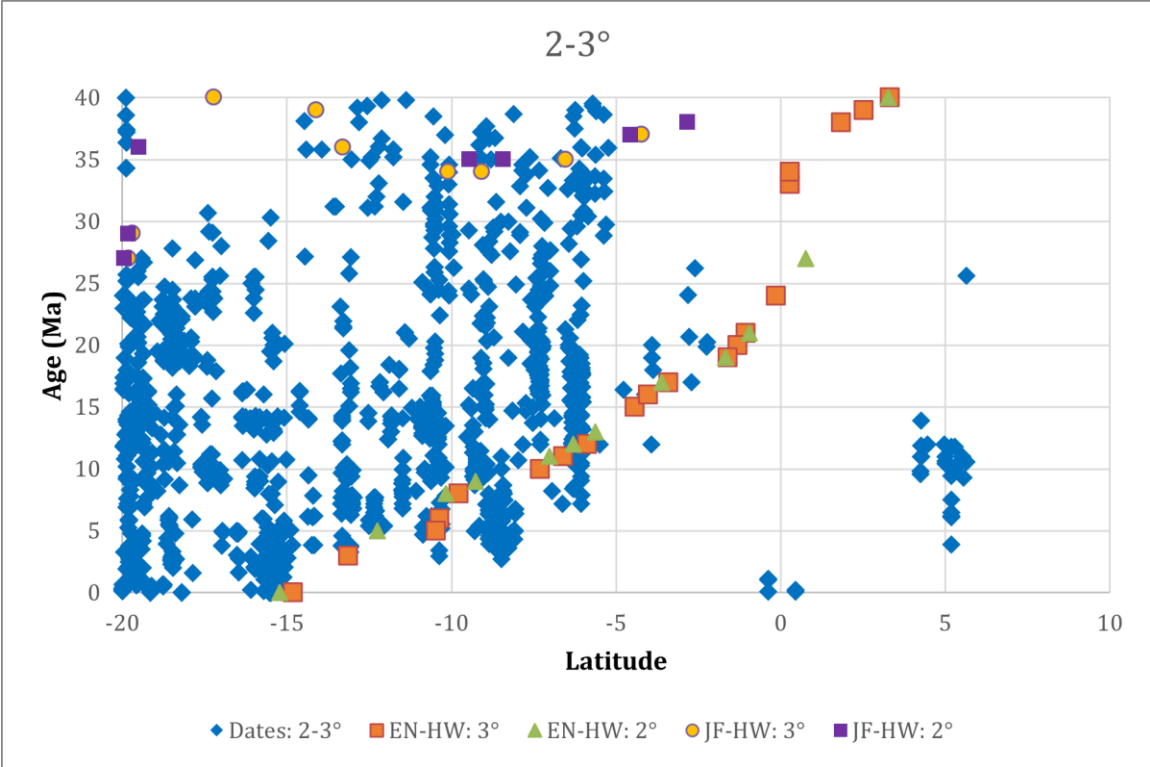
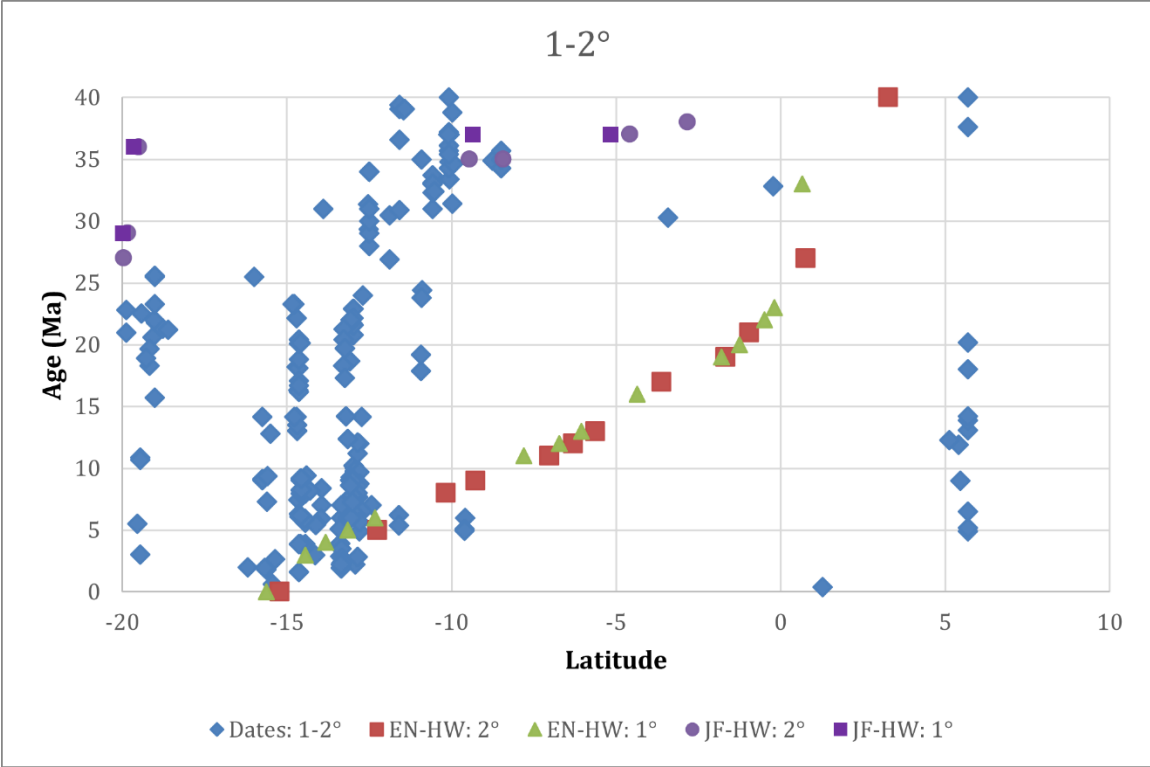
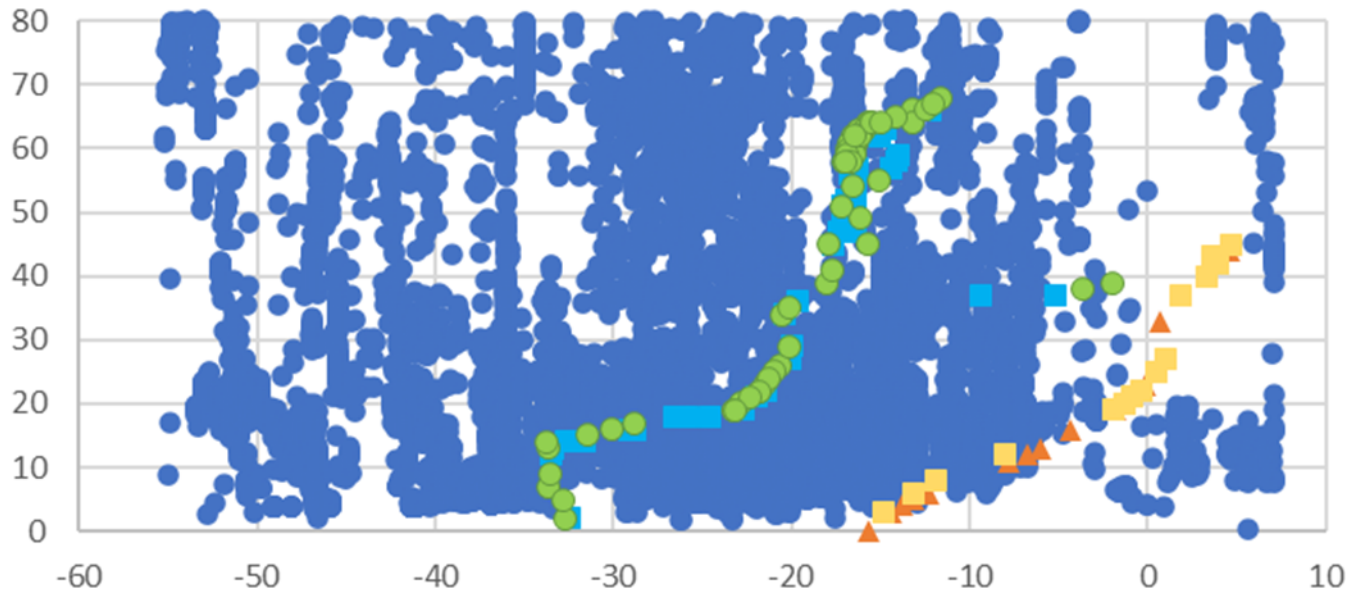


Figure 7.

Anticipated Age



● Dates ▲ 36-21: 1° ■ 36-21: 0° ■ 34-21: 1° ● 34-21: 0°

Figure 8.



Data SIO, NOAA, U.S. Navy, NGA, GEBCO
Image Landsat / Copernicus

Google Earth

Figure 9.



W80°

S50°

S30°

W60°

S10°

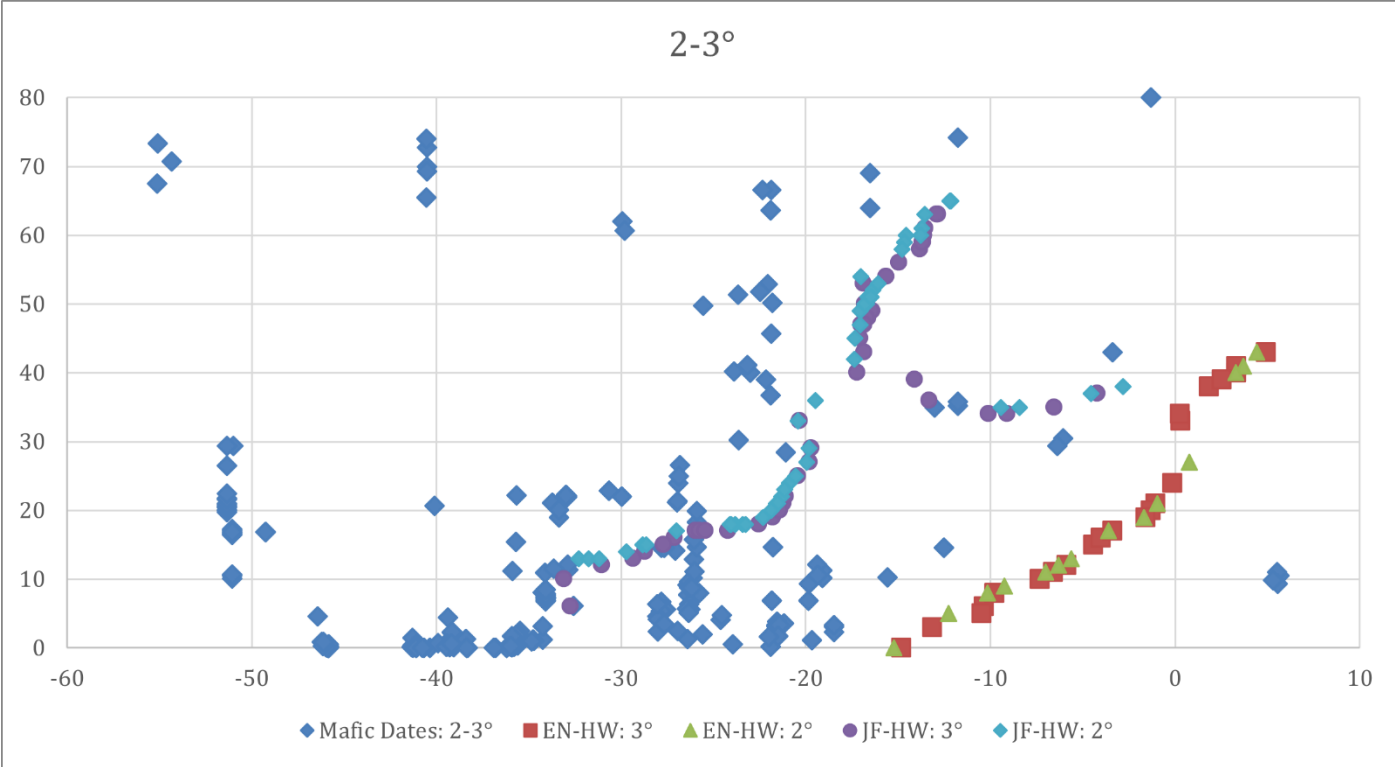
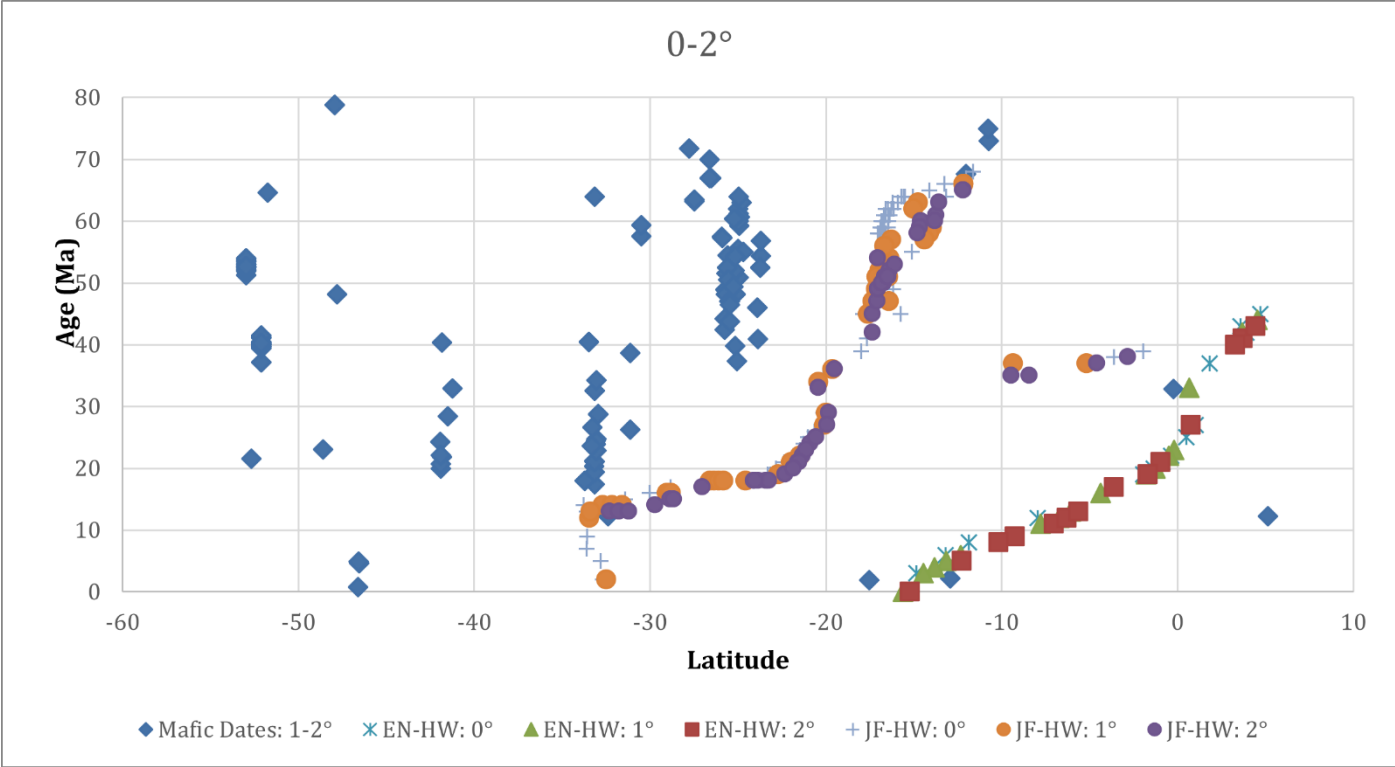
Equator

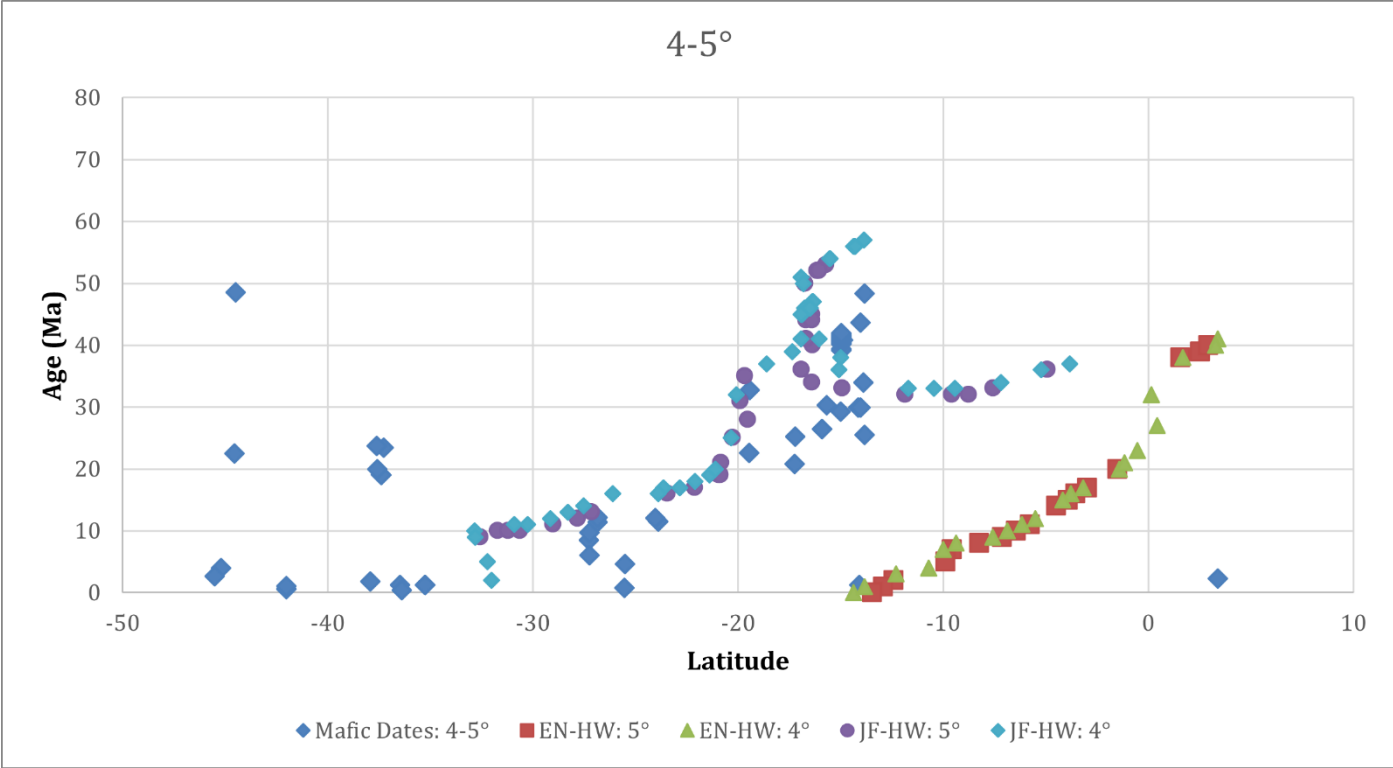
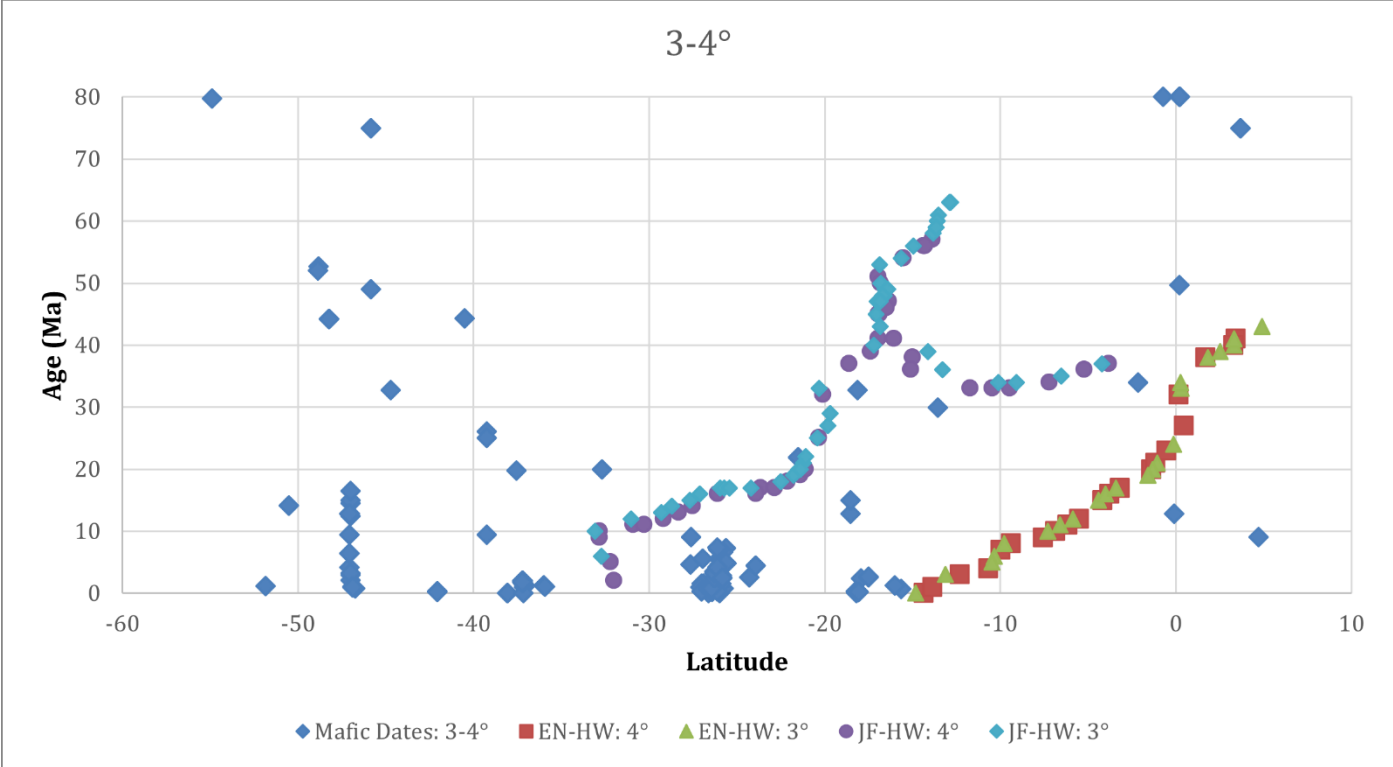
Capricorn

Data SIO, NOAA, U.S. Navy, NGA, GEBCO
Image Landsat, Copernicus
Image PGC, NASA

Google Earth

Figure 10.





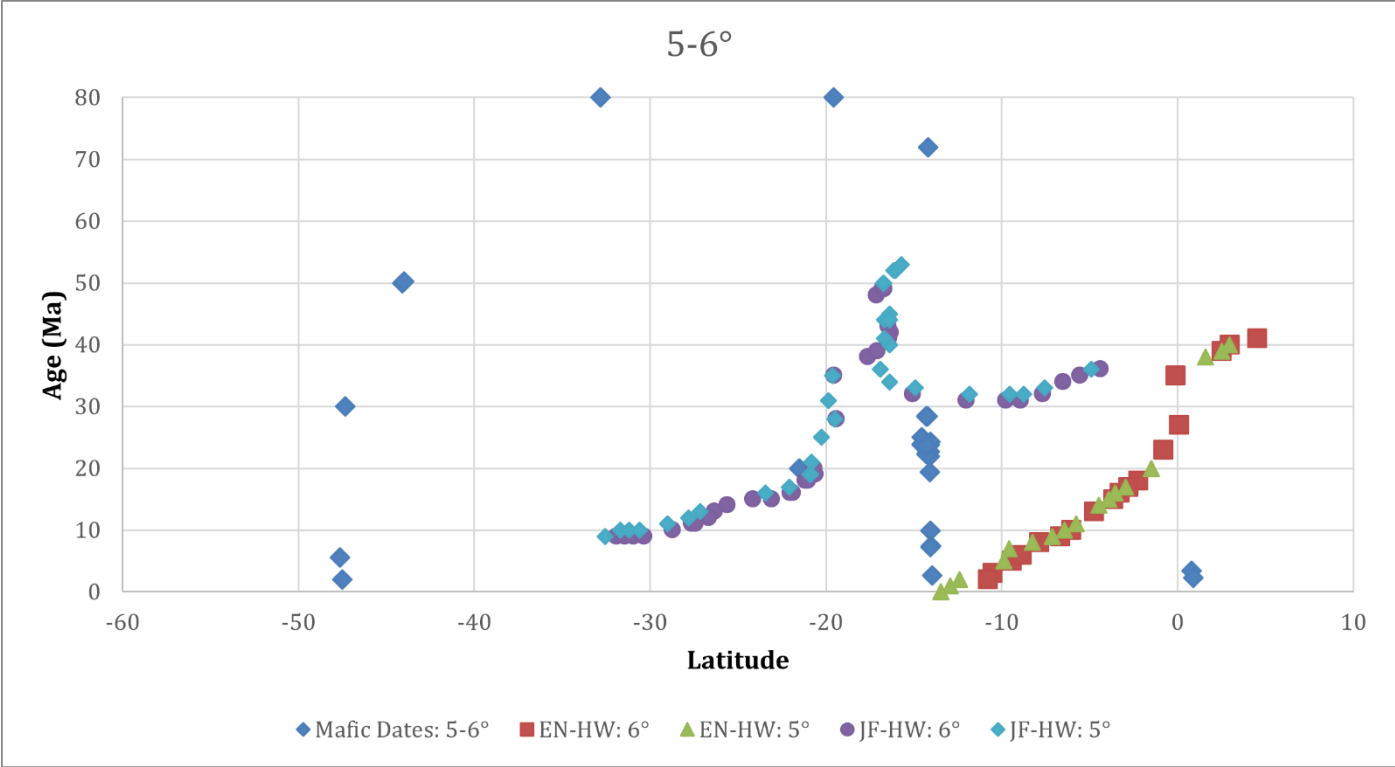


Figure 11.



Figure 12.

Figure 13.

Nazca/Farallon-South America Velocity - 1 m.y. Interval

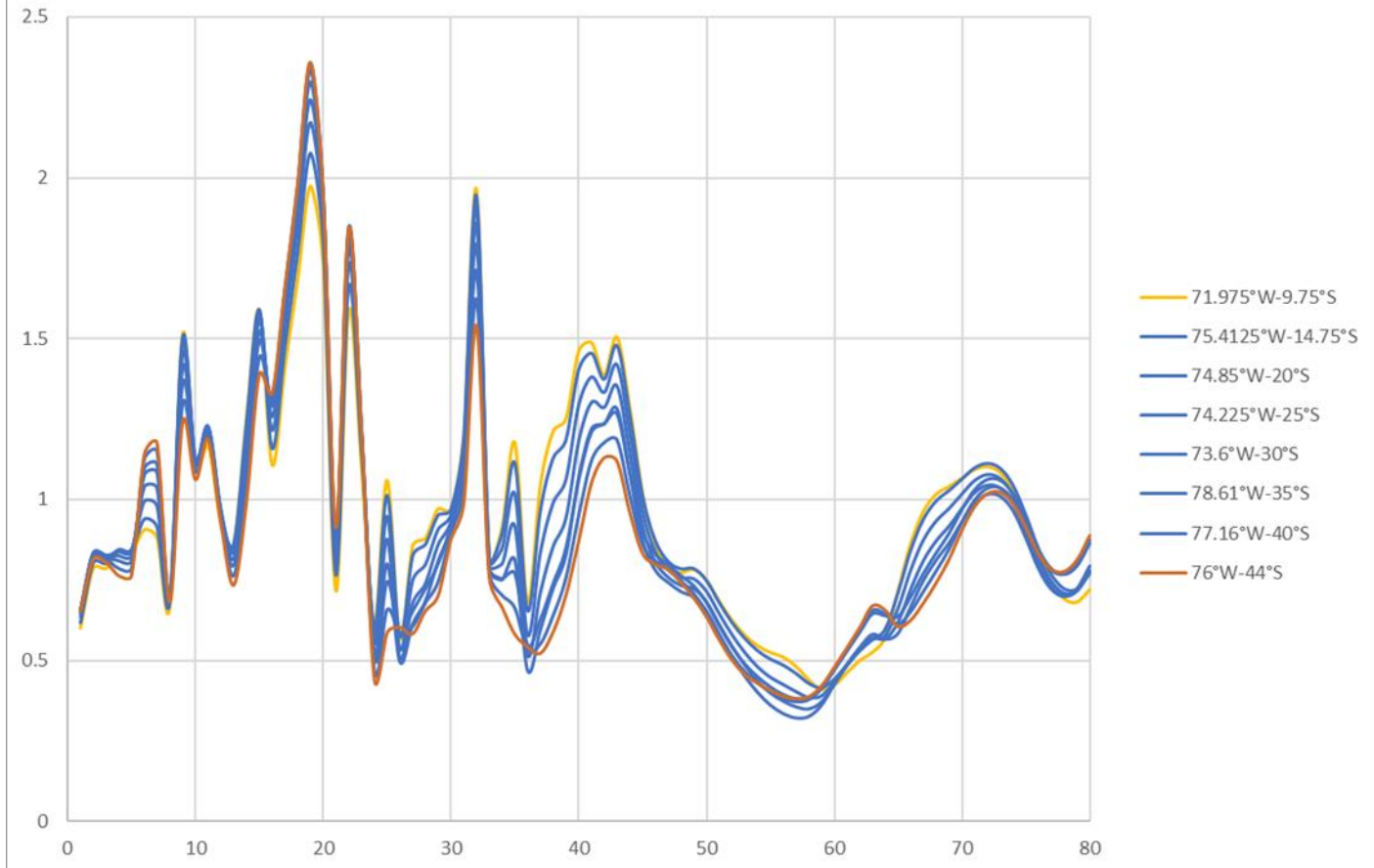
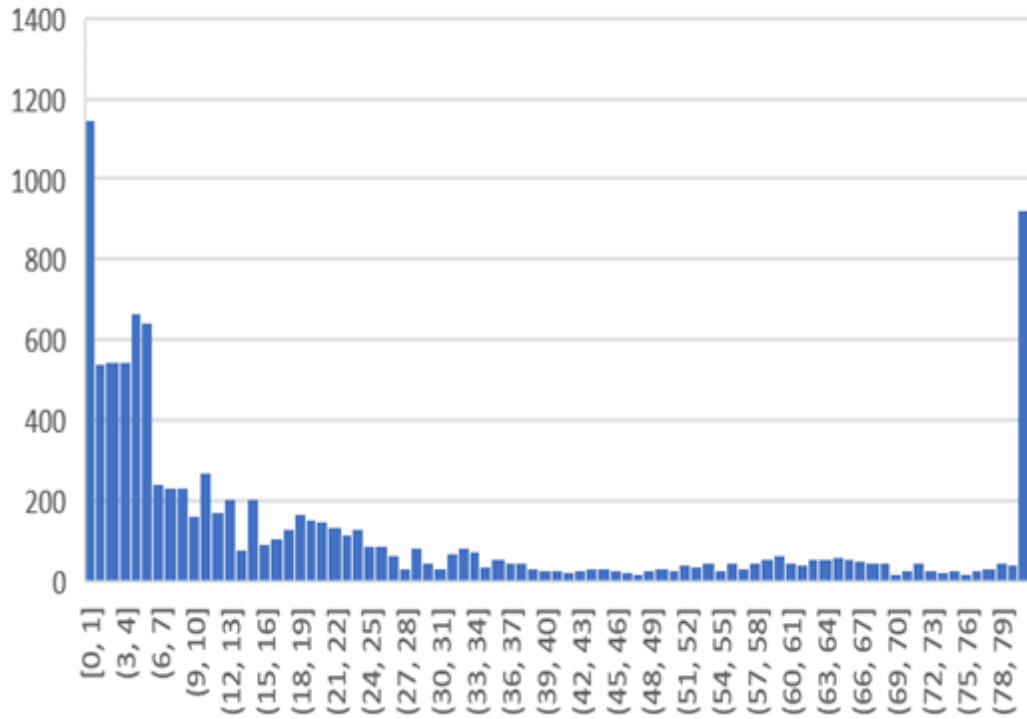
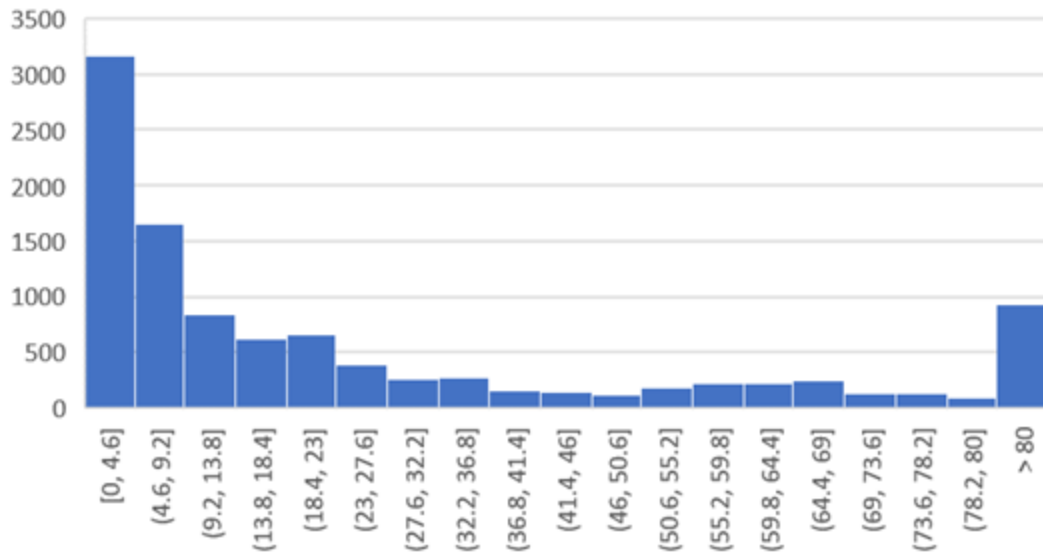


Figure 14.

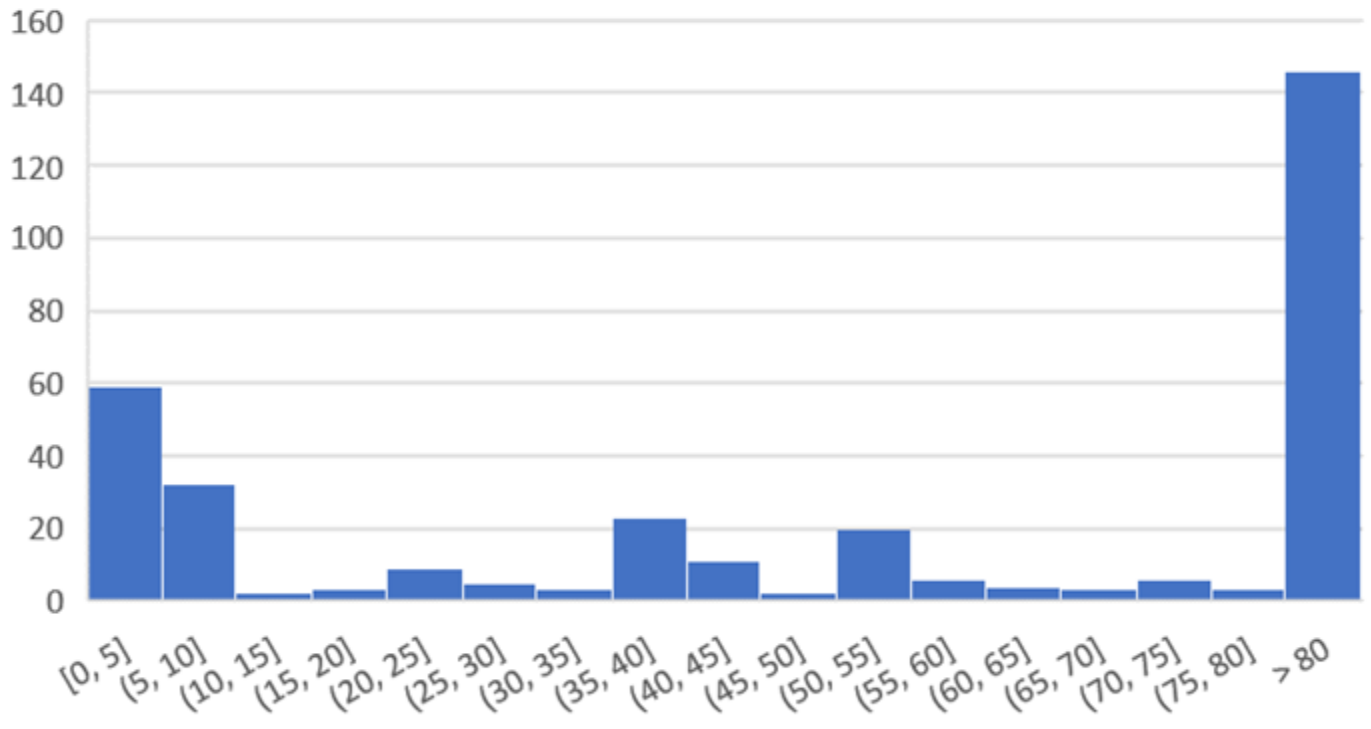
All - 0-80 Ma



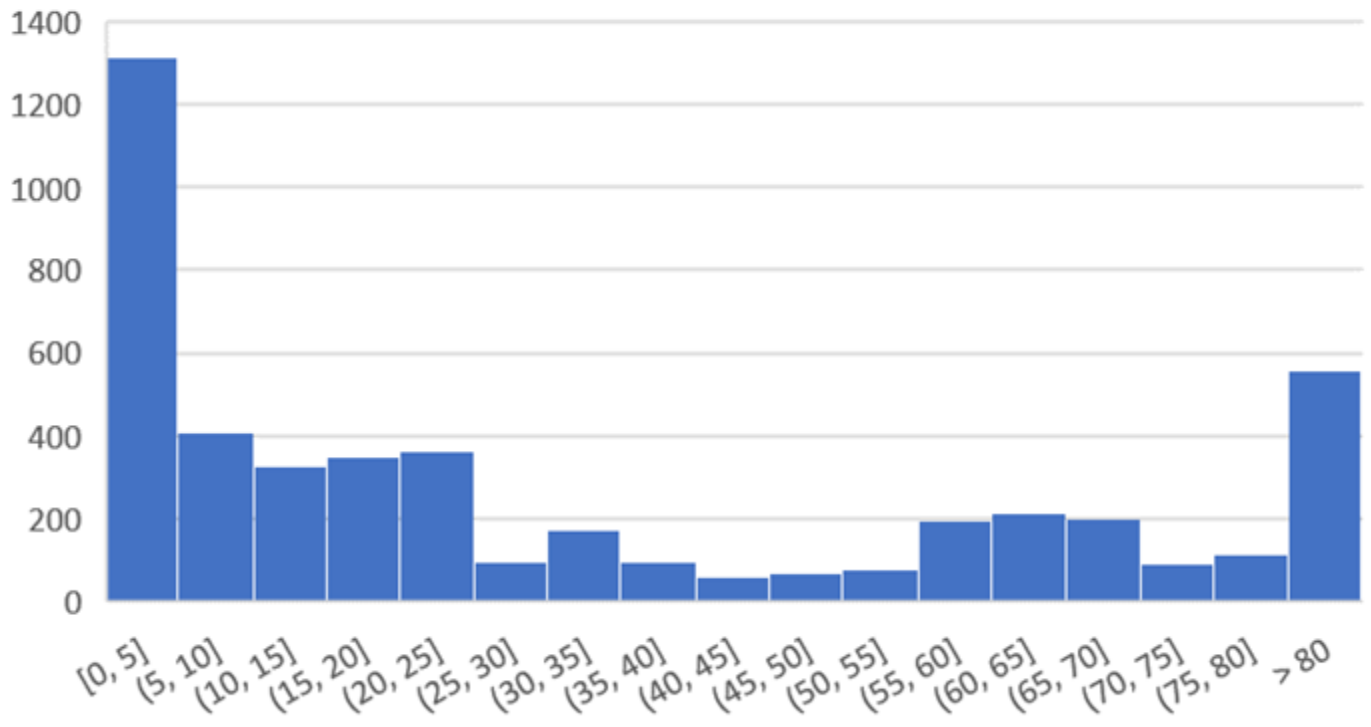
All - 0-80 Ma



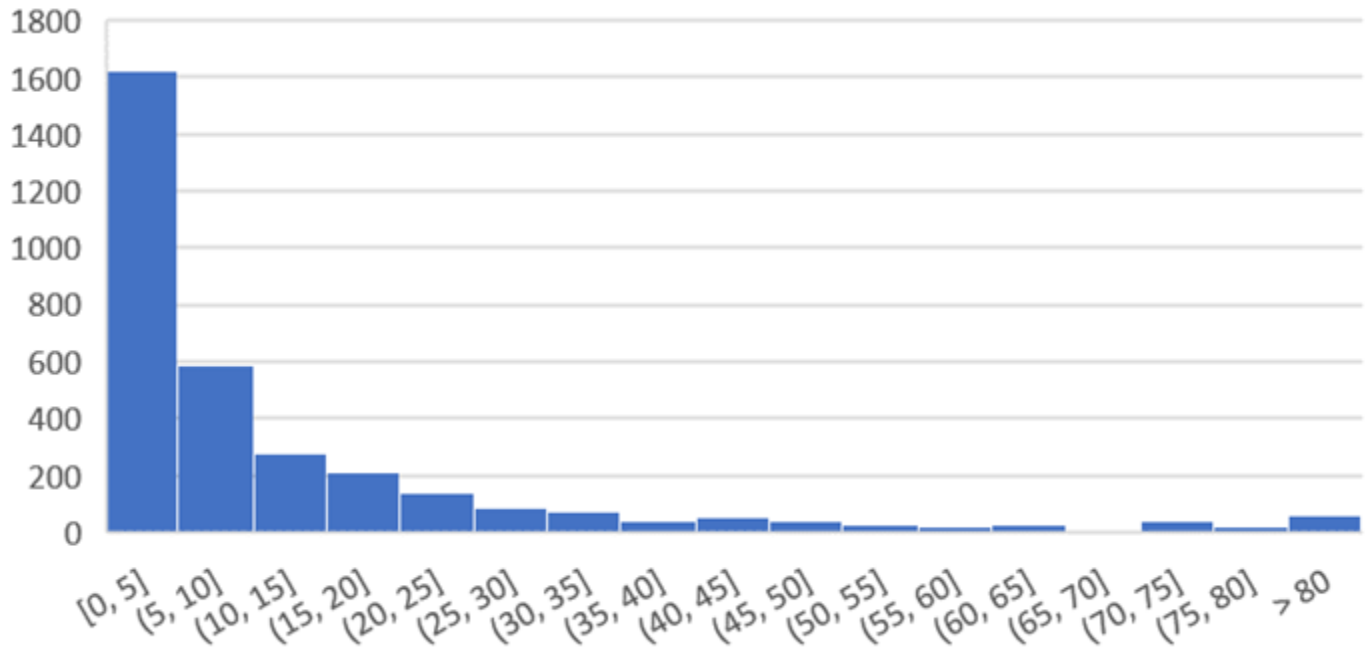
0-150 km



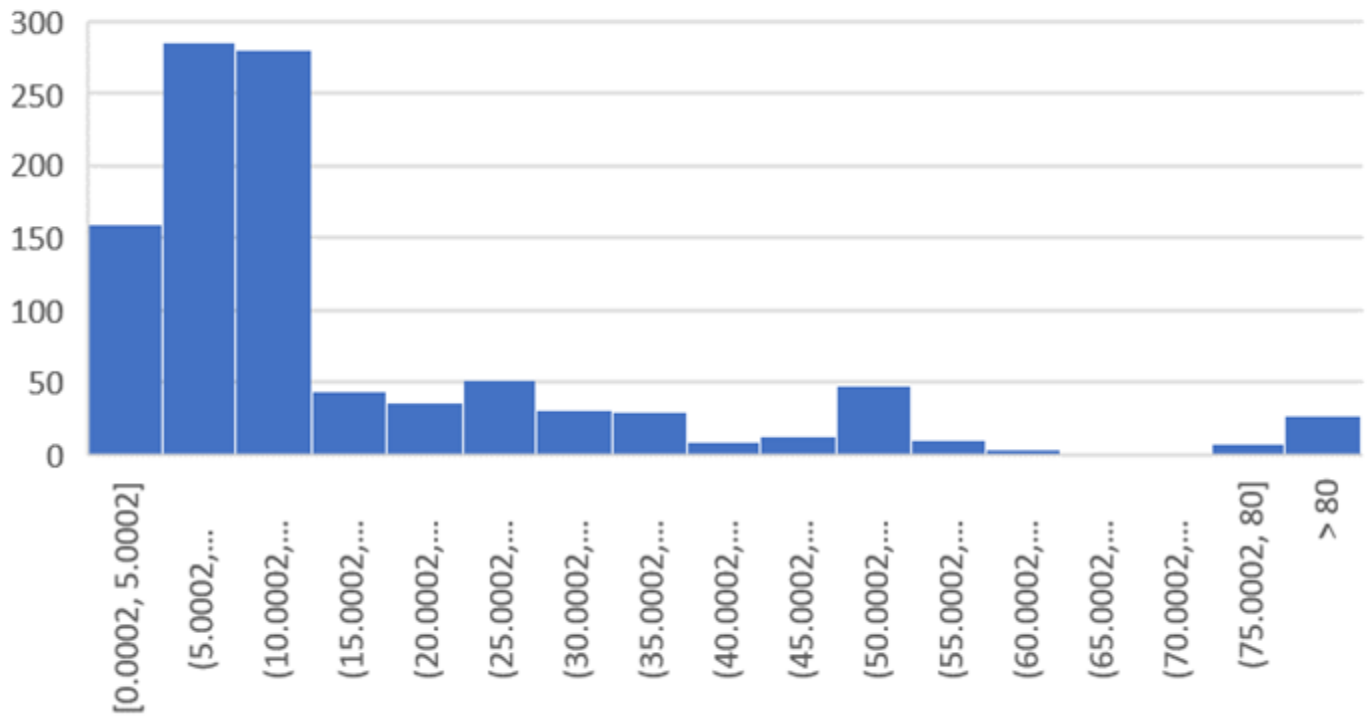
150-300 km



300-450 km



450-600 km



600-750 km

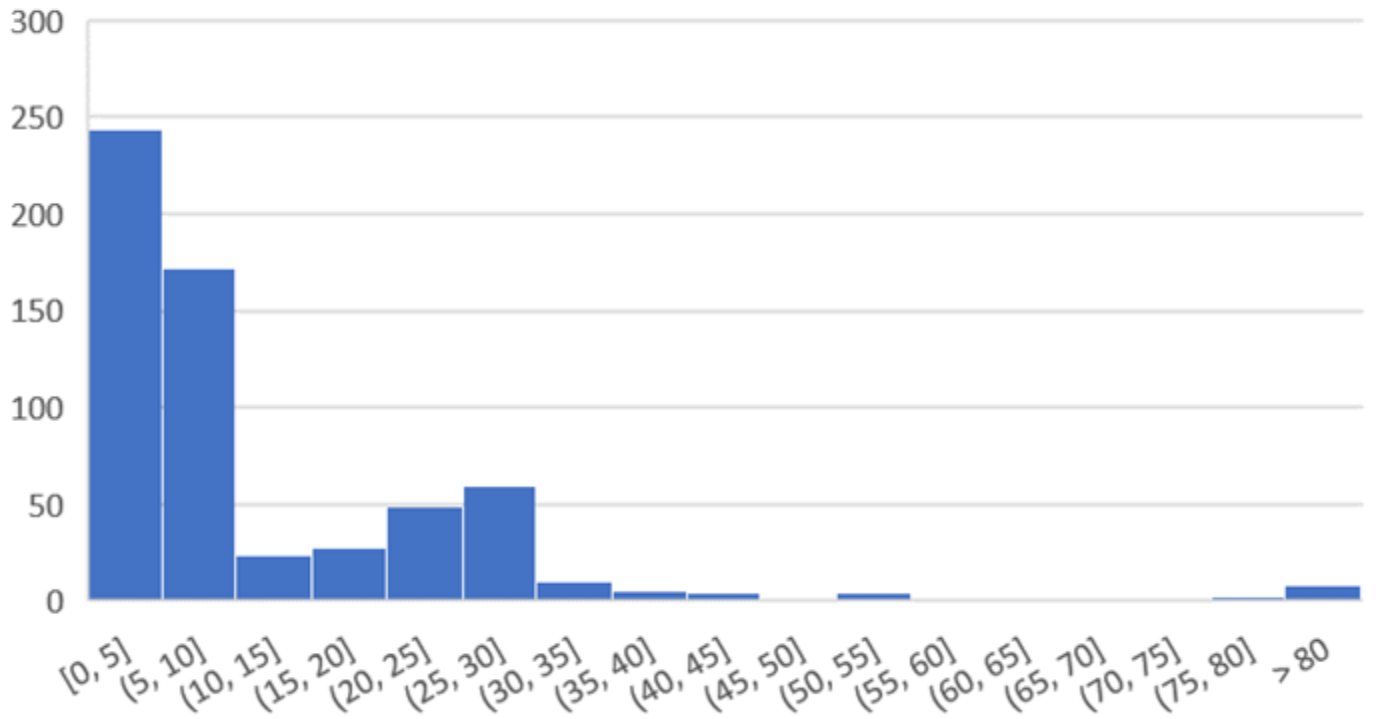


Figure 15.

Cross-Correlation, 0-80 Ma, 1 m.y. interval

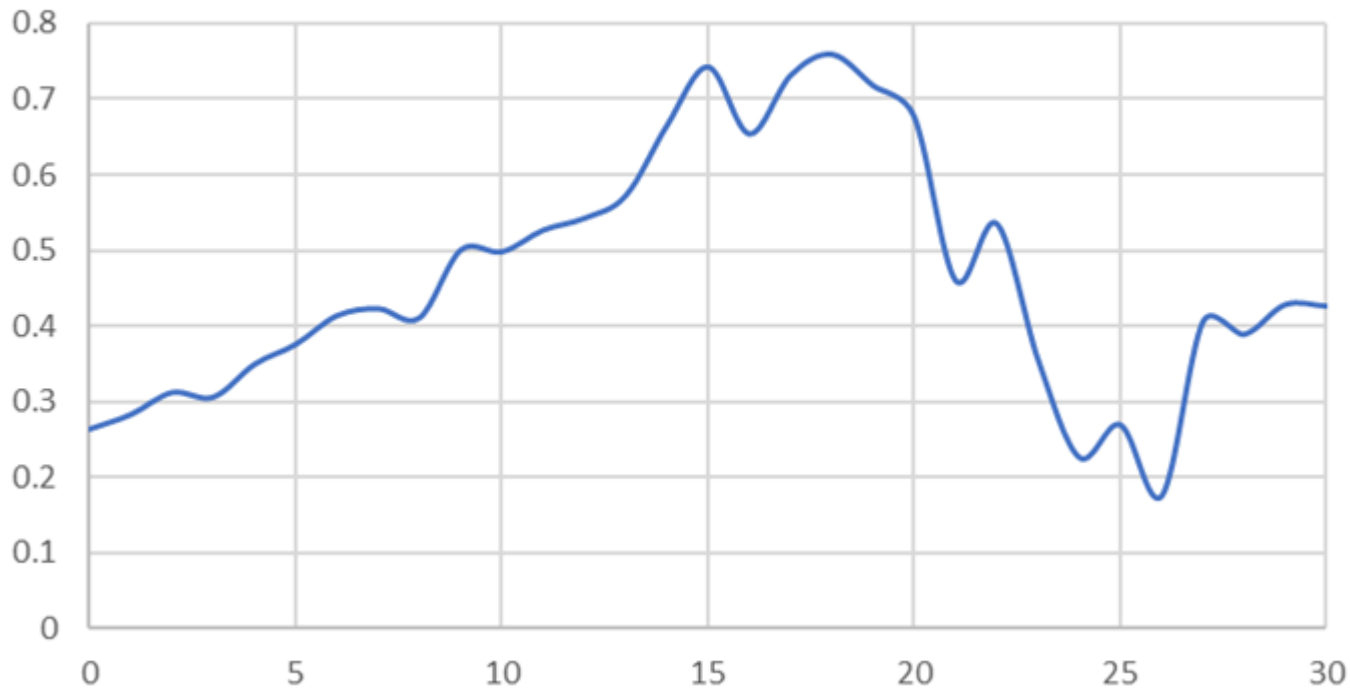
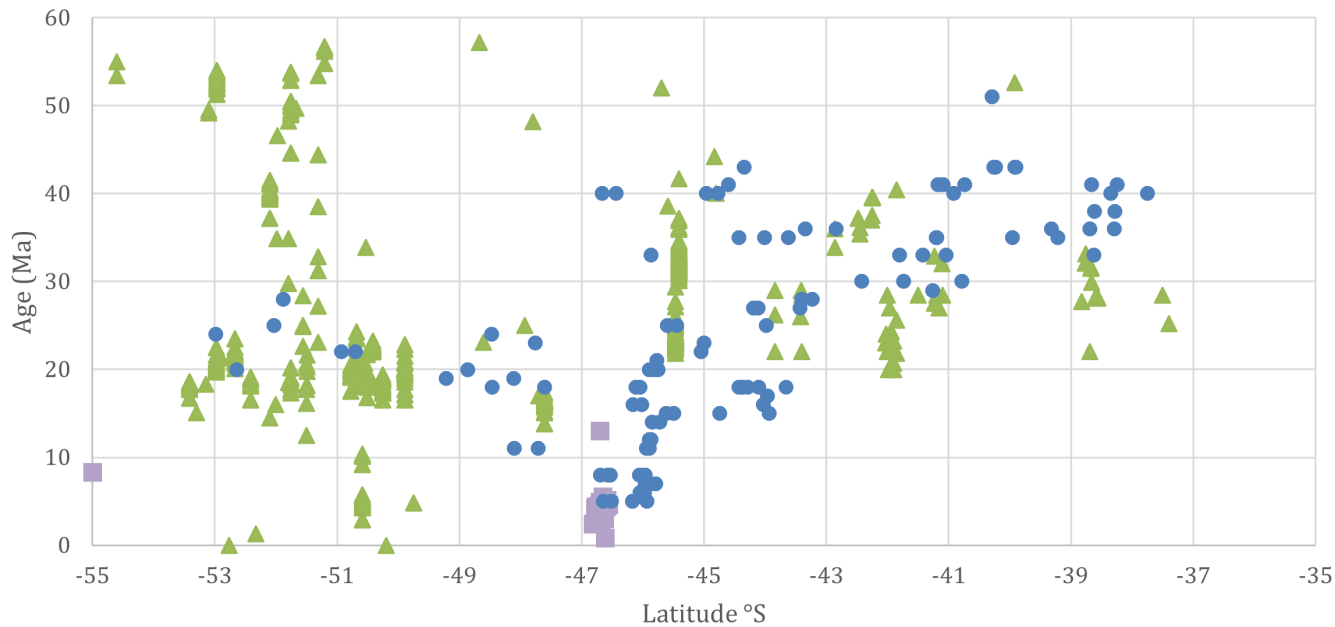


Figure 16.

Ridge-Trench Intersection



■ Dates: 0-1° ▲ Dates: 1-2° ● Ridge-Trench

Figure 17.

